Development of a Magnetic Levitation System for Additive Manufacturing Processes

by

Parichit Kumar

A thesis
presented to the University of Waterloo
in fulfillment of the
thesis requirement for the degree of
Doctor of Philosophy
in
Mechanical and Mechatronics Engineering

Waterloo, Ontario, Canada, 2022

Examining Committee Membership

The following served on the Examining Committee for this thesis. The decision of the Examining Committee is by majority vote.

External Examiner:	Mohamed Youssef, Professor Dept. of Mechanical Engineering Ontario Tech University
Supervisor:	Mir Behrad Khamesee, Professor Dept. of Mechanical and Mechatronics Engineering University of Waterloo
Supervisor:	Ehsan Toyserkani, Professor Dept. of Mechanical and Mechatronics Engineering University of Waterloo
Internal Member:	Sanjeev Bedi, Professor Dept. of Mechanical and Mechatronics Engineering University of Waterloo
Internal Member:	Hamid Jahed Motlagh, Professor Dept. of Mechanical and Mechatronics Engineering University of Waterloo
Internal Member:	Eihab Abdel-Rahman, Professor Dept. of Systems Design Engineering University of Waterloo

Author's Declaration

I hereby declare that I am the sole author of this thesis. This is a true copy of the thesis, including any required final revisions, as accepted by my examiners.

I understand that my thesis may be made electronically available to the public.

Abstract

Magnetic levitation and Additive Manufacturing (AM) are both highly innovative fields that have changed the trajectory of development within a wide variety of applications. Magnetic levitation techniques offer noncontact levitation forces that highlight high compatibility with metal AM operations like Laser Directed Energy Deposition via Powder Feeding (LDED-PF) techniques. The research presented in this report aims to highlight the novel implementation of a magnetic levitation system compatible with LDED-PF operations. The suspension of a conductive paramagnetic material geometry through repulsive magnetic levitation techniques will serve as the substrate to build a part through LDED-PF operations.

The research contributions are as follows: First, this research develops a novel magnetic levitation system capable of supporting AM operations. The compatibility of the levitation system has been tested through simulations and experiments. Second, the levitation system can support time-varying loads over time without losing stability during AM operations. Finally, a novel parameter to determine the compatibility of different paramagnetic materials with magnetic levitation applications was developed and verified through this research.

Two magnetic levitation systems were developed. The first system was composed of a laminated core. This entailed the use of several hundred sheets assembled together to form the core within which the coils were embedded. This resulted in a reduction in eddy current losses within the core, however, the sheets sizes were predefined which resulted in the loss of flexibility for optimization. The second system was composed of a solid core system. This system was subjected to higher eddy current losses, however, offered significantly higher flexibility for optimization. The prototypes were optimized, manufactured, assembled, and tested. Both prototypes successfully highlighted the ability to levitate aluminum discs.

Following the successful development of the levitation system prototypes, the next step was the development of a feedback controller to facilitate stable suspension at the desired setpoint. Through the incorporation of a simple Proportional Integral and Derivative (PID) controller using a laser sensor, the rise time was improved. However, a significantly high settling time was still encountered. To overcome this, a PID controller with a compensator component modeling the anticipated initial value of the voltage input was incorporated into the feedback PID controller. Through the implementation of the PID controller with the compensator component, the overshoot was eliminated and the settling time was reduced by 3.9 s.

Subsequently, the performance of the levitation system was tested without a feedback controller within the LDED-PF machine experimentally. Copper alloys were deposited on

an aluminum alloy build surface that was levitated. Under a high powder feed rate and high laser power, the levitation system was successfully able to support powder deposition activities. The build surface for powder deposition was also maximized through the incorporation of the levitation system within the AM machine.

Finally, this research also develops a parameter set that utilizes the material properties of different paramagnetic materials to determine their compatibility with magnetic levitation techniques. Conventionally, there is a strong reliance on the use of experimental implementation to determine whether a material is compatible with magnetic levitation techniques. However, by comparing the ratio of electrical conductivity to the density of the material, the compatibility of the material with magnetic levitation techniques can be determined without any experimental implementation.

Acknowledgements

I would like to take this opportunity to thank everyone who made the progression of my research possible.

I would like to offer my sincerest and deepest gratitude to my supervisors and mentors, Dr. Mir Behrad Khamesee and Dr. Ehsan Toyserkani. Their constant support, patience, guidance, and mentorship helped me achieve the goals of my research and helped make me a better engineer.

I would like to thank the committee members, Dr. Mohamed Youssef, Dr. Sanjeev Bedi, Dr. Hamid Jahed Motlagh, and Dr. Eihab Abdel-Rahman for their time, comments, and recommendations.

I would also like to thank the collaborators of this research: First, Dr. Yuze Huang, who helped with the initial feasibility testing and working principal development. Next, Mr. Saksham Malik acted as a collaborator for the development of the first prototype of the magnetic levitation system compatible with AM operations. Finally, Dr. Mazyar Ansari helped with the setup and implementation of the DMDIC106 AM machine. Thank you all for your fruitful corporation.

A special thank you to Neil Griffett (the Electronics Technician at the University of Waterloo), Rob (from MCI Ltd.), Andrew Urschel, Jeff McCormick (Student Shop Instructors at the University of Waterloo), and Richard Forgett (Machine shop at the University of Waterloo) who have served as invaluable resources throughout this research.

Finally, I would like to thank my colleagues and peers - Chanuphon Trakarnchaiyo, Heba Farag, Zhenchuan Xu, Saksham Malik, Pooriya Kazemzadeh Heris, Azeem Singh Kahlon, and Curtis Stewart. It was a pleasure to be surrounded by such a dedicated and intelligent group of people.

Dedication

I would like to dedicate this thesis to my family and friends. Your love and support made it possible for me to achieve my dreams.

Table of Contents

List of Figures

List of Tables

List of Abbreviations

AM: Additive Manufacturing
LDED-PF: Laser Directed Energy Deposition via Powder Feeding
RMS: Root Mean Square
AC: Alternating Current
FEM/FEA: Finite Element Method / Finite Element Analysis
NDT: Non-Destructive Testing
FF: Fill Factor
SF: Stacking Factor
EM: ElectroMagnetic
RLC: Resistor Inductor Capacitor
MMF: Magneto Motive Force
AWG: American Wire Guage
SP: Set Point
PID: Proportional Integral Derivative

Chapter 1

Introduction

1.1 Problem Identification

[1] is a patent developed by Beoing Inc. It deals with the development of a levitation system for Additive Manufacturing (AM) applications. The part levitation is tackled through the application of principles of acoustic and magnetic levitation. A feature can be built by adding material on a levitated 'nugget' that can be moved and rotated in free space.

For the scope of this research, the emphasis is placed on the magnetic levitation technique. A variety of magnets are placed beneath the part being built to generate the lift force to overcome the gravitational force of the part. The materials employed here may comprise ferromagnetic, paramagnetic, or diamagnetic materials. An array of electromagnets and permanent magnets are used in conjunction to generate a magnetic field (now called the primary magnetic field). The primary magnetic field results in the induction of electrical currents within the part. These induced electrical currents produce a secondary magnetic field which repels the primary magnetic field, causing the part to be levitated.

The reference provides a high-level view of the conceptualization of several embodiments of the levitation system, including the implementation of electro-magnets, permanent magnets, and super-cooled conductors. However, to the knowledge of the author, there has been no prior attempt to effectively develop a working prototype of a magnetic levitation system for AM applications.

There are critical advantages to eliminating the need for the build platform using magnetic levitation. First, the levitated part can be manipulated in all axes to allow for the development of highly complex features. Next, through magnetic levitation techniques,

multiple material nozzles can be incorporated to accelerate the build process. Through the incorporation of multiple material nozzles, multiple different materials can be used to build the part, resulting in a truly heterogenous feature formation. Finally, the magnetic levitation technique would also allow the fabrication of features without the need for part support development.

The reference plays a significant role in highlighting the advantages offered by the non-contact forces of magnetic levitation techniques. The applications of the magnetic levitation system can be extended even further. For instance, the principle of repulsive levitation techniques relies on the induction of currents within the levitated geometry. The ohmic losses associated with the induced currents in the levitated geometry can contribute to the heating of powders placed on the levitated geometry.

1.2 Challenges of Implementation and Solutions

The critical challenges of implementation of the magnetic levitation system within the AM environment are discussed in this section.

- Dimensional Constraints on the System
  - A key challenge of the development of a magnetic levitation system for AM machines was the dimensional constraints presented by the available build surface of AM machines. AM machine build surfaces can be as small as 100 mm in diameter and 95 mm in height, as specified within the EOS M 100 machine [2] and 35x35x35 cubic cm in DMDIC106 [3].
  - For manipulation within the axial, lateral, and rotational axes, the incorporation of several different permanent magnetic and electromagnets are recommended. However, the incorporation of dimensional constraints deters the incorporation of multiple electromagnets. Thus, given the dimensional constraints, the emphasis is placed on the controllability of levitation within the z-axis.
- Levitation of Paramagnetic Materials
  - Conventional magnetic levitation techniques rely on the levitation of ferromagnetic materials. Ferromagnetic materials are highly magnetized in an externally applied magnetic field and have a high magnetic permeability. However, AM

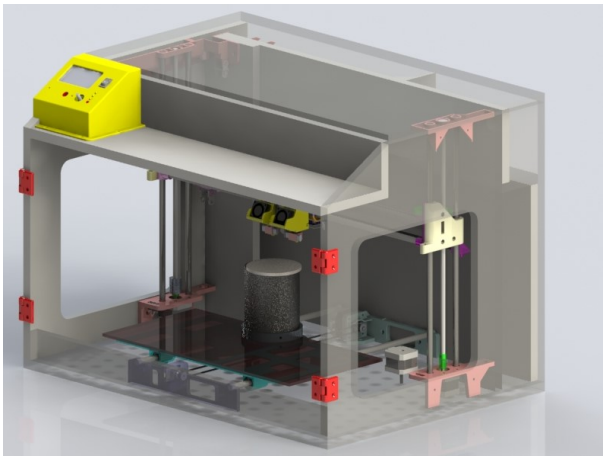

(a) Anticipated Implementation of a Prototype in LDED-PF Machine

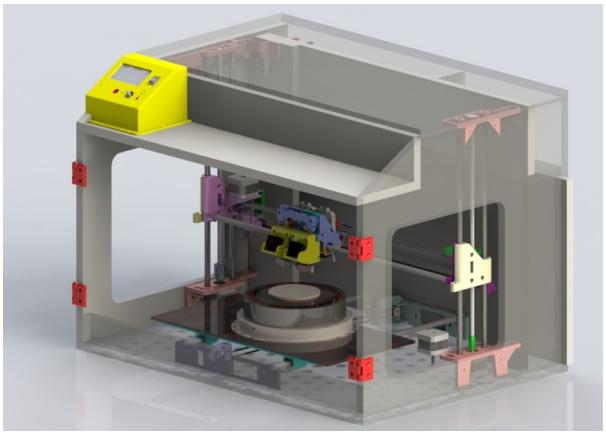

(b) Anticipated Implementation of another Prototype in LDED-PF Machine

Figure 1.1: Anticipated Implementation of the Levitation Systems within an AM Machine

operations use several paramagnetic materials. Paramagnetic materials are materials that are weakly attracted by an externally applied magnetic field and have a constant relative magnetic permeability of slightly more than 1.

– The levitation of paramagnetic materials is accompanied by trade-offs, with the most critical being the controllability of forces within the lateral axes. Thus, the scope of this research was constrained to the levitation and controllability of forces within the z-axis.

1.3 Motivations and Goals of this Research

Magnetism and magnetic levitation, as well as AM technologies, have received significant interest within the research environment. While there has been some growth in the overlapping research between the two fields, the integration of a magnetic levitation system within AM environment has yet to be developed. The research presented in this report aims to bridge that gap.

The non-contact nature of magnetic levitation and suspension techniques makes it a prime candidate for integration within the AM environment. **The goal of this research is the development of a repulsive levitation system capable of suspending a paramagnetic material (like aluminum) to provide the build surface necessary**

for AM operations, specifically Laser Directed Energy Deposition via Powder Feeding (LDED-PF). The anticipated implementation of the system has been highlighted in Fig. 1.1.

There are several key motivations for this approach. First, the levitated build surface (also known as the substrate) is anticipated to be a part of the final part built. Thus, there is a significant reduction in the amount of post-manufacturing operations to which the built part will be subjected. These post-manufacturing operations include (but are not restricted to) the removal of supporting structures and the separation of the part from the built surface. These processes can be time-consuming and subject the part to avoidable damage.

Second, since the levitation part is suspended through non-contact forces of magnetic fields, the build surface available for deposition activities can also be increased by flipping the levitation substrate. This facilitates deposition on both sides of the levitated build surface. This can allow for complex geometries to be built on either side of the build surface. This can also significantly improve LDED-PF repair and reconditioning capabilities, since the levitated build surface can be the part being subjected to repair operations, depending on the geometry of the part being repaired.

Finally, levitation techniques have been emphasized quite heavily for ferromagnetic materials, as highlighted in Section 3.1.2. However, there are several paramagnetic conductors that have applications within the additive manufacturing environment. Applications of materials like aluminum, copper, titanium, et cetera have been explored quite limitedly within the magnetic levitation sphere. Thus, there has been a need to emphasize the suspension of paramagnetic materials using magnetic levitation techniques.

Through the incorporation of these advantages presented by the magnetic levitation technique, the applications of AM operations within the field of repair and reconditioning, and coating can be extended further. Conventionally, there is a need for creative clamping to allow for deposition activities to occur on both sides of the substrate. Through magnetic levitation, the non-contact forces allow for levitation of the substrate to allow for deposition activities on both sides without negatively affecting the health of the deposited layer on the previous side.

1.4 Contributions of this Research

Having established the goal of developing a repulsive magnetic levitation system for LDED-PF applications, the critical contributions of the research presented in this report are as

follows:

- **Development of a magnetic levitation system with positional stability in the axial (z-axis) and lateral (x-, y-axes) axes with compatibility with AM operations**. This entails the continuous stable suspension of a levitated geometry (which is a disc) that can maintain stability despite AM operational factors like powder deposition and incorporation of a high-power laser while protecting the critical electrical components of the levitation system.
- **Development of a magnetic levitation system with the ability to support time-varying loads during AM operations without losing its suspension stability**. This requires the system to support an increase in payload due to deposition activities encountered within the AM environment while maintaining stable suspension.
- **Development of a feedback controller to facilitate stable suspension of the levitated geometry.** This includes the ability to change the levitation height (i.e. the relative position of the levitated geometry with the levitation system in the z-axis) of the levitated geometry by changing the input (i.e. RMS current) to the levitation system.
- **Development of a novel parameter set to determine the compatibility of different materials with magnetic levitation applications.** Metal AM applications usually employ the use of paramagnetic materials with varying material properties. Thus, it becomes critical to determine the compatibility of the material with magnetic levitation application without relying on experiments, since it can be time-consuming and inefficient. Thus, through analytical modeling, a novel parameter is developed to determine the 'levitation ability' of different materials while bypassing its reliance on experimental implementation to determine their compatibility.

1.5 Research Objectives

As described in Sections 1.3 and Section 1.4, the primary goal of this research is the development of a levitation system utilizing the principles of repulsive levitation. To accomplish the research goal and achieve the contributions of this research, the following objectives were designed and met through this research.

- Development and optimization of several novel magnetic levitation system prototypes conducive to the LDED-PF machine within both simulation and experimental environments.
- Determination of the compatibility of the levitation system with LDED-PF operations through simulation analyses. This entails determining the system's ability to support time-varying payloads and sustain the impact of powder deposition.
- Determination of the compatibility of the levitation system within an LDED-PF machine through experimental implementation.
- Development of a feedback controller to facilitate stable suspension and variable levitation height controllability
- Development of a 'levitation ability' parameter to theoretically determine the compatibility of different paramagnetic materials with the magnetic levitation technique.

1.6 Thesis Outline

This thesis includes 10 chapters. The overall workflow of the research highlighted in this thesis has been highlighted in Fig. 1.2.

Chapter 1 presents a brief overview of magnetism and magnetic levitation techniques. This chapter also presents an introduction to AM and its associated techniques. The goals, motivations, and research objectives have also been emphasized in this chapter.

Chapter 2 emphasizes the pertinent literature review that drives integral decision-making throughout the research.

Chapter 3 highlights the pertinent theory associated with the implementation of a magnetic levitation system for AM applications. This includes the governing equations driving the working principle. Secondary considerations like the EM coils presented as an RLC circuit and analytical modeling of the levitation system as an RLC circuit have also been presented.

Chapter 4 depicts the establishment of the initial feasibility of a magnetic levitation system for AM applications. The simulation model was subjected to extremely strict constraints. The outer diameter of the system is restricted to 70 mm. The system successfully outlines the feasibility of a levitation system for AM applications.

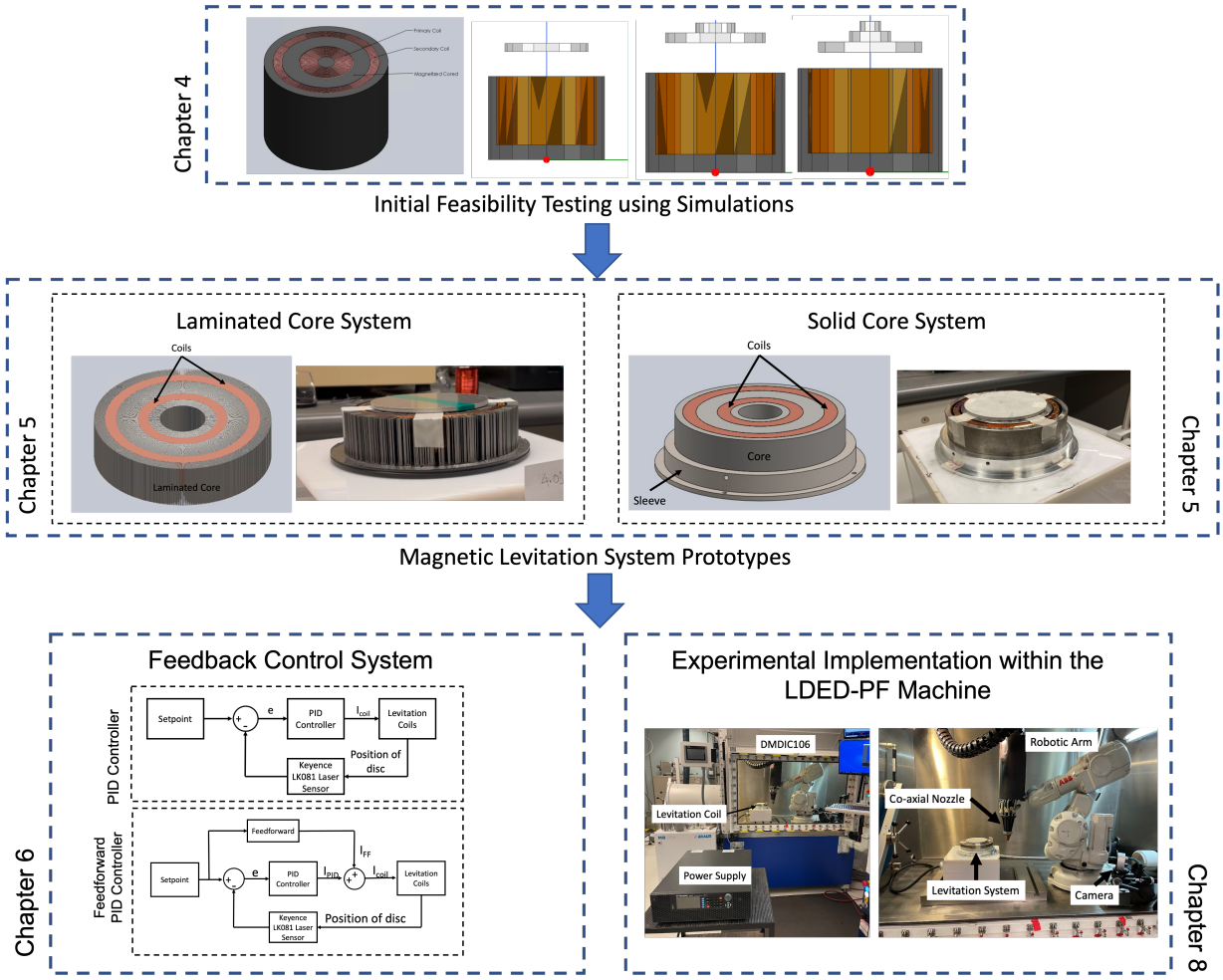

Figure 1.2: Graphical Abstract Highlighting the Progression of the Research

Chapter 5 emphasizes the development of a system prototype subjected to experimental implementation. With highly relaxed constraints ($< 40\%$ volume of the available volume of AM machine), this system achieves improved levitation while significantly improving the efficiency of the system. The compatibility of this system with AM operations is tested through simulations.

Chapter 6 highlights the development of a simple feedback controller to facilitate stable suspension of the levitated disc. The controller development is first conducted within a simulation environment, following which the implementation is conducted experimentally. A simple PID controller and a PID controller with a compensator component have been developed.

Chapter 7 stresses the development of a novel parameter to determine the compatibility of different paramagnetic materials without relying on experiments.

Chapter 8 emphasizes the experimental implementation of the levitation system prototypes developed in Chapter 6. Several different analyses are conducted to test the performance of this levitation system. This chapter establishes the successful experimental performance of the levitation system with AM operations

Chapter 9 highlights the conclusions and recommended future work obtained through the investigations conducted in this research.

Chapter 2

Literature Review

2.1 Suspension of Different Geometries using Magnetic Levitation

[4] revolves around the levitation of a homogenous sphere. A homogenous sphere, under the influence of a magnetic field, produces electrical currents (eddy currents) whose magnetic field is the equivalent of a magnetic dipole. The sphere is broken down into smaller current-carrying loops (secondary loops). The force between the primary current-carrying loops (electromagnet) and secondary loops is computed through the determination of the mutual inductance between the co-axial current loops. Through the principle of superposition, the overall force experienced by the sphere is computed. The system studied here consists of a primary conical coil at the bottom and a planar coil at the top. The top coil is responsible for producing restoring forces, in the event of part displacement. This ensures stable levitation at the equilibrium point. The system studied and the analytical model developed was subjected to experimental verification. The results generated from the experiments were similar to the analytical model developed, thus depicting the viability of the model.

[5] looks at the suspension of an aluminum disc using the principles of magnetic levitation. Due to the high complexity of the analytical models developed, the article uses simulation software (FEMM software) to generate the vertical force generated in the disc. The primary objective of the work conducted was to optimize the dimensions of the disc in consideration. An iterative methodology was implemented where simulations were conducted repeatedly until the peak force in the z-axis was obtained. The core is made of

electric steel. The iterative simulations are run by varying one of three parameters while keeping the other two parameters constant. The optimized system and simulation results were verified experimentally.

[6] presents the electrodynamic suspension of an aluminum disc. The system is simulated in COMSOL and the results are verified through experiments. No core is employed in this system. The input current supplied is 20 A at 50 Hz. N1 = 960, N2 = 576. The system results in the levitation of the aluminum disc at 11.8 mm above the levitation system.

2.2 Magnetism in LDED-PF

[7] highlights the use of a solenoid coaxially aligned with the laser beam in an LDED-PF operation to improve the overall convergence of the power stream (composed of ferromagnetic powders). The improved convergence of the powder stream results in a higher catchment efficiency (which is the ratio of the laser beam area to the powder stream area [8]) and improves the overall material efficiency by 25%.

[9] discussed the use of permanent magnet arrays to improve the convergence of the powder stream composed of non-magnetic conductive materials. The research concludes that particles with a particle radius of 300 μm can be concentrated to a 15-degree angle at 600 kHz, therefore highlighting the potential of magnetic focusing to narrow the powder stream.

[10] has also utilized the principles of magnetism within the AM environment. The article highlights the development of non-destructive testing (NDT) sensor to detect defects at different depths within parts manufactured through AM techniques. The system utilizes the principle of eddy current-based probes designed to detect artificial depths in parts composed of stainless steel and titanium alloys.

2.3 Optimization Techniques in Magnetic Levitation Systems

[11] studied the optimization for a 2D magnetic levitation transporter system comprising high-temperature superconducting bulk. The lift and restoring forces are studied closely for optimization. Six samples of permanent magnets are considered. Several parameters like the number of permanent magnets, the distance between permanent magnets, and the air

gap between the HTS Bulk and the levitated object are taken into account in the selection of the six samples. The measurement of these forces is conducted through experiments. A load cell is used for the measurement of these forces. Through this trial-and-error-based method, the optimum permanent magnet array structure was optimized.

[12] studies the use of diamagnetic levitation principles for stable suspension. The array of permanent magnets is optimized here to maximize the levitation force. Eight configurations of the permanent magnets are studied here. The thrust force is measured experimentally. Through trial and error, the optimal arrangement of the magnetic system was developed to maximize the thrust force.

[5] studies the optimization of an aluminum disc levitated over a pre-defined levitator setup. This article was also used to develop the initial EDS system. The article uses FEA for optimization. The trial and error direct substitution was used to optimize the levitated disc. The objective was to maximize the levitation force.

[13] uses the Fabry factor (G) to parameterize coil dimensions. Using heat dissipation as the cost function, the ideal and optimum dimensions of the coils are obtained to the maximum force generated by the EM coils.

[14] highlights the incorporation of several techniques like the feasible direction interior point algorithm, genetic algorithm, and extensive search, amongst others to optimize a superconducting linear magnetic bearing. The use of FEM software ANSYS is at the center of this analysis. The genetic algorithm optimization method produced the best output, with extensive search optimization also producing high-quality results.

2.4 Core Material Selection

2.4.1 Core - Laminated vs Solid

According to [15], cores exposed to time-varying magnetic fields are vulnerable to induced eddy currents. The laminated cores are used to ensure that these induced currents are minimized to maximize efficiency. That serves as the primary reason for using laminated cores.

[16] emphasizes the focus on increasing the efficiency of electric motors. The improvement of performance is contingent on minimizing two major losses encountered in cores: Magnetic losses and power losses. Laminated cores are used to minimize the intensity of currents induced within the core. The focus is placed on producing laminations with thinner and thinner layers in the lamination to maximize performance.

[17] focuses on the study of transformer core constructions. A transformer core is used to provide the path for the magnetic field to maximize the induction of current in the secondary coil. Two primary losses are studied here: Hysteresis losses and eddy current losses. Ideally, bringing the two coils in close proximity can increase the currents inducted by maximizing the magnetic coupling. However, this would also result in a significant increase in the currents induced within the core. Laminated cores are used to minimize these induced currents. These cores have high permeability and high resistivity to maximize the efficiency of the system. These cores have a permeability of 1500. By using a core with lamination, the magnetic efficiency of the system was optimized.

[18] studies the flux distribution and impedance of solid and laminated cores. It accounts for the effects of permeability, conductivity, and permittivity on the magnetic flux distribution and impedance as a function of frequency. The article uses ferrite cores since ferrite cores are commonly used in high-frequency applications. With frequency varying from several hundred kHz to 10 MHz, several parameters like permeability and conductivity vary as a function of frequency. For the impedance study, the article documents the impedance at different frequencies using FEM and experimental methods. The sample used here is a ring core with an outer diameter of 25 mm, an inner diameter of 15 mm, and a height of 10 mm. Wayne Kerr 6550B was used to experimentally measure the impedance of the system. The permeability of the solid core is similar to the laminated core at lower frequencies. However, at higher frequencies, the laminated core produces higher permeability. This results in a higher impedance value in laminated cores. Thus, this study concludes that solid cores produce lower impedance when compared to laminated cores.

[19] studies the use of laminated silicon steel cores for an inductor. Subsequently, the article studies the behavior of laminated cores and their impedance at different frequencies. The authors also consider the skin depth effect and the proximity effect during the analysis. The Sweep Frequency Response Analysis (SFRA) is the technique used to study the windings and the laminated core. It was documented that the winding resistance of the inductor increases with an increase in frequency due to the decrease in the degree of penetration of the conductor by magnetic flux. The impedance of the system increases with an increase in frequency until the resonant frequency. Beyond this frequency, the impedance decreases. This is because, below the resonant frequency, the reactance of the winding is inductive dominant. Beyond the resonant frequency, the reactance is capacitive dominant.

2.4.2 Materials - Pure Iron vs Ferrite

[20] studies the comparison of ferrite cores with other materials. The key primary difference between ferrite (compared to other magnetic materials) is that ferrites are oxide materials. Ferromagnetism of ferrite is derived from the unpaired electron spins in only a few metal atoms, these being iron, cobalt, nickel, manganese, and some rare earth elements. The oxides suffer from a dilution effect of the large oxygen ions in the crystal lattice. Thus, ferrite has significantly lower magnetic saturation. The oxygen ions play the role of insulating the metal ions, thus, increasing the resistivity of the material. This material is great to minimize the induction of eddy currents due to its low resistivity. Ferrite is great for high flux applications like generators, motors, and power transformers for frequency < 1 kHz. The primary disadvantage of ferrite cores is the limited size of parts.

[21] states that the ferrite core is a ferromagnetic metal oxide with high resistivity and high permeability. However, due to its low saturation magnetization nature, it is limited in its applications in low-frequency applications. Ferrite is specifically great for inductive applications (like transformers).

[22] talks about the use of different core materials in inverters. Inverters are primarily used for converting stored DC energy to high-voltage AC energy. There are two types of inverters:

- Pure iron core inverters: These are used for low-frequency conversion applications. They convert low-frequency AC voltage to high-frequency AC voltage.
- Ferrite core inverters: These are suitable for high-frequency applications. These convert low-voltage DC voltage to high-frequency AC voltage. The range of frequencies suitable for ferrite core inverters is from a few kHz to MHz.

2.5 Implementation of Feedback Control Strategies for Magnetic Levitation System

[23] highlights the levitation of a ferromagnetic ball through a single electromagnetic coil. The magnetic field output of the coil is controlled using voltage adjustments. An opto-electronic sensor is used to provide positional feedback to the controller. Two distinct strategies are used to control the suspension of the spherical ball: First, a non-linear control model was used in conjunction with a feedback linearization method. Second, the

non-linear model was linearized around the equilibrium point. The two approaches were simulated and verified experimentally.

[24] also studies the stable suspension of a ferromagnetic ball using a single coil system. A light sensor is used to provide positional feedback to the controller. A simple PID controller is used. To minimize the sensitivity of the controller to feedback noise, a derivative filter was also added to the PID controller. Through the incorporation of the differential filter, an improvement in rising time, overshoot, settling time, and the steady-state response are observed.

[25] also studied the suspension of a ferromagnetic ball using a single coil. To address the inherent instability of the levitation system, a simple PD controller is used. A photodiode provides positional feedback to the control system. Pulse width modulation was used to improve the overall efficiency of the system.

2.5.1 Selection of Sensor for Feedback to Controller

[26] studies the development of a magnetically guided robot. It is crucial to note that magnetic-based actuation systems are inherently unstable. Thus, to ensure the stability of the system, a closed-loop controller needed to be developed. These closed-loop controllers are heavily dependent on sensor feedback to ensure stable levitation. Optical sensors like laser sensors, cameras, or x-ray and ultrasound sensors are ideal for transparent environments. However, these sensors have major shortcomings in non-transparent environments. In addition, these sensors tend to be quite expensive. Thus, an alternate sensor using the magnetic field of the levitation system was studied to determine the viability of the sensor for the system.

Hall effect sensors are used for the detection of the magnetic flux of the system in [26]. The system utilized a combination of linear Hall effect sensors, 2 on the x-axis and 2 on the y-axis to determine the position of the levitated robot in the lateral axes. A 4th order polynomial curve was used to develop a relationship between the magnetic flux of the robot and the position of the robot. Through experimentation, it was validated that the resulting accuracy of the position was within 0.4 mm RMS error. Thus, the resulting sensor system was adequate for stable levitation.

[27] studies the use of a magnetic levitation system responsible for levitating a neodymium magnet suspended in a voltage-controlled magnetic field. Electromagnets are used to generate the magnetic field necessary to facilitate levitation. Adhering to Earnshaw's law, a closed-loop controller relying on sensor feedback was used to ensure the stability of the system. The feedback for the controller is obtained through the use of hall effect sensors.

Through simulation and experimentation, it was verified that the sensor feedback obtained from the Hall effect sensor is satisfactory for the stable levitation of the magnet.

[28] studies the design and implementation of a magnetic levitation system with a feedback controller. Here, a steel object is suspended using an electromagnet. The system schematic uses a light-emitting diode to get the feedback to alter the current input to the electromagnet.

[29] studies the use of sensors to monitor in-process parameters for DED AM. First, the laser position was monitored using photo-diodes. The feedstock delivery was monitored using filtered cameras. The article also describes the use of weight sensors under the substrate to determine the amount of feedstock deposited. The melt pool geometry was monitored using co-axial imaging systems. And finally, the deposition height of each layer was monitored using optical sensors and charged coupled imaging sensors. Thus, these sensors could provide new means to track the position of the levitated object as well.

[30] studies the pre-processing and in-process monitoring of AM parameters like temperature, melt pool geometry, laser strength, and plume formation. It also studies these parameters for powder bed fusion and direct energy deposition. Some of the sensors studied here are:

- Melt pool: Coaxial in-line filtered imaging through optics. Also utilizes image illuminating strategies for the implementation
- Plume monitoring: Plume is the conical geometry of deposition. It is monitored through sensors like spectrometers, photodiodes, and filtered cameras.

[31] studies the use of thermal imaging using an infrared setup to study an online in-process detection of anomalies in part geometry. The article studies the melt pool to extract features that may point to a part anomaly.

Chapter 3

Theoretical Concepts Associated with the Magnetic Levitation System

3.1 Introduction to Magnetism and Magnetic Levitation

Magnetism is associated with electric charges. Magnetic fields are defined as a space where the magnetic force of magnetism acts, usually around a magnetic substance or a moving electric charge. The magnetic field is operationally defined as three measured quantities: (1) the velocity of a charged particle, (2) the electric charge, and (3) the magnetic force experienced by the particle. [32]. One of the more popular applications of magnetism and magnetic fields is the use of magnetic levitation systems.

Magnetic levitation/suspension is defined as the method to suspend an object using the interactions of magnetic fields alone. Magnetic levitation has found applications in a wide variety of fields ranging from small-scale objects requiring vibrational isolation [33] from its environment, suspension and propulsion of maglev vehicles [34], damping capability [35], levitation and manipulation of a magnetized object [36], energy harvesting [37], sensing applications [38], manipulation of magnetorheological fluid (MRF) [39] amongst several others

Magnetic levitation has been classified based on several different criteria. The two most critical classifications are based on the mechanism of levitation and the materials for levitation.

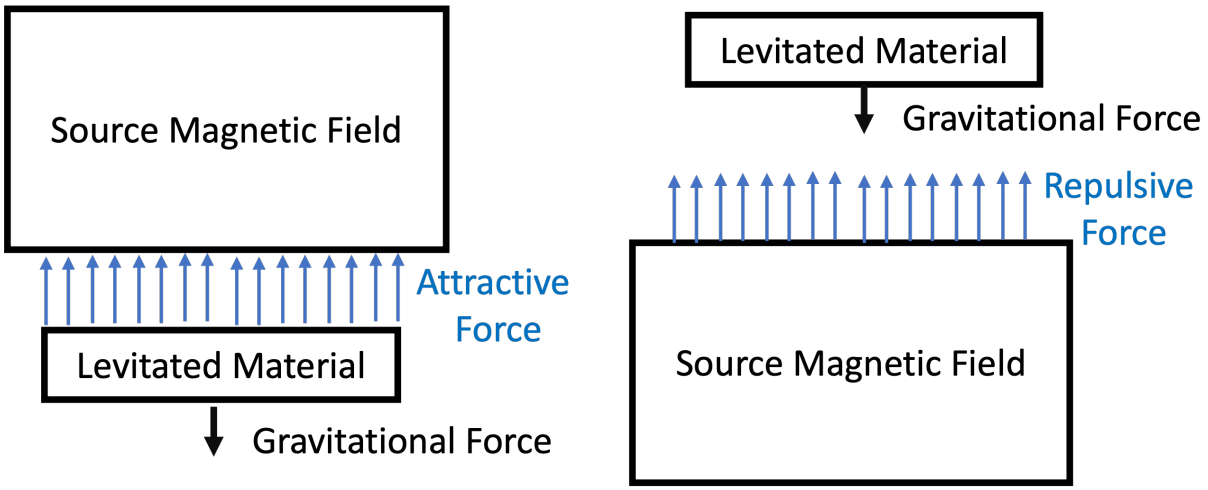

(a) Magnetic suspension and levitation using attractive levitation technique

(b) Magnetic suspension and levitation using repulsive levitation technique

Figure 3.1: Magnetic Levitation Techniques

3.1.1 Types of Magnetic Levitation Techniques and Applications

There are two critical and popular magnetic levitation techniques. The first utilizes attractive force between a magnetic field source and ferromagnetic materials, as highlighted in Fig. 3.1a. This technique is referred to as electromagnetic suspension. The second technique utilizes repelling forces generated by a magnetic field source producing a time-varying magnetic field (e.g. through relative motion or around a magnetic material) relative to electrical conduction, as highlighted in Fig. 3.1b. This technique is referred to as electrodynamic suspension [40].

Electromagnetic suspension techniques have been utilized in several applications like magnetic bearings [41]-[42], ground transportation such as magnetic levitation trains [43], precision-based non-contact manipulation of ferromagnetic materials [44] amongst several others.

Electrodynamic suspension systems have also found applications in a wide variety of fields. For instance, electrodynamic suspension systems are utilized in high-speed magnetic levitation train applications [45]-[46], precision position controllability [47], levitation applications within wind tunnels [48], vibration isolation [49], induction melting applications [50] amongst several others.

3.1.2 Types of Materials for Magnetic Levitation and Applications

The material properties of the material subjected to levitation applications are also critical. The materials are broadly classified into 4 fields: Diamagnetic materials, paramagnetic materials, ferromagnetic materials, and superconducting materials.

Diamagnetic materials are those which are freely magnetized in the presence of a magnetic field. The applied magnetic field induces a magnetic field within the material in the opposite direction resulting in the generation of a repulsive force. This includes materials like water, proteins, diamonds, etc. [51]. Diamagnetic levitation has found applications in fluid dynamics [52], development of high-precision gyroscope [53], development of force sensors [54], magnetic bearings [55] amongst several others.

Paramagnetic materials are conducting materials that are weakly attracted to magnets. The source magnetic field induces a magnetic field in the material which results in the generation of an attractive force. This includes materials like aluminum, silver, gold, etc. Levitation of paramagnets has found applications in spheres like magnetic levitation transportation using aluminum [56], and measurement of the density of liquids [57], amongst others. However, there is significant scope for further exploration within this field.

Ferromagnetism is a type of magnetism associated with the elements iron, cobalt, nickel, and some alloys or compounds containing one or more of these elements. The study of ferromagnetic materials has been the most popular among the various magnetic levitation applications. Owing to their relative magnetic permeability being greater than 1, the magnetic fields induced in these materials are in the same direction as the source magnetic field. This results in the generation of an attractive force between the material and the magnetic field. Due to the special properties of ferromagnetic materials, they have found applications in fields like magnetic bearings [58], position manipulation [59], and magnetic navigation [60] amongst several others.

Finally, superconducting materials have also found significant interest within academic environments for research-related activities. Superconducting magnets are made from superconducting wires cooled to cryogenic temperatures during operations. Through this, these materials have negligible resistance. Thus, significantly higher amounts of currents can be sustained in this material with no losses due to heat dissipation. Superconducting materials have found applications in the study of MagLev train technology [61], magnetic bearings [62], positional manipulation [63], amongst others.

3.2 Introduction to Additive Manufacturing

AM has also been a primary point of emphasis for research within the academic environment. AM deviates from conventional subtractive manufacturing techniques by building structures using a 'layer-by-layer' approach. This approach offers significant flexibility and versatility in terms of the complexity of shapes, customizability, and application of parts built. The use of a wide variety of materials like metals, ceramics, and polymers also makes the technique highly appealing for several applications [64].

The prevalence of AM in fields like tooling, repair, and reconditioning [65], the aerospace industry [66], medical implants [67] with a special focus on the development of metallic implants [68], dental devices [69] and micro-fabrication of microrobots [70] amongst several others has significantly strengthened the importance of the field. There are several different techniques that fall under the umbrella of AM techniques.

3.2.1 Types of AM Techniques

Vat Photopolymerisation

Photopolymerisation utilizes liquids, resins, or photopolymers that react to the radiation of UV lights to solidify using chemical reactions. Vat polymerization is an AM technique that uses this technique to 3D print complex geometries by curing these materials in a layer-by-layer fashion [71]. This technique offers some advantages like good accuracy, good surface finish, and build-in volumes. However, this technique also requires support structures, post-processing, and post-curing, and is a relatively expensive process. Vat Photopolymerization has found applications in fields like bioprinting [72], tooling applications [73], amongst others.

Material Jetting

In this AM process, droplets of build material are selectively injected onto a substrate and cured by UV light in successive layers [74]. This technique facilitates the fabrication of flexible parts from rigid opaque to rigid transparent while offering high resolution and high accuracy. However, this technique is relatively expensive, requires support material, and is vulnerable to shrinkage and creep. This technique has found applications in fields like biomedical applications [75], ultrasound applications [76], amongst others.

Binder Jetting

While most other AM techniques require the use of a heat source to facilitate fabrication, binder jetting relies on the use of glue to bind particles layer-by-layer to fabricate a part. Thus, binder jetting bypasses the need for a heat source [77]. Binder jetting AM offers high speed of fabrication, versatility, simplicity, and minimal wastage of materials. However, the functionality of parts produced is relatively limited, usable materials for this technique are also restricted, and the overall surface finish is also not ideal. This technique has found applications in fields like electrochemical energy storage [78], and biomedical applications [79] amongst others.

Material Extrusion

This technique is based on the thermoplastic extrusion technique. It simply relies on a syringe-based injection of material on a layer-by-layer basis. The material state (i.e., molten or solid) is controlled using temperature [71]. This technique facilitates the fabrication of functional polymeric parts and makes material change easy for subsequent operations. However, this technique also has restricted accuracy, unpredictable shrinkage, and relatively poor surface quality. The process is also slow and requires the use of support structures. The technique is useful to develop models for conceptualization and has also found applications within the biomedical industry [80].

3.2.2 Metal Additive Manufacturing

Metal AM processes are reliant on the delivery of feedstock materials like sheets, powder, or wire on a substrate/object, melting the feedstock materials using a reliable energy source like lasers, electron beam/arc amongst others, and the subsequent solidification of the material in a layer-by-layer approach [81]. The ability to make complex parts using metals makes it a prime candidate for further research.

Laser Powder Bed Fusion Additive Manufacturing

Laser powder bed fusion AM (LPB-AM) is a metal AM technique that utilizes a pointed source like lasers or electron-beam to fuse powders being spread by a roller from storage to build a part [82]. This technique has several advantages including the use of several

different types of metals for the application and development of complex parts with relative ease. However, the technique also requires post-processing operations, the use of support structures, and high residual stress and porosity of the part. LPB-AM has found applications in fields like aerospace [83], biomedicine [84], and tooling applications [85].

Laser Directed Energy Deposition via Powder Feeding (LDED-PF)

Also known as Laser Powder Fed Additive Manufacturing (LPF-AM), this AM technique relies on the dispersion of powders through a nozzle onto a build surface. A high-power pointed heat source like a laser, electron beam, or plasma arc is then used to melt the powder. The melted powder solidifies in the desired shape of the part being built [86]. The key advantages of this technique are the ability to use several different metal powders, the fabrication of objects with embedded sensors [87], and the improved quality of parts produced. This technique has found applications in fields like aerospace [83], biomedical [88], repair and reconditioning [89], and coating [90] amongst many others.

3.3 Focus of this Research

From a magnetics perspective, critical emphasis is placed on the use of repulsive levitation techniques to facilitate the suspension of paramagnetic materials like aluminum, copper, titanium, etc. The key reasoning behind the decision was dictated by the applications of various materials within the AM environment. As explained in Chapter 7, paramagnetic materials like aluminum, titanium, copper, et cetera have significant applications within the AM environment. While ferromagnetic metals like iron also have applications within AM environment [91, 92], the other materials discussed have significantly more applications and a better track record.

From an AM perspective, the LDED-PF technique has been emphasized in this research. The LDED-PF technique generates tool paths for deposition using sliced cross-sectional dimensions obtained from CAD models. The material nozzle head carries the material (usually powder form) along with an inert gas (e.g. argon) to deliver the feedstock material onto the build surface. Through the use of a power source (e.g. laser), the material deposited is melted and solidified to build parts using the layer-by-layer approach, as described in [93]. This makes the technique most compatible with a magnetic levitation system to replace the build surface.

According to [94], the critical process parameters associated with the implementation of the LDED-PF technique arise from two critical steps: The delivery of heat and mass

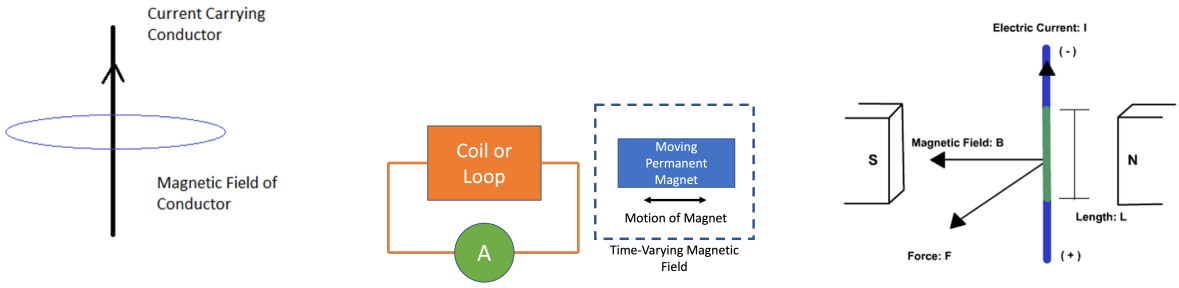

(a) Ampere's Law (b) Faraday's Law (c) Lorentz Law

Figure 3.2: Visual Representation of Governing Equations

onto the build surface and the interaction of the heat and mass at the build surface. The parameters of relevance include laser source ignition, gas-powder delivery, powder stream, laser beam interaction, and melt pool formation by heat conduction, amongst several others. These parameters aid to determine the quality of parts built with LDED-PF.

3.4 Governing Equations

3.4.1 Ampere's Law

Ampere's Law (shown in Fig. 3.2a) relates the integrated magnetic field around a closed loop to the electric current passing through the loop. This is shown empirically in Equation 3.1. In integral form, the equation is given by 3.2.

$$\nabla \times B = \mu_0 J \tag{3.1}$$

$$\oint B.dl = \mu_0 I_{enc} \tag{3.2}$$

where B is the magnetic field, μ_0 is the permeability of free space, and I_{enc} is the current enclosed within the Amperian loop.

3.4.2 Faraday's Law

Faraday's Law (shown in Fig. 3.2b) states that a time-varying magnetic field induces an electric field within a conductor placed within close proximity of the magnetic field source. This induced electric field results in the production of an induced EMF within a conductor placed within the sphere of influence of the magnetic field. Empirically, Faraday's Law is given by Equation 3.3. The differential form of the equation (through the application of Stoke's theorem) is given by 3.4.

$$\oint E.dl = -\frac{d\phi}{dt} \tag{3.3}$$

$$\nabla \times E = -\frac{\delta B}{\delta t} \tag{3.4}$$

where E is the electric field, ϕ is the magnetic flux, and l is the length of the conductor.

The induced EMF within the conductors results in the production of a current within the conductor. These induced currents are called eddy currents.

3.4.3 Lorentz' Force Law

The Lorentz force law relates the force generated by magnetic fields interacting with moving charges, shown in Equation 3.5. Fig. 3.2c shows the pictorial representation of the law.

$$F = Q[E + (v \times B)] \tag{3.5}$$

where Q is the moving charge moving with a velocity v in a magnetic field B.

Since currents in conductors are charges per unit time passing a given point, Equation 3.5 can be transformed to Equation 3.6

$$F = \int [E + (v \times B)]dq = \int [E + (v \times B)]\lambda dl$$

Here, λ is the charge density, and v is the speed of a charge in a magnetic field B. The relationship between the induced eddy currents and the charged particles is described next.

$$J = \lambda v$$

where J is the current in the conductor.

$$F = \oint [\lambda E + J \times B] \tag{3.6}$$

Thus, the relationship tracking the interactions between the magnetic fields and current-carrying conductors has been clearly established. It can also be assumed that the electric field of the system is 0. Thus, the Lorentz force equation is shown in Equation 3.7.

$$F = \oint J \times B \tag{3.7}$$

3.5 Working Principle

The various laws presented in Section 3.4.1, 3.4.2, and 3.4.3 all contribute to the development of the working principle of the system.

From Ampere's Law, it can be concluded that the time-varying current supplied to a set of coils will produce a time-varying magnetic field. These fields have both radial and axial components.

From Faraday's Law, the time-varying magnetic field produced by the coil induces an electric potential on the conductor placed in the sphere of influence of the coil. This electric potential results in the induction of currents (also known as eddy currents).

Finally, from Lorentz Law, the induced currents on the plates interact with the magnetic fields of the coil to produce a force. This resultant force is referred to as the levitation force from here on. This theory serves as the basic working principle of the levitator design.

3.5.1 Vertical Force for Stable Levitation

The induced eddy currents interact with the primary time-varying magnetic field. According to the principle of Lorentz' force, there is a force generated through the interactions of the magnetic fields of the induced eddy currents with the magnetic fields of the coil. This results in the generation of a force that results in the stable suspension of the solid. The Lorentz force is defined by Equation 3.8, presented in Section 3.4.3.

$$F = \int\int\int_V J \times B dV \tag{3.8}$$

As shown in Equation 3.8, the vertical levitation force is a function of the induced eddy currents and the magnetic field of the primary coil setup. Both of these parameters are primarily dependent on the magnitude of the applied current (peak current), the frequency of the alternating current supply, and the material properties of the levitated geometry.

3.5.2 Position Relative to the Levitation System

In order to conduct AM operations, it is necessary to gain positional control of the suspended object. In conventional methods, the substrate provides the relevant constraining forces necessary to prevent motion during the operation. Thus, it is necessary to hold the object at the desired height with stability. Since the stability in the vertical direction is primarily dependent on the vertical force imposed on the object, the position of the suspended object is also dependent on the magnitude of the applied current and the associated frequency of the alternating current supplied to the coils. By altering the input current and associated frequency of the levitation system, the position of the levitated geometry can be controlled.

3.6 Description of the Levitation System

The levitator setup consists of two cylindrical coils carrying time-varying sinusoidal current, as shown in Fig. 3.3a. The coil closer to the center (i.e. the primary coil) is used for the generation of the primary vertical force. The coil closer to the outer edge (i.e. the secondary coil) is utilized for the generation of stabilizing lateral forces. These coils are embedded within a high magnetic permeability material called the core to facilitate improved magnetic focusing of the levitation system. The two coils carry current in the opposite direction, as highlighted in Fig. 3.3b. The overall system implementation schematic has been highlighted in Fig. 3.3c.

3.6.1 Fill Factor of Coils

To determine the height of the coil, the concept of the fill factor was utilized. The fill factor is the ratio of the area of the electrical conductor (c/s area of the wire) to the area

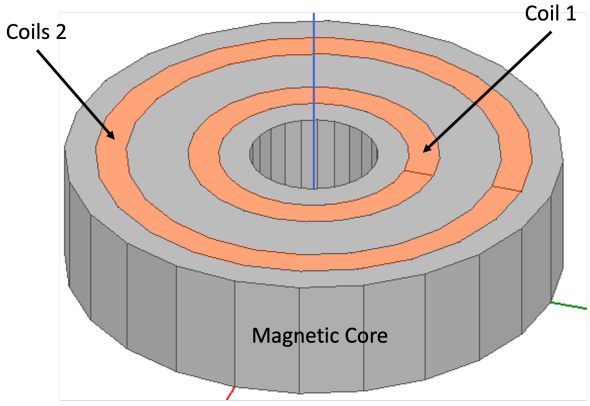

(a) Levitation System Model

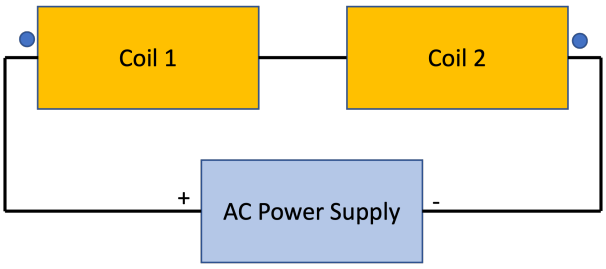

(b) Schematic of levitation system

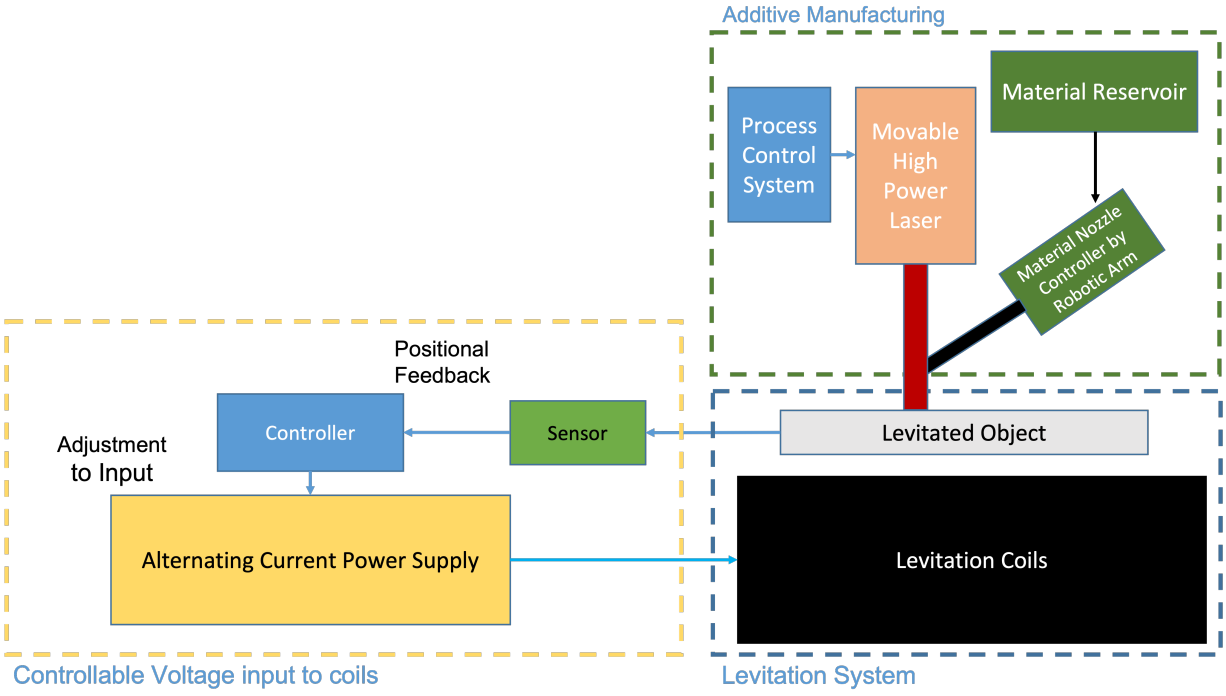

(c) Schematic for the overall envisioned system

Figure 3.3: Magnetic Levitation System

of the provided space (c/s of the coil), as shown in Equation 3.9. If all dimensions (i.e. the dimension of the conductor, number of turns, and mean radius of the coil) are known, the fill factor can be used to determine the dimension of the coil.

$$FF = \frac{\frac{\pi}{4} d^2 N}{b.h} \tag{3.9}$$

Where FF is the fill factor, d is the diameter of the wire used, N is the number of turns of the coil, b is the coil width and h is the coil height.

3.6.2 Skin Depth Effect

Eddy currents are produced within a characteristic length called the skin depth. There are very minimal eddy currents produced beyond this length since the reactionary magnetic field cancels out the effects of the primary magnetic field. Beyond this length, there are eddy currents induced within the conductor [95]. The skin depth is calculated using Equation 3.10.

$$\delta = \sqrt{\frac{1}{\pi f \mu \sigma}} \tag{3.10}$$

Where f is the frequency, μ is the relative permeability and σ is the conductivity of the material.

3.6.3 Electromagnetic (EM) Coils as RLC Circuit

As explained in [96], the impedance of the EM Coils, which is the overall resistance offered by the levitation system is a combination of its DC resistance, inductive reactance, and capacitive reactance is given by the Equation 3.11.

$$Z = \sqrt{R_{DC}^2 - (X_L - X_C)^2} \tag{3.11}$$

where X_L is the inductive reactance, X_C is the capacitive reactance, R_{DC} is the DC resistance and Z is the impedance of the levitation system. The inductive and capacitive reactance is given by Equation 3.12.

$$X_L = 2\pi fL \ , \ X_C = \frac{1}{2\pi fC} \tag{3.12}$$

where L is the inductance of the coils, C is the system's parasitic capacitance, and f is the frequency of the input.

3.6.4 Analytical Modelling of RLC Circuit

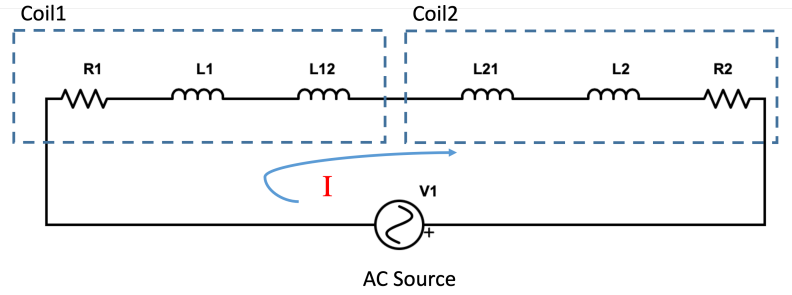

Figure 3.4: Circuit modeling of Two Concentric Coils Carrying Current in the Opposite Direction

Fig. 3.4 represents the RLC circuit modeling of the levitation system. The levitation system is made up of two coils. Each coil can be treated as an inductor with some internal resistance. The interaction of the magnetic field between the two coils also results in the induction of mutual inductance between the two coils.

Using Kirchhoff's voltage loop rule, the circuit can be represented in Equation 3.13.

$$-V1 + I.R_1 + j.\omega.L_1.I - j.\omega.L_{12}.I - j.\omega.L_{21}.I + j.\omega.L_2.I + I.R_2 = 0 \tag{3.13}$$

Here, R_1 is the internal resistance of the inner coil (coil 1), R_2 is the internal resistance of the outer coil (coil 2), L_1 is the self-inductance of coil 1, L_2 is the self-inductance of coil 2, L_{12} and L_{21} is the mutual inductance between the two coils, ω is the angular frequency $(2.\pi.Frequency)$, j is the square root of -1.

The coil characteristics can be measured and the Equation 3.13 can be solved to determine the current through the coil for given voltage input. Since ANSYS Maxwell calculates the input current from the voltage definition, using the analytical model is an excellent strategy to double-check whether the simulation inputs defined are correct.

3.6.5 Magnetomotive Force of Coils

The force of levitation is directly affected by the Magnetomotive Force (MMF) of the coils. The MMF is the product of the number of turns of the coils to the current through the coils [97]. According to [5], the average force of levitation is derived as:

$$F_{Z_{avg}} = \frac{(N_1 - N_2)^2 I_0^2 \mu_0 A_{airgap}}{4z^2} \tag{3.14}$$

where N1 and N2 are the numbers of turns of coil 1 and coil 2 respectively, I_0 is the current through the coils, μ_0 is the permeability of free space, A_{airgap} is the area of the air gap under the disc and z is the distance of the disc from the levitation coil. $N \times I$ is the magnetomotive force, which is the line integral of the magnetic intensity around a closed line. Maximizing $N \times I$ is the objective function of the development of this system while minimizing inductance 'L', as well as the resulting impedance 'Z' which is the cost function. A higher resultant levitation force is a necessity to counteract the opposing force (weight) imposed by the deposition of material on the disc substrate in an AM environment. The inductance of a multi-coil, multi-core system is a non-linear property, and theoretical calculation of the same is not an objective for this research, it will be calculated and minimized through simulations using ANSYS Maxwell.

3.7 Modelling the Impact Forces of Powder Deposition

In order to develop a magnetic levitation system suitable for AM applications, it is imperative to determine the impact forces of powder deposition on the substrate. Since the research presented in this report deals with LDED-PF, the impact forces of powder deposition are modeled. The analysis presented here makes some assumptions. These are:

- The analysis assumes a steady flow of powders and the impact of air friction is negligible. Since AM operations occur in a vacuum, this assumption is fair.
- Since the size of the particles is very small and originates at the same source, the collisions between the particles can be ignored.

The theorem of transfer of momentum is given by Equation 3.15.

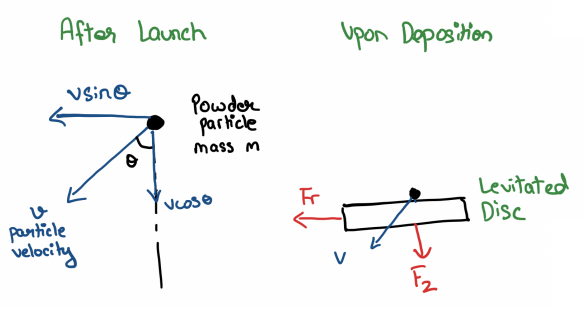

Figure 3.5: Model of Powder Particle

$$F\triangle t = m.v \tag{3.15}$$

where m is the mass of the powder particle, v is the velocity of the particle, F is the impact force and $\triangle t$ is the instantaneous time of impact, as shown in Fig. 3.5. The impact forces are decomposed to their axial (F_z) and radial (F_r) directions. This is given by Equation 3.16.

$$\begin{aligned} mvsin\theta &= F_r\triangle t \\ mvcos\theta &= (mg + F_z)\triangle t \end{aligned} \tag{3.16}$$

According to [98], the velocity of powder particles employed during LDED-PF operations is about 2 m/s. The exact velocity of powder particles will be calculated based on the dimensions of the nozzle and the volumetric feed rate of the coupled powder and gas flow and is given by Equation 3.17 obtained from [99].

$$v_p = \frac{\dot{V}}{\pi(r_0^2 - r_i^2}} \tag{3.17}$$

Where v_p is the velocity of powders, $\dot{V}$ is the volumetric feed rate of the coupled powder and gas flow, r_o is the outer radius of the nozzle outlet and r_i is the inner radius of the nozzle outlet.

Chapter 4

Feasibility of a Magnetic Levitation System with Additive Manufacturing Applications

This chapter presents the development of the very first prototype of a magnetic levitation system to implement within the additive manufacturing environment. The system was only implemented within the simulation environment to highlight the initial feasibility of a magnetic levitation system for Laser Powder Fed Additive Manufacturing Applications.

The Electrodynamic Levitation System consists of two concurrent coils carrying currents in opposite directions. The two coils are embedded within a ferrite core, which is a high magnetic permeability material that houses the coils and is meant to improve the magnetic focusing capabilities of the coils. For the analysis conducted here, the radius of the disc levitated was taken to be 25 mm. The material selected for the disc is AlSi12, a common aluminum alloy used for AM applications. The maximum outer diameter of the levitator was taken to be 70 mm due to spatial restrictions. The remaining constant parameters are highlighted in Table 4.1.

Table 4.1: Initial and Constant Parameters for Optimization

Constant Parameters	
Input to Coils	
Frequency	1000 Hz
Input Current	5 Amperes
Dimensions of Core	
Outer Diameter of Levitation System	70 mm
Levitation system height	50 mm
Coil Characteristics	
Coil1 width	20 mm
Coil 2 width	10 mm
Initial Coil Height	30 mm
N1	1000
N2	500

4.1 Optimization of Coil

4.1.1 Optimization of Radial Placement of Coils

The levitator setup was optimized with consideration for lateral and axial forces. The optimization was conducted to obtain the optimum position of the two coils within the ferrite core. The optimization parameter is the ratio of the mean radius of the primary coil (coil responsible for the development of the levitation force) and the secondary coil (coil responsible for the lateral restoration force). Two different scenarios were considered here – The levitation disc is placed at its equilibrium point (X = 0, Y=0, Z=0) and the levitation disc is given a displacement (X = 5 mm, Y=0, Z=0). The lateral and axial forces for the two scenarios are plotted. It can be seen in Fig. 4.1 that R1 = 10 and R2 = 25 produce the best combination of the vertical and lateral forces in the two situations.

4.1.2 Optimization of Height of Coils

22 AWG wires were used for the analysis ($d_w = 0.6438mm$). Copper wires possess some internal resistance. This puts an upper limit on the maximum current that a wire can support. This maximum current is, thereby, a function of the wire resistance. The wire resistance is a function of the dimensions of the wire. Thus, it is crucial to determine the

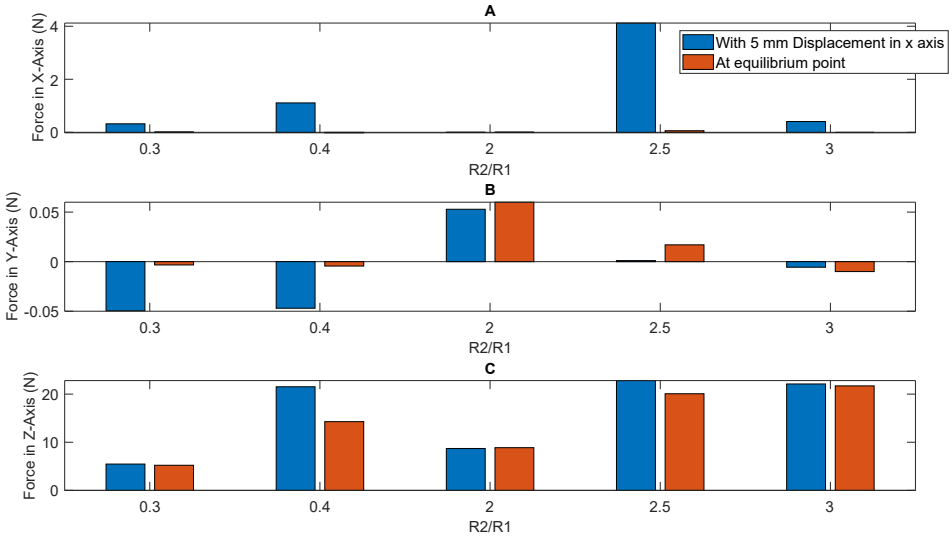

Figure 4.1: Levitation Force vs Optimization Parameter R2/R1 (a) Lateral Forces in X-Axis (b) Lateral Forces in Y-Axis (c) Axial Forces in Z-Axis

wire gauge for the coil. Since the anticipated current supplied to the system isn't expected to exceed 5 A, a 22 AWG wire can be utilized for the prototyping endeavors.

Since round wires will always have some gap, and wires also have some space required for insulation between turns and between layers, the fill factor, as described in Section 3.9, is always smaller than one. A 20% tolerance was assumed for the analysis. Thus, the fill factor was assumed to be 0.8.

All dimensions pertinent to the calculated height of the coil using the principle of fill factor are known. Thus, using Equation 3.9, the calculated height of coil 1 is given by Equation 4.1 and the calculated height of coil 2 is given by Equation 4.2.

$$h_{Coil1} = \frac{\frac{\pi}{4}.0.6438^2.1000}{10.(0.8)} = 40.69mm \tag{4.1}$$

$$h_{Coil2} = \frac{\frac{\pi}{4}.0.6438^2.500}{5.(0.8)} = 40.69mm \tag{4.2}$$

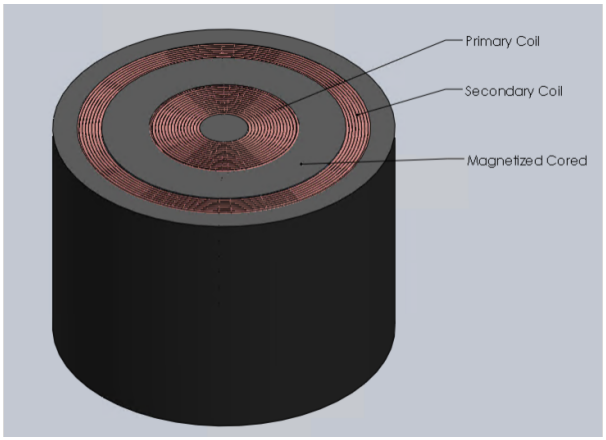

(a) CAD model of the prototype developed

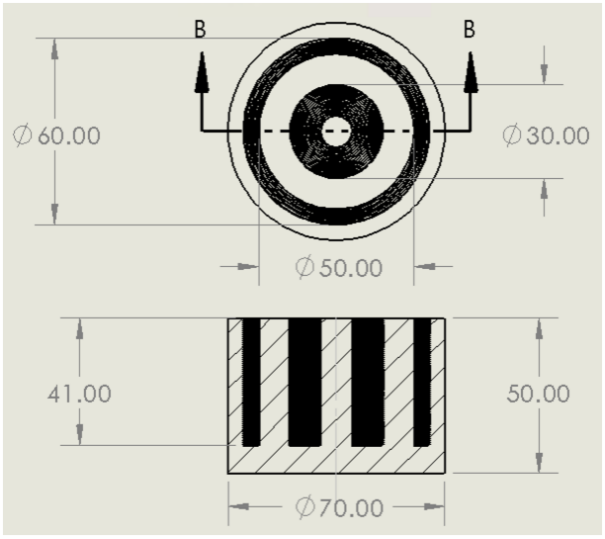

(b) Pertinent dimensions of the prototype developed

Figure 4.2: Visual Overview of the Overall Prototype

4.2 Simulations and Results

4.2.1 Test Cases for Analysis

The RMS current and the frequency of the alternating current supplied are the key parameters driving the magnitude and direction of the levitation force generated. ANSYS Maxwell has been used to determine these parameters.

For this analysis, three separate cases were considered. Some specifications for the system are shown in Table 4.2. The test cases mimic the addition of deposited layers and the associated levitation forces generated. The first test case only considers the initial disc. The second test case considers the addition of a disc on top of the initial disc. The third test case considers the addition of two discs on top of the initial disc. It should be noted that the solids suspended are composed of AlSi12.

Table 4.2: Specifications of the Three Cases Considered

Case	Base Plate	Layer 1	Layer 2
Case 1	r = 25 mm h = 5 mm Mass = 0.026 kg	-	-
Case 2	r = 25 mm h = 5 mm Mass = 0.026 kg	r = 20 mm h = 5 mm Mass = 0.0047 kg	-
Case 3	r = 25 mm h = 5 mm Mass = 0.026 kg	r = 20 mm h = 5 mm Mass = 0.0047 kg	r = 5 mm h = 5 mm Mass = 0.0011 kg

4.2.2 Calculation of Lift Current

First, the emphasis is placed on the calculation of the lift current. The lift current is defined as the minimum RMS current required to stably levitate the objects (details in Table 4.2) at specific frequencies (800 - 1000 Hz). The analysis is done to calculate the RMS current 8mm and 15 mm away from the levitator. The calculation is conducted through the use of the principle of least square fitting.

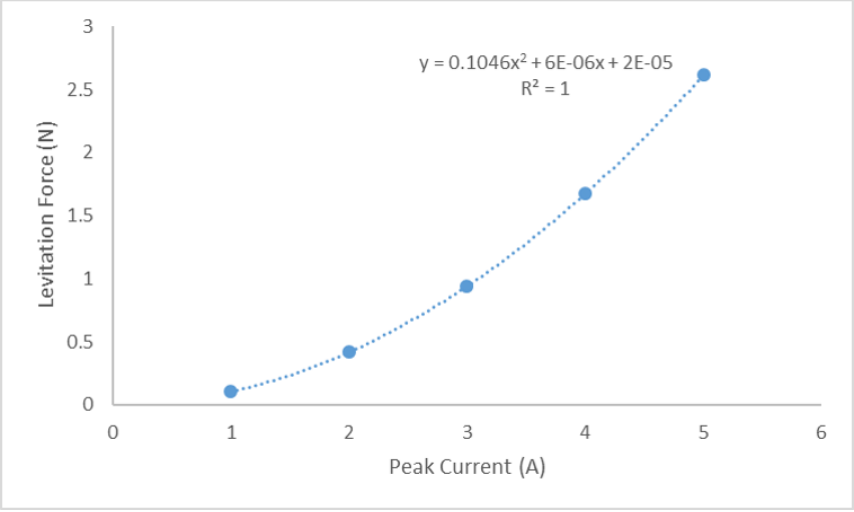

Figure 4.3: RMS Current vs Levitation Force

To do this, a plot depicting the relationship between the magnitude of the current

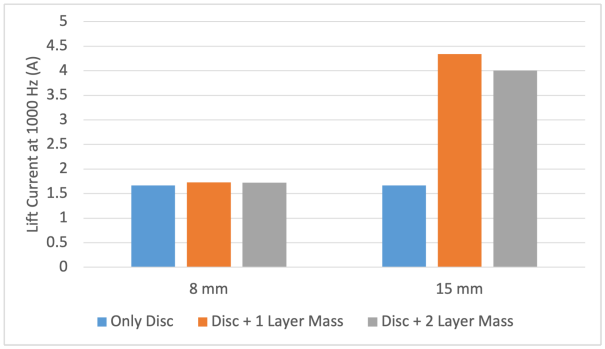

(a) RMS lift current calculated for 1000 Hz supply for all cases

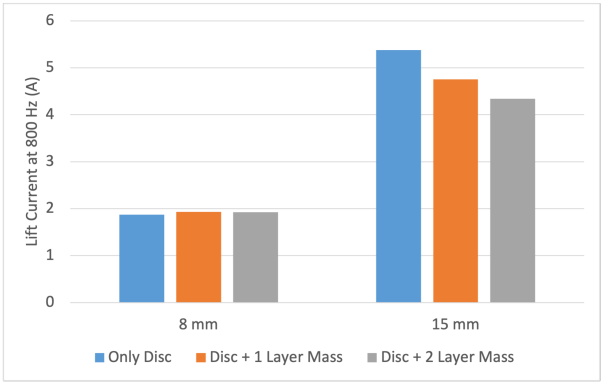

(b) Calculated lift RMS current of AC current for 800 Hz frequency

Figure 4.4: Calculation of Lift Currents for Different Frequencies

of the AC Supply and the z-component of the levitation force was developed. This was obtained by documenting the levitation force for various current inputs for an alternating current supply. The levitation force was documented for the various RMS currents at 1000 Hz frequency. Through least square fitting, the equation of the curve was obtained. This equation was then used to interpolate the required RMS current for stable levitation. The required force (i.e. the weight of the disc suspended) was given a tolerance of 10%. The plot is shown in Fig. 4.3.

Finally, the fit equation was equated to the gravitational force of the mass to be suspended, as shown in Equation 4.3. Solving, the 'lift' current, i.e., the current required to be supplied to the current carrying coil to stably levitate the mass is obtained. This is shown in Equation 4.3. As shown in Fig. 4.3, the goodness of fit is 1. This shows that the least square curve fit equation represents the behavior of the system quite strongly.

$$\begin{aligned} LevForce &= 0.1405I^2 + 6 \times 10^{-6}I + 2 \times 10^{-5} \\ 0.026 \times 9.81 &= 0.1405I^2 + 6 \times 10^{-6}I + 2 \times 10^{-5} \\ I &= 1.636A \end{aligned} \tag{4.3}$$

The process was repeated for all cases for 1000 Hz and 800 Hz situations. The results are shown in Fig. 4.4a and 4.4b.

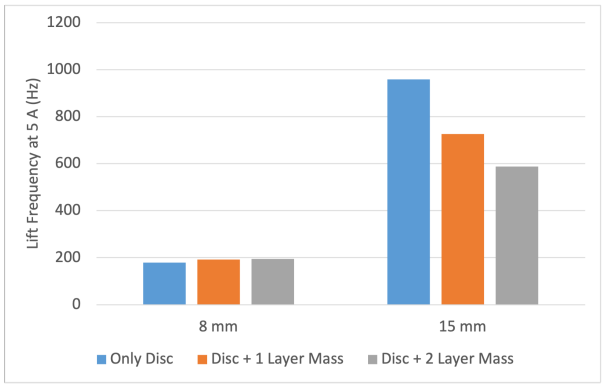

(a) Calculated lift frequency of AC current for 5 A RMS current

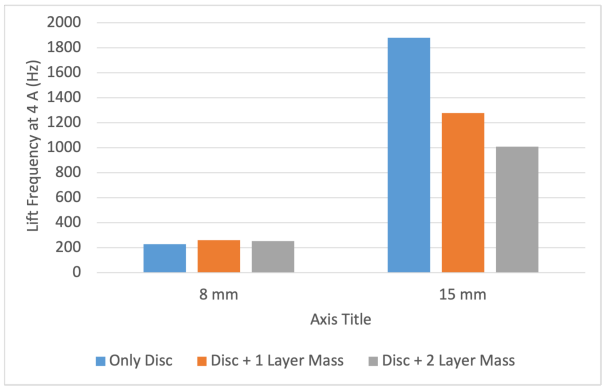

(b) Calculated lift frequency of AC current for 4 A RMS current

Figure 4.5: Calculation of Lift Frequencies for Different Currents

4.2.3 Calculation of Lift Frequency

Next, the emphasis was placed on the calculation of the lift frequency. The lift frequency of the AC supply is defined as the minimum frequency required to stably levitate the solids (Table 4.2) at specific RMS currents (4 & 5 A). The calculation of the RMS frequencies is also conducted using least-squared fitting. Similar to the analysis shown for the calculation of the lift current, a plot of frequency vs levitation force is developed and used to develop the least squared fitting equation. The analysis is done for all cases at 8 mm and 15 mm away from the levitator. The results are shown in figure 4.5a and 4.5b.

4.3 Validation

In an attempt to verify the calculated currents and frequencies, an analysis was conducted in the transient domain. The Transient Module for ANSYS Maxwell 2D was used. The module provides the capability to observe the variation of several parameters (like force, position, velocity, etc.) as a function of time. ANSYS 2D module was used to ease meshing and thereby reduce computation time.

The primary objective of the analysis here is to show that the lift current calculated here was sufficient for the stable levitation of the solid. For this verification, Case 1 (Table 4.2) was used. The mass of the solid suspended is 0.026 kg. The alternating current supplied to the levitator is shown in Fig. 4.6a. It shows the characteristics of the input current

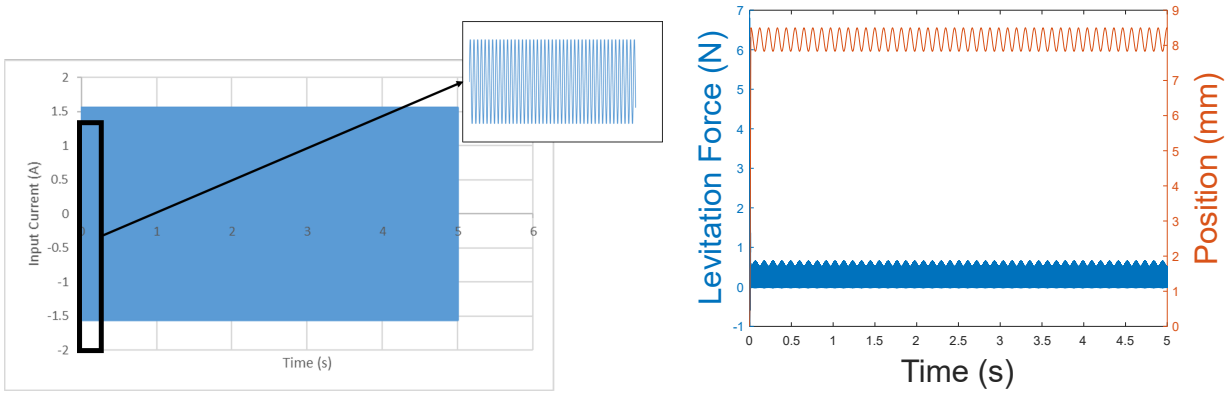

(a) Input current supplied to the levitator

(b) Position and axial force of the disc

Figure 4.6: Input Current, Position of Disc and Levitation Force vs Time - ANSYS Maxwell

(1.636 A RMS Current, 1000 Hz Frequency). The current calculated stably levitates the solid at 8 mm above the levitator setup.

4.3.1 Parameters vs Time

The simulations are conducted based on the model described. The primary parameter that needs to be observed to validate the model is the position of the solid as a function of time. Ideally, the solid would rise to the desired height (8 mm above the levitator) and stay there. However, due to the sinusoidal nature of the forces produced, slight oscillations are acceptable. The plots for the position of the solid as a function of time (as shown in Fig. 4.6b) and the vertical levitation force (as shown in Fig. 4.6b) are obtained.

4.3.2 Temperature vs Time

The method discussed here depends on the generation of eddy currents. Due to the production of these currents, there are some heat losses within the solid being levitated. Thus, it is crucial to conduct a thermal analysis on the system to ensure that the material stably levitated does not heat up excessively too quickly. Thus, to conduct this analysis, ANSYS transient thermal module was used.

The induced eddy currents primarily exist within a characteristic length known as the skin depth (δ) [95], as described in Section 3.10. The induced eddy currents that exist

beyond this characteristic length are very small, and thereby can be ignored. The skin depth is a function of the frequency, permeability, and density of the materials. For the test cases discussed here, the δ value computed is shown in Equation 4.4. Since the currents are produced within this depth, the heat losses originate within this band.

$$\delta = \sqrt{\frac{1}{\pi f_0 \mu}} = 2.593mm \tag{4.4}$$

where f_0 is the frequency of operation, mu_r is the relative permeability and μ_0 is the permeability of free space

To depict the sustainability of the model, the maximum value of the heat losses produced amongst all nodal points (extracted from the ANSYS EM Maxwell module) is uniformly fed to all nodal points within the skin depth of the disc. This ensures that the temperature estimated is higher than the actual temperature distribution of the disc. The primary objective of this estimation technique is to ensure that even in relatively harsh circumstances, the system can be feasible. For the analysis, the ambient temperature is assumed to be 22° C.

Fig. 4.7a shows the variation of the temperature of the solid as a function of time. The analysis is conducted for 12 seconds here. As it can be seen, the maximum temperature increase after 12 seconds is about 4° C. Using least squared fitting, the time required to heat the system to the Melting Point of AlSi12 (660° C) is computed. The fitted curve for the temperature vs time function is shown in Fig. 4.7b. As can be seen, the melting point of the solid is achieved after 2850 seconds. Thus, with external cooling, stable levitation can be achieved for extended periods without melting the solid being suspended.

4.4 Summary

The research presented in this chapter aims to highlight the initial viability of a magnetic levitation system for AM applications. This is established by highlighting that the levitation system can suspend aluminum alloys (like AlSi12) for extended periods. The initial system developed has been optimized to levitate a 25 mm radius and 5 mm height AlSi12 disc. The lift current and lift frequencies to levitate the disc 8 mm and 15 mm above the levitation system have been calculated. Three specific cases were considered: Suspension of the disc, suspension with one layer on the disc, and suspension of 2 layers on the disc. The performance of the calculated parameters was subsequently verified through the use of the transient module within ANSYS Maxwell. The variation of critical output parameters

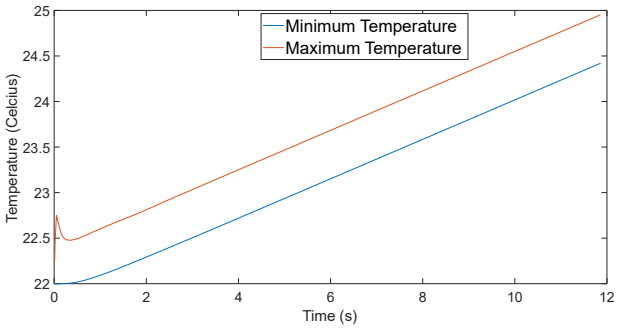

(a) Minimum and maximum temperature of the solid vs time

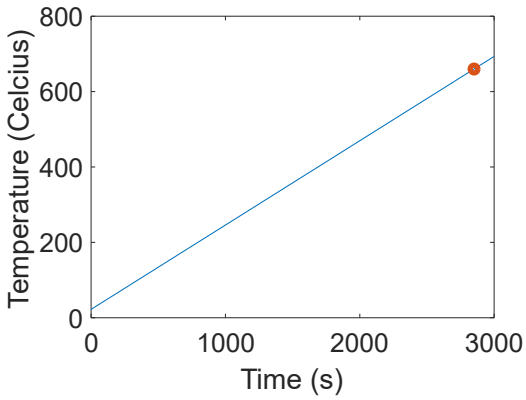

(b) Fitted curve (from maximum current) for temperature vs time with the melting point of aluminum (660°) plotted

Figure 4.7: Temperature vs Time - Simulation

like the position of the disc vs time and levitation force vs time were obtained from ANSYS Maxwell and the results were compared with the expected outcomes. Since the outcomes from ANSYS Maxwell matched closely with expectations, the overall system performance was verified. Thus, the system successfully highlights the initial compatibility of the magnetic levitation system for AM applications. There is a strong dependence on the use of simulations through ANSYS Maxwell. However, given the high fidelity of the simulation results and the reliability of these simulations, the results presented are well grounded.

However, there is a very harsh constraint on the outer diameter of the levitation system of 70 mm. In addition, only 22 AWG wires were considered for the analysis, resulting in a relatively low current carrying capacity of the coils. Several pertinent coil parameters (like the width of coils) could also be modified to improve the overall system performance. Thus, the current system was only developed in the simulation environment. The constraints on this system were relaxed to further improve the overall system performance.

Chapter 5

Laminated and Solid Core System

5.1 Need for Laminated and Solid Core System

A working prototype of a magnetic levitation system with compatibility within the AM environment has been developed by the authors in [96]. The research has been subsequently emphasized in my colleague's thesis, as highlighted in [100].

To summarize, a magnetic levitation system prototype with a dimensional constraint of 90 mm on the outer diameter of the system was developed. The system operated on the same working principle as highlighted in Section 3.5. Two coils were embedded in a high-permeability pure iron core. The inner coil consists of 920 turns and the outer coil consists of 800 turns, resulting in a $N_{inner\ coil} : N_{outer\ coil} = 1.15$. The levitation system is successfully able to facilitate stable suspension of an aluminum disc with a diameter of 50 mm and a height of 5 mm and a mass of 26 g.

However, there were some critical challenges encountered with the levitation system. First, the harsh constraint of 90 mm placed on the outer diameter of the levitation system resulted in a decrease in the efficiency of the system. In order to produce the levitation forces necessary for stable suspension, a high number of turns were needed. This resulted in an increase in the height of the levitation system. This, subsequently, resulted in a stark increase in the impedance of the levitation system. Thus, there was a clear need to revise the constraint placed on the system. The levitation system was constrained based on the volume occupied by the levitation system, as opposed to the outer diameter of the levitation system.

Second, the pure iron core utilized has a maximum allowable permeability of 9500. However, the high permeability is encountered at a high magnetic field output of 1.5 T of

the coils. However, with the maximum allowable input to the coils, the maximum magnetic field measured is within the range of 0.1 - 0.2 T. This results in a significant reduction in the permeability of the core of 700. Thus, there was significant scope to improve the permeability of the core of the levitation system.

Finally, as highlighted in Article [96], the strength of the outer coil is very high. This results in the generation of sufficient forces in the lateral axes. However, as highlighted in Section 3.6.5, the inner coil and outer coil are in constant competition to determine the overall strength of the coils. Thus, to compensate for the high strength of the outer coil, a 40 Ω resistor was added in parallel to the levitation coil. This results in a reduction in the current output of the outer coil, therefore, reducing the current through the outer coil. However, this also results in a reduction of the efficiency of the system, since the current supplied to the resistor is essentially wasted energy.

The levitation systems developed in this chapter aim to improve the system's overall performance developed in Article [96].

5.2 System Description

Laminated cores are comprised of sheets coated with insulated materials stacked together to form the core. Laminated cores are used to prevent the induction of eddy currents within the core, therefore minimizing the losses occurring due to the induced eddy currents, as highlighted in Section 2.4.1. Pre-defined sized lamination sheets were used to replace the core within which the levitation coils are embedded.

Following the development and successful implementation of the laminated core system, it was also deemed relevant to develop a levitation system comprised of a solid core system. The use of a solid core offers significantly more flexibility with the optimization of dimensions, resulting in a potential improvement of the system. This is because the laminated core sheets were selected from preexisting and pre-cut lamination sheets to facilitate cheaper and faster fabrications. However, the solid core system would offer significantly more control over design variables, offering avenues for improved performance. The implementation of both levitation systems has also been presented in [101].

Parameter	Value
Coil 1 Width	11 mm
Coil 1 IR	34 mm
Coil 2 Width	11 mm
Coil 2 IR	67 mm
N1	314
N2	280
Disc levitation height	2 mm above levitation system
Current input	5A
Frequency of input	50 Hz

(a) System description for stacking factor analysis

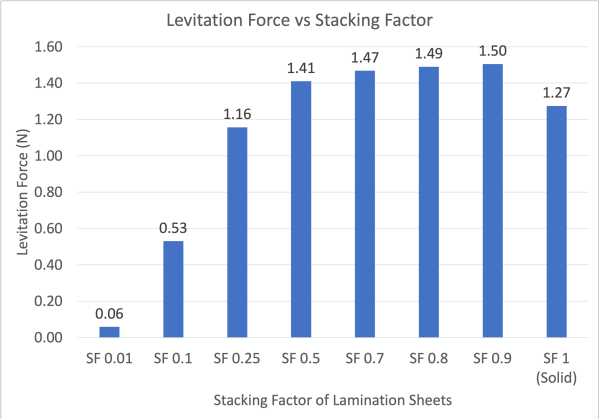

(b) Levitation force vs stacking factor from ANSYS Maxwell

Figure 5.1: Stacking Factor Analysis

5.3 Comparison of Laminated and Solid Core System Performance

The stacking factor (also known as the lamination factor or space factor) is the ratio of the volume of the electrical core material to the overall volume available. Since lamination sheets have some electrical insulation coatings, the stacking factor, by definition, is less than one.

The stacking factor has a significant impact on the performance of the levitation system. As highlighted in [102], with a decrease in the stacking factor of the laminated core, there is a reduction in the relative permeability of the material. This would impact several critical parameters like the magnetic field, levitation force, etc.

Since the laminated core is free from eddy current induction within the core, there is a stark improvement in the system performance for relatively high lamination stacking factors (< 0.7). This was verified using ANSYS Maxwell. For the analysis, the material property of the stacking factor was varied and the levitation force was studied. The pertinent system parameters have been highlighted in Fig. 5.1a.

The variation of the levitation force as a function of the stacking factor of the core has been presented in Fig. 5.1b. As it can be seen, for low stacking factors, there is a significant reduction in levitation forces. However, for stacking factors of 0.7 to 0.9, the levitation forces are relatively similar. When compared to the solid core system with the

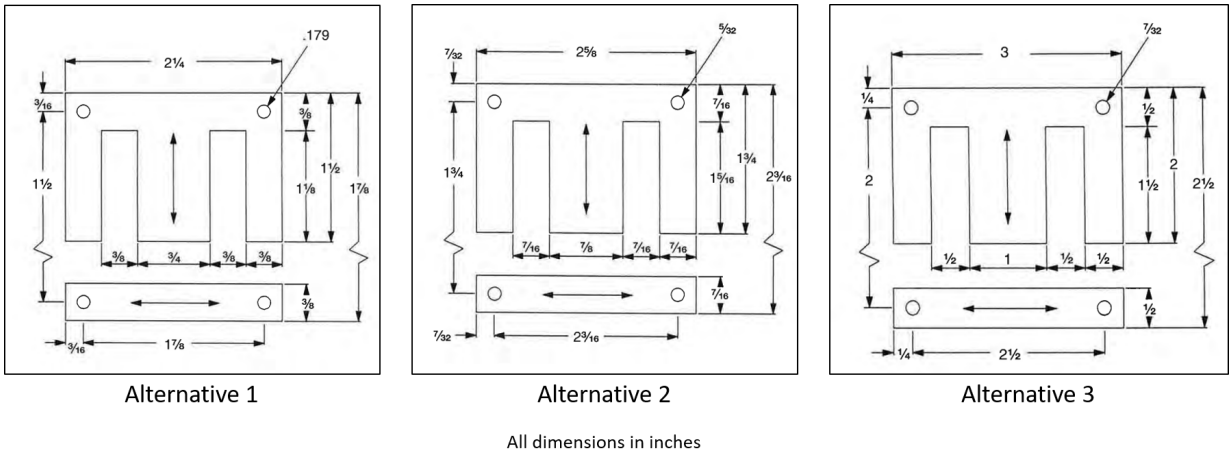

Figure 5.2: Lamination Sheets Alternatives Compared

same system specifications, the laminated cores have a significantly better performance. Thus, the viability of a laminated core system has been highlighted through this analysis.

5.4 Optimization of Laminated Core Levitation System

Laminated sheets are usually available in pre-defined dimensions. It is possible to cut custom-sized sheets to build the core. However, the process of cutting hundreds of sheets to a custom size would be too time-consuming, and existing lamination sheet sizes can also produce satisfactory system performance. Thus, in order to facilitate fast fabrication, pre-defined lamination sheets are used for the research.

5.4.1 Selection of Lamination Sheet Size

Three different alternatives of lamination sheet sizes were obtained from a local manufacturer's catalog and have been presented in Fig. 5.2. These laminated sheets were then subjected to simulation analyses using ANSYS Maxwell. It should be noted that all these laminated sheets were stacked around the z-axis. A central hole of 23 mm was added to all alternatives to maintain consistency. 18 AWG (with a current carrying capacity of 5 A) was used within all lamination core systems. The levitation force on a disc of 60 mm

radius and 5 mm height made of aluminum and placed 2 mm above the levitation system was studied and plotted. The input supplied to the system is 5 A at 60 Hz. A stacking factor, which is the ratio of the volume of lamination sheets within the assembly to the total volume available, of 0.7 was considered and a fill factor, which is the area of copper wires in coils to the total area available, of 0.7 was considered for the simulations.

Sizes of lamination sheets smaller than these alternatives produced very low levitation forces, with forces < 1 N for 1 mm levitation height which is lower than the weight of the disc (1.49 N). Sizes higher than these produced a very high impedance (over 60 ohms), therefore losing the ability to provide a 5 A current input to the coils with a 300 V voltage input.

Fig. 5.3 highlights the output specifications of the laminated core system. The number of turns has been presented in Fig. 5.3a. As expected, alternative 2 has the highest number of turns for both the inner and outer coil. However, as highlighted in Fig. 5.3b and 5.3c, the output inductance and impedance of the alternative 3 are the highest as well. Most notable, however, the levitation force of alternative 2 is the highest, as highlighted in Fig. 5.3d. The power output of alternative 2 (as highlighted in Fig. 5.3f) was also lower than that of alternative 3. With all parameters considered, alternative 2 was pursued in this application.

5.4.2 Wire AWG Selection

For the initial phase, the wire AWG was selected arbitrarily as 18 AWG but applied to all alternatives to maintain consistency. However, several important considerations such as the number of turns of coils, the strength of coils, which is the product of the difference of the number of turns of the outer and inner coils to the current through the coils, inductance, impedance, and levitation force are contingent on the wire AWG. Thus, a deeper analysis is conducted for the wire AWG selection using ANSYS Maxwell. For the analysis, 16-20 AWG wires are considered.

Fig. 5.4a highlights the number of turns of the inner and outer coils for the various wire sizes. It should be noted that the fill factor used for the analysis was 0.7. The current carrying capacity of these wire AWG alternatives is presented in Fig. 5.4b. The maximum current was capped at 10 A, based on the maximum current output of the hardware used. With the development of the number of turns and maximum current carrying capacity, the strength of the two coils was calculated and presented in Fig. 5.4c. As can be seen, the use of 20 AWG produces the best strength of coils. The performance of the different wires was also studied in ANSYS Maxwell. While 20 AWG wire has the highest impedance, as

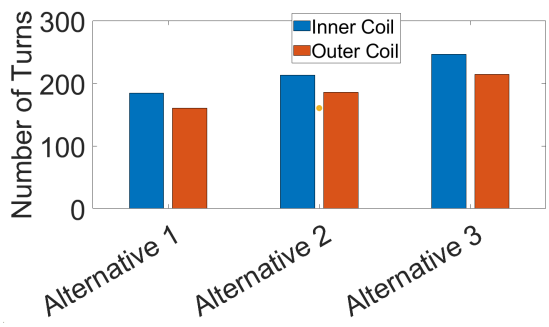

(a) Number of turns of inner and outer coil for all alternatives

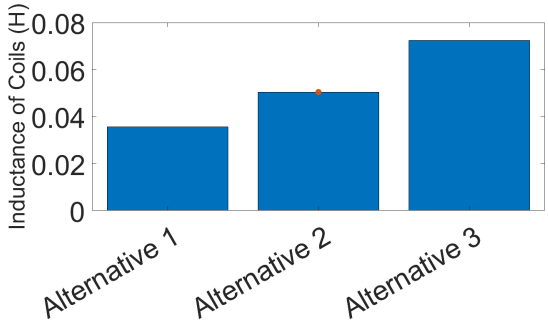

(b) Inductance of both coils in series for all alternatives

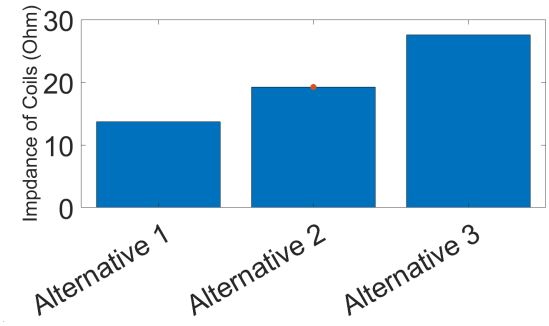

(c) Impedance of both coils in series for all alternatives

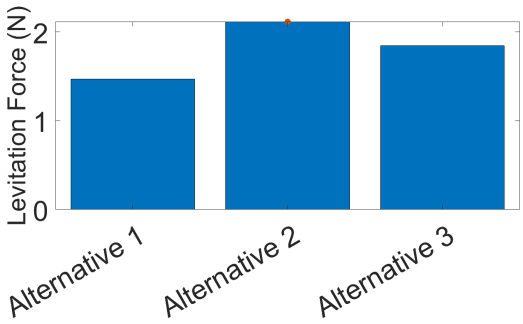

(d) Levitation force on disc for all alternatives

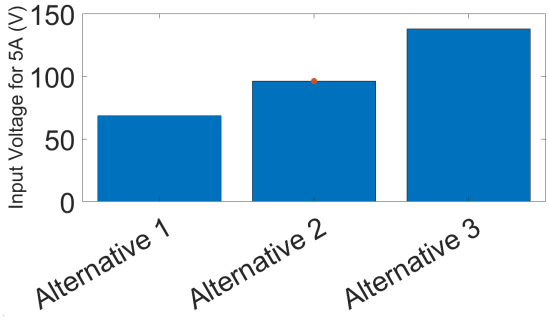

(e) Input Voltage for 5 A input for all alternatives

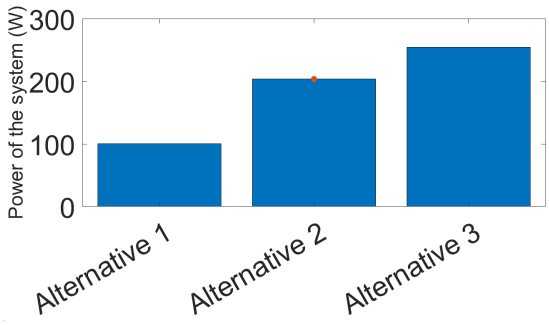

(f) Output power for all alternatives

Figure 5.3: Performance of Lamination Sheets Alternatives

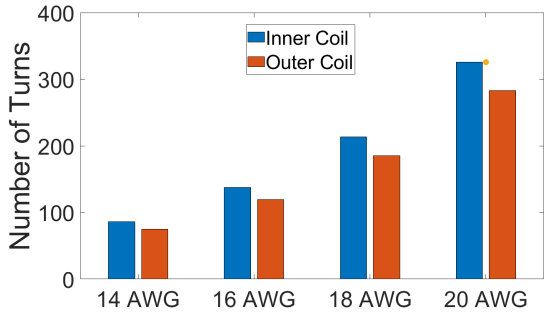

(a) Number of turns of inner and outer coil for all alternatives

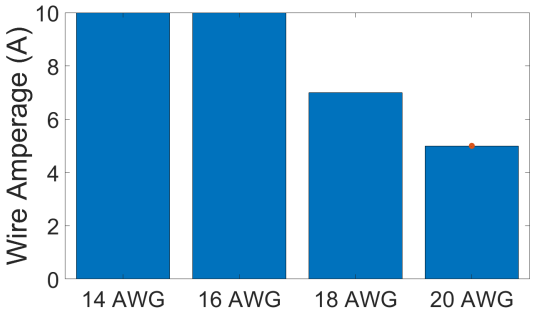

(b) Current carrying capacity for all alternatives

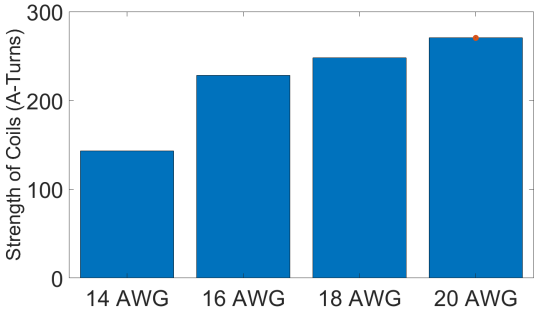

(c) Strength of coils for all alternatives

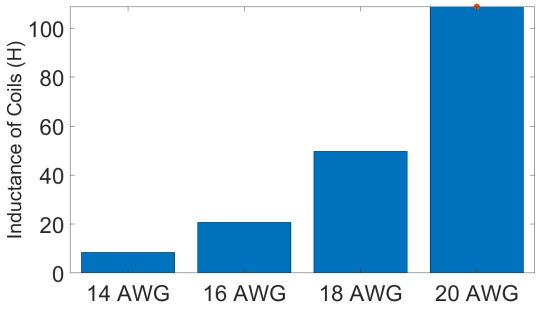

(d) Inductance of both coils in series for all alternatives

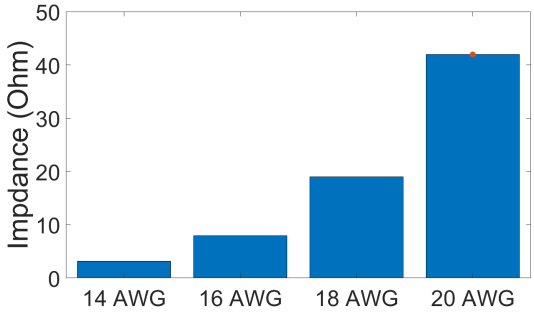

(e) Impedance of both coils in series for all alternatives

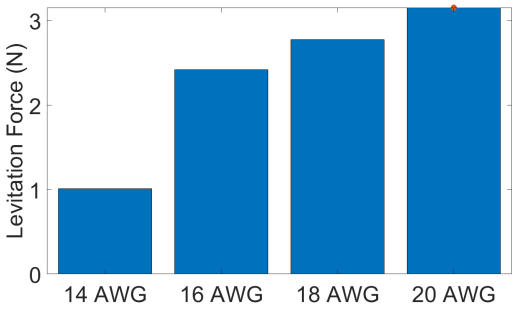

(f) Levitation force on disc for all alternatives

Figure 5.4: Performance of Different Wire AWG

Table 5.1: Initial and constant parameters

Parameter	Value
Input Current	5 A
IR1	34 mm
IR2	67 mm
Radius of Hole	23 mm
Height of Coils	33.5 mm
Levitated Material	Aluminum
Height of Disc	2 mm above levitator
Frequency	50 Hz
Wire AWG	18 AWG (6 A Max)
Core Material	Low Carbon Steel

shown in Fig. 5.4d, the impedance is still low enough to facilitate the supply of 5 A with 300 V input. The levitation force produced with 20 AWG wire was also the highest. Thus, 20 AWG was pursued in this application.

5.5 Optimization of the Solid Core System

For the optimization of the solid core, the direct substitution method was employed after reviewing several other strategies highlighted in Section 2.3. This optimization strategy has been employed for the development of the first iteration of the levitation system developed by the authors [96]. For the optimization, the selected dimensions of the laminated core system were taken as the initial parameters. The dimensions of the coils are subjected to the optimization process. The initial parameters have been listed in Table 5.1. The critical constraint placed on the system was that the impedance should not exceed 50 ohms, to ensure a 5 A current input with a 300 V input at 50 Hz.

5.5.1 Optimization of Coil Widths

Fig. 5.5a and Fig. 5.5b highlight the variation of levitation force and impedance as a function of the width of the inner coil (coil 1) and outer coil (coil 2) respectively. It should be noted that the number of turns for both coils is adjusted in accordance with the dimension. For dimensions of coil width greater than 14 mm, the impedance of the

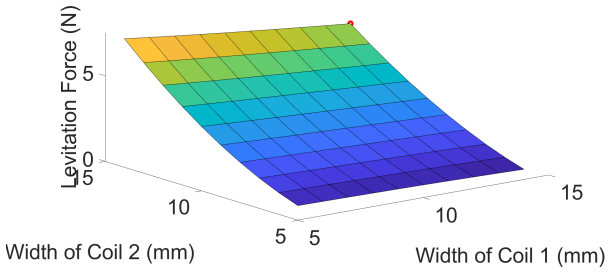

(a) Levitation force vs width of Coils

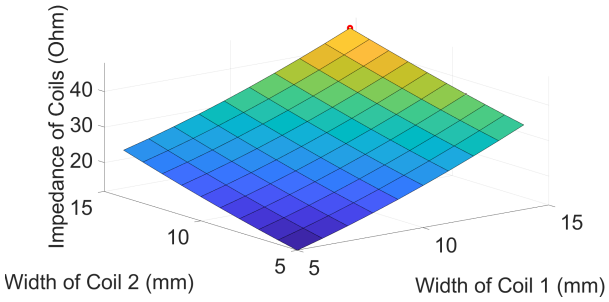

(b) Impedance vs width of coils

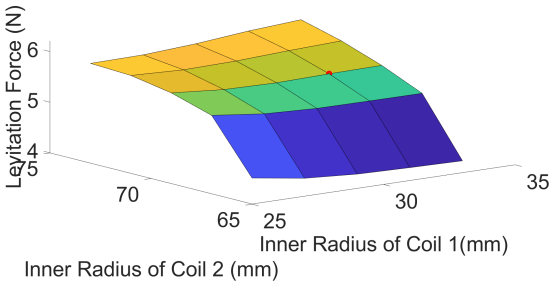

(c) Levitation Force vs inner radius of coils

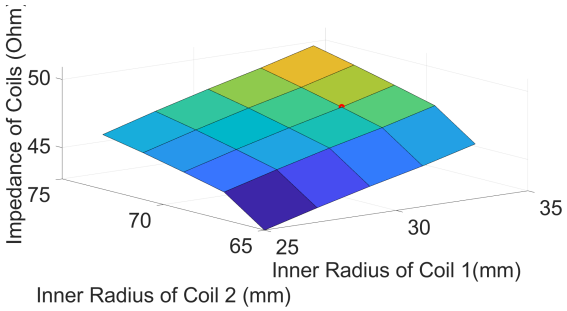

(d) Impedance vs inner radius of Coils

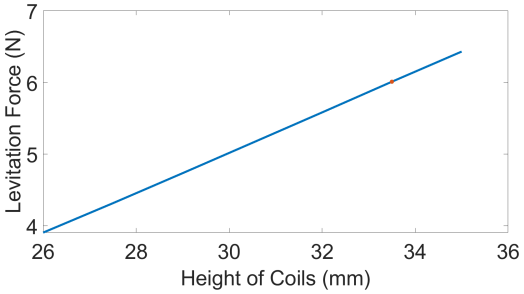

(e) Levitation force vs the height of coils

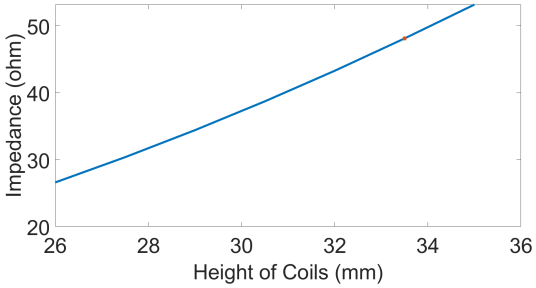

(f) Impedance vs the height of coils

Figure 5.5: Optimization of Coils

system is higher than 60 Ω, resulting in the input current being lower than 5 A, which is the current carrying capacity of 18 AWG wire. As it can be seen, the width of both the inner coil and outer coil produces the highest levitation force and an acceptable impedance is obtained at a width of 14 mm.

5.5.2 Optimization of Radial Placement of Coils

Fig. 5.5c and Fig. 5.5d highlight the variation of levitation force and impedance of the system as a function of the inner radius of the coils respectively. With the coil width determined, the determination of the inner radius of the coils determines the radius placement of the coils. The optimized radial placement results in the inner radius of coil 1 as 31 mm and the inner radius of coil 2 as 67 mm, as highlighted in Fig. 5.5c and 5.5d.

5.5.3 Optimization of Height of Coils

The height of the levitation system has been varied and the resulting levitation force (Fig. 5.5e) and impedance (Fig. 5.5f) have been obtained. It should be noted that the number of turns for both coils is adjusted in accordance with the dimension. As it can be seen in Fig. 5.5f, for coil heights greater than 33.5 mm, the impedance of the system is higher than 50 ohms. Thus, the ideal height was taken to be 33.5 mm and was pursued.

5.5.4 Wire AWG Selection

Fig. 5.6a and 5.6b highlight the variation of levitation force and impedance respectively for different wire diameters. Previously, the analysis was restricted to low-frequency inputs. However, the analysis was extended to higher frequency inputs as well. When restricted to relatively low frequencies like 50 Hz, the use of 20 AWG wires would be feasible, as highlighted previously. However, as shown in Fig. 5.6a, there is a significant increase in levitation force for all wire diameters. However, the impedance goes above the 50 Ω resistance limit for all wire AWG except 16 AWG. Thus, for the solid core system, 16 AWG wire was selected.

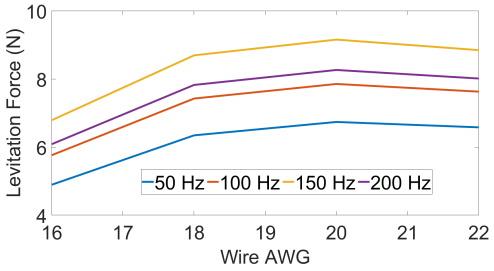

(a) Number of turns of inner and outer coil for all alternatives

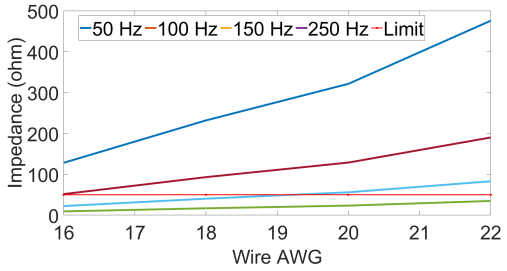

(b) Current carrying capacity for all alternatives

Figure 5.6: Performance of Different Wire AWG

5.6 Simulation vs Experiment Comparison

For the comparison of simulation data when compared to experimental data, two different approaches were taken. First, the current measured through simulations and experiments was compared since input current determines other relevant factors like the magnetic field, levitation force, etc., it was deemed best to compare the performance of simulation using the same. For the analysis, the coils were connected in series and carrying current in the opposite direction. As shown in Fig. 5.7a, the simulation data was in close agreement with experimental data, with a maximum error of 3.84%. This error can be attributed to meshing errors associated with simulation using FEA. This verifies the validity of the simulation data studied so far.

The specifications of the levitation system were also subjected to the analytical model developed in Section 3.6.4. The self-inductance of the inner coil (L_1), the outer coil (L_2), and the total inductance of the two coils in series and oriented to carry current in the opposite direction (L_{tot}) were measured using a Keysight U1732B LCR meter. The measured values are highlighted in Equation 5.1.

$$L_1 = 0.05286H, L_2 = 0.08549H, L_{tot} = 0.1229, R_1 = 2.115\ \Omega, R_2 = 3.372\ \Omega \tag{5.1}$$

The resulting data were compared with the experimentally measured current values. The data obtained from the analytical model is in close agreement with the experimental data, with a maximum error of 2.62%. Thus, the analytical model was deemed to be a success.

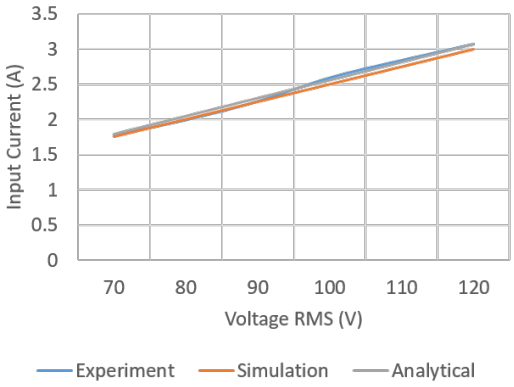

(a) Laminated Core: Current measurement using simulation and experiment

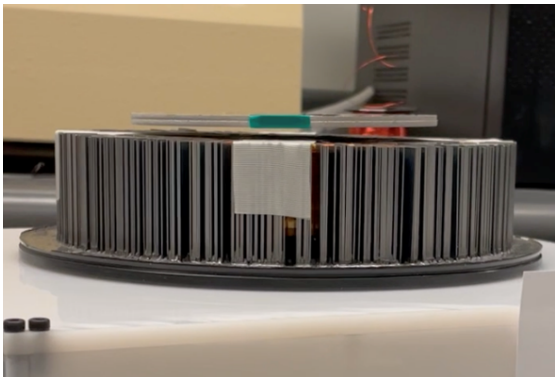

(b) Laminated Core: Steady state position observed experimentally

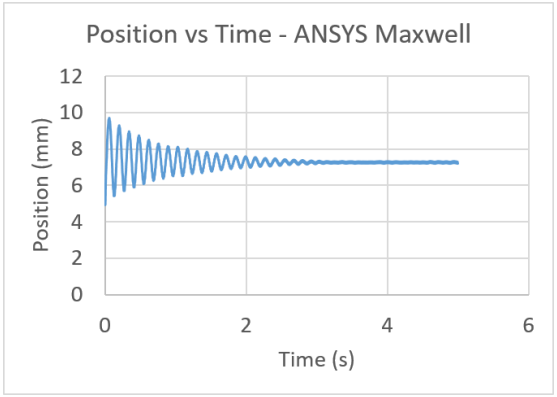

(c) Laminated Core: Steady state position measured through simulation

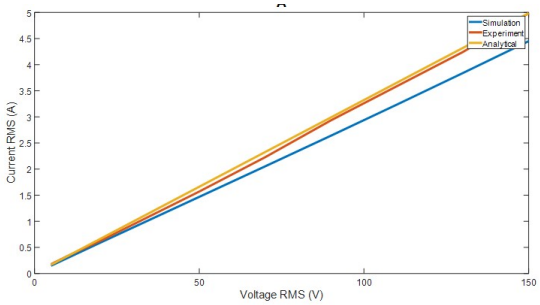

(d) Solid Core: Current measurement using simulation and experiment

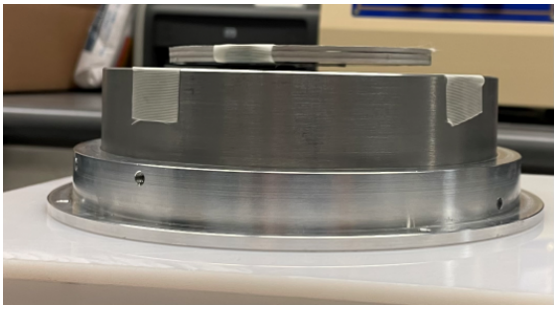

(e) Solid Core: Steady state position observed experimentally

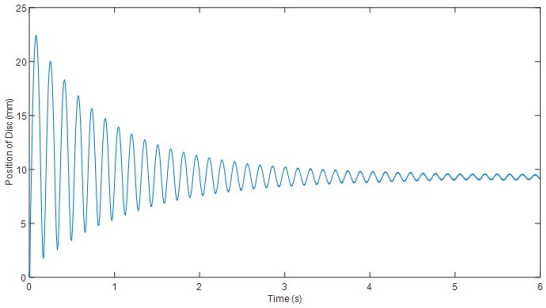

(f) Solid Core: Steady state position measured through simulation

Figure 5.7: Simulation vs Experiment Comparison

The second approach was to compare the steady state position of the levitated disc obtained experimentally to the steady state position obtained through simulation. Fig. 5.7b highlights the steady state position with a 5 A at 50 Hz input observed experimentally. The position of the disc is observed to be 7 mm above the levitation system. The simulation data highlighting the variation of position as a function of time, as presented in Fig. 5.7c, is in close agreement with the experimental data.

The experimental approach of the comparison of simulation and experimental data was repeated for the solid core system. As it can be seen in Fig. 5.7d, the current measurement is in close agreement with each other, with a maximum error of less than 10%. Thus, the validity of simulation data has been verified. As done previously in the laminated core system, the specifications of the levitation system were also subjected to the analytical model developed in Section 3.6.4. The measured coil parameters are highlighted in Equation 5.2.

$$L_1 = 0.005H, L_2 = 0.0084H, L_{tot} = 0.0956H, R_1 = 0.65\ \Omega, R_2 = 1.14\ \Omega \tag{5.2}$$

The resulting data were compared with the experimentally measured current values. The data obtained from the analytical model is in close agreement with the experimental data, with a maximum error of 6.21%. Thus, the analytical model was deemed to be a success.

Fig. 5.7e - 5.7f highlights the steady state position observed experimentally (Fig. 5.7e) and using the transient mode of ANSYS Maxwell (Fig. 5.7f). As it can be seen, the simulation data is in close agreement with experimental data.

5.7 Levitation Experiment

The levitation experiment conducted was deemed a success, as highlighted in Fig. 5.7b and 5.7e. The experimental analysis was further tested for different system inputs and dimensions of the disc.

For the laminated core system, Fig. 5.8a highlights the levitation of a disc of 60 mm radius and 4 mm height at 75 Hz. Fig. 5.8b highlights the levitation experiment with a disc of the same diameter and height of 6 mm at 75 Hz. Fig. 5.8c and 5.8d highlights the levitation experiment with the dimensions of disc presented previously at 90 Hz. Thus, the ability of the laminated core levitation system to stably suspend a disc has been clearly

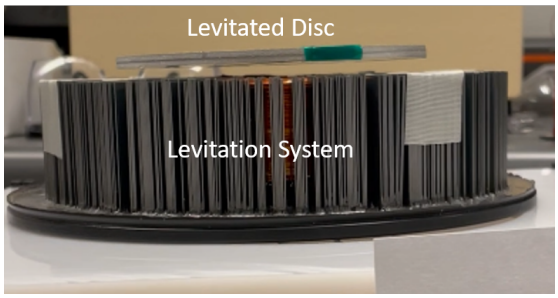

(a) Laminated Core: Disc of 60 mm radius, 4 mm height at 75 Hz

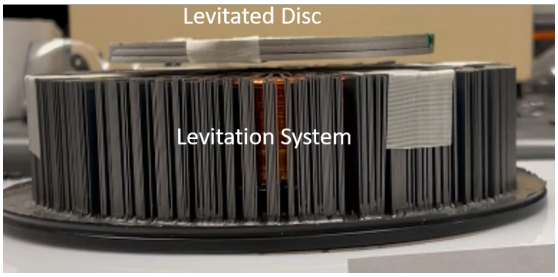

(b) Laminated Core: Disc of 60 mm radius and 6 mm height at 75 Hz

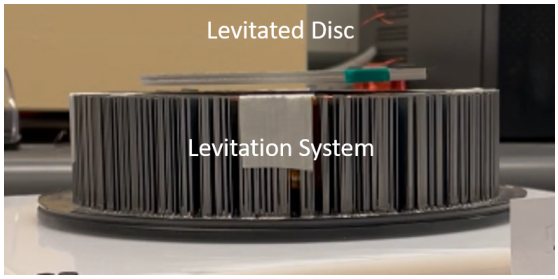

(c) Laminated Core: Disc of 60 mm radius, 4 mm height at 90 Hz

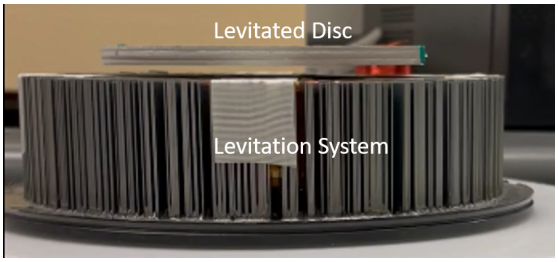

(d) Laminated Core: Disc of 60 mm radius, 6 mm height at 90 Hz

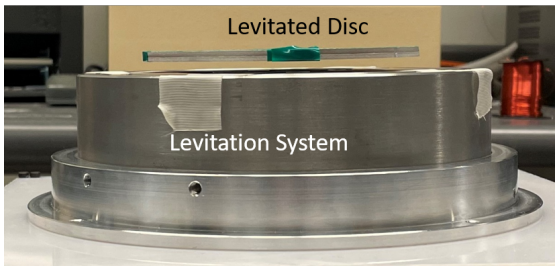

(e) Solid Core: Disc of 60 mm radius, 4 mm height at 150 Hz

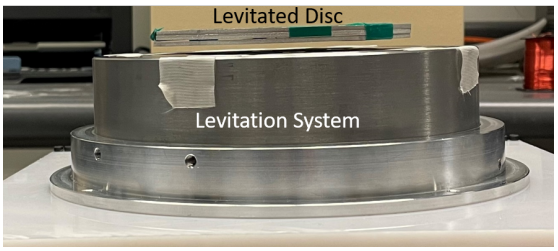

(f) Solid Core: Disc of 60 mm radius, 6 mm height at 150 Hz

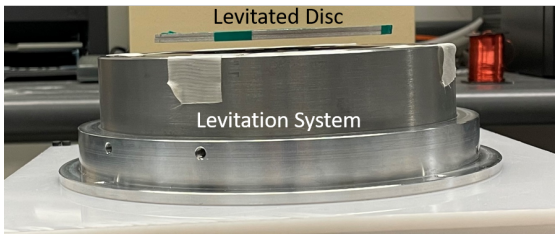

(g) Solid Core: Disc of 60 mm radius, 4 mm height at 250 Hz

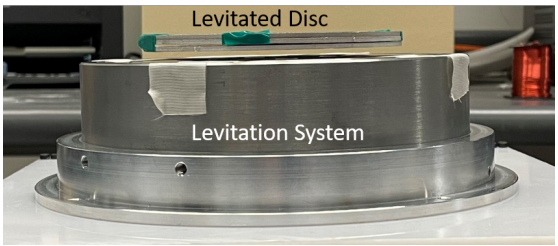

(h) Solid Core: Disc of 60 mm radius, 6 mm height at 250 Hz

Figure 5.8: Successful Levitation Experiment - Solid and Laminated Core

established. The versatility to support the levitation experiment at several inputs has also been highlighted.

The same versatility of the levitation system with a solid core was highlighted. Fig. 5.8e and Fig. 5.8f highlight the performance of the system at 150 Hz and Fig. 5.8g and Fig. 5.8h depict the system performance at 250 Hz. Thus, the system has been highlighted to perform satisfactorily with these inputs.

5.8 Compatibility with Additive Manufacturing Experiment

The primary objective of this experimental apparatus is to support AM operations. To test the feasibility of the same, it was critical to highlight and test certain performance criteria. This includes the system's ability to support additional payload and the lateral and axial stability following powder deposition.

5.8.1 Suspension of Additional Payload

As explained in [96], a critical objective of the levitation system is to support additional mass as a function of time. This is because of the mass added due to powder deposition to build geometries using AM. Thus, it is integral for the levitation system to support additional mass as time goes on. Fig. 5.9b highlights the system's ability to support an additional payload of 15.2 g during levitation. Fig. 5.9c highlights the addition of a 66.74 g mass on the levitated disc.

Fig. 5.9e highlights the ability of the solid core system to support added payload as a function of time. This experiment highlights the solid core system's ability to handle/cope with payload variation as a function of time. This variation occurs primarily due to the mass deposition activities encountered within the AM environment.

With the ability to support 66.74 g of aluminum in addition to the levitated disc with minimal loss of functionality and performance, as highlighted in Fig. 5.9f, it has been clearly highlighted that the solid core system can sustain additional payloads as a function of time.

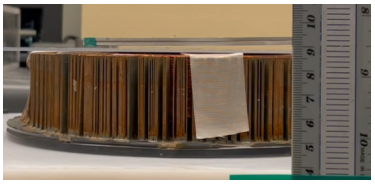

(a) Laminated Core: Levitation experiment with no added payload

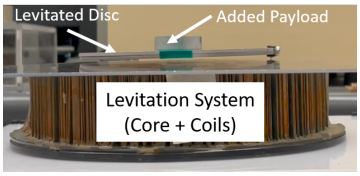

(b) Laminated Core: Levitation experiment with 15.2 g added payload

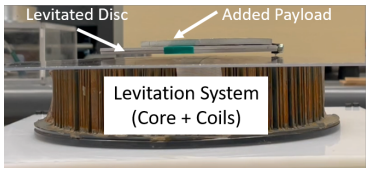

(c) Laminated Core: Levitation experiment with 66.74 g added payload

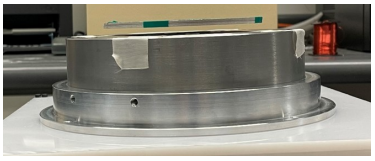

(d) Solid Core: Levitation experiment with no added payload

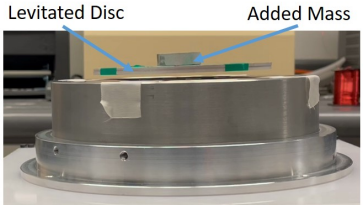

(e) Solid Core: Levitation experiment with 15.2 g added payload

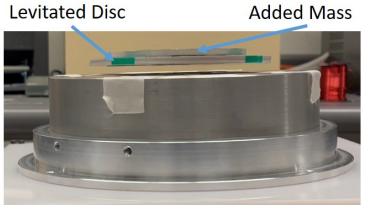

(f) Laminated Core: Levitation experiment with 66.74 g added payload

Figure 5.9: Successful Levitation Experiment with Added Payloads

5.8.2 Impact of Powder Deposition

The impact of powder deposition is another crucial phenomenon that needs to be verified to ensure the satisfactory performance of the levitation system. Assuming a mass flow rate of 1 g/min [103], the velocity of powder of 2 m/s [104] and a nozzle angle of 60-degree [103], the calculator impact force of powder deposition as a worst-case scenario analysis was found to be 0.01 N in [96] within the axial axis. Adding this as an additional force in the negative axial axis, the levitation force and levitation position are studied as a function of time using the transient mode of ANSYS Maxwell.

The resulting levitation force vs time and position of disc vs time plots obtained from ANSYS Maxwell has been presented in Fig. 5.10a and Fig. 5.10b respectively. As can be seen, the levitation height reduces from 9.1 mm to 8.97 mm, which is a 1.3% reduction in levitation height. Thus, the incorporation of the powder deposition force does not significantly impact the overall stability of the levitated disc. Thus, the compatibility of the levitation system has been highlighted effectively.

Fig. 5.10c highlights the levitation force as a function of time. The levitation force is much higher than the impact force of powder deposition. Thus it is safe to assume the retention of stability despite powder deposition. Fig. 5.10d highlights the position of

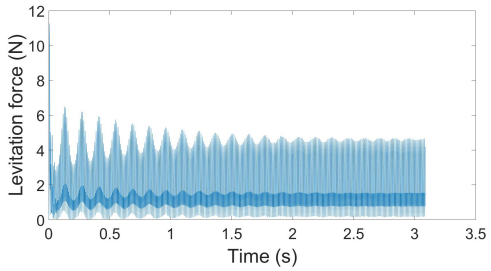

(a) Laminated Core: Levitation force with powder deposition

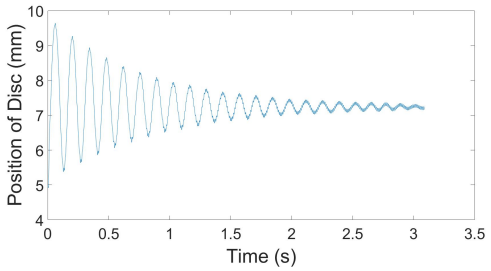

(b) Laminated Core: Position of disc with powder deposition

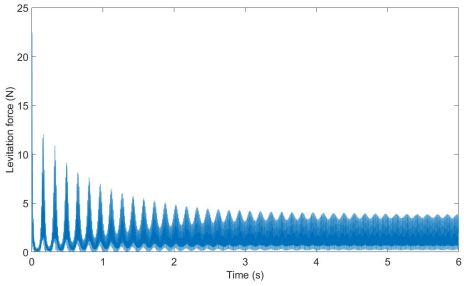

(c) Solid Core: Levitation force with powder deposition

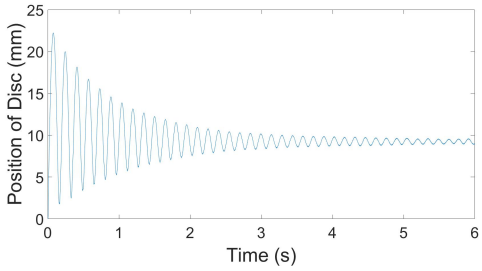

(d) Solid Core: Position of the disc with powder deposition

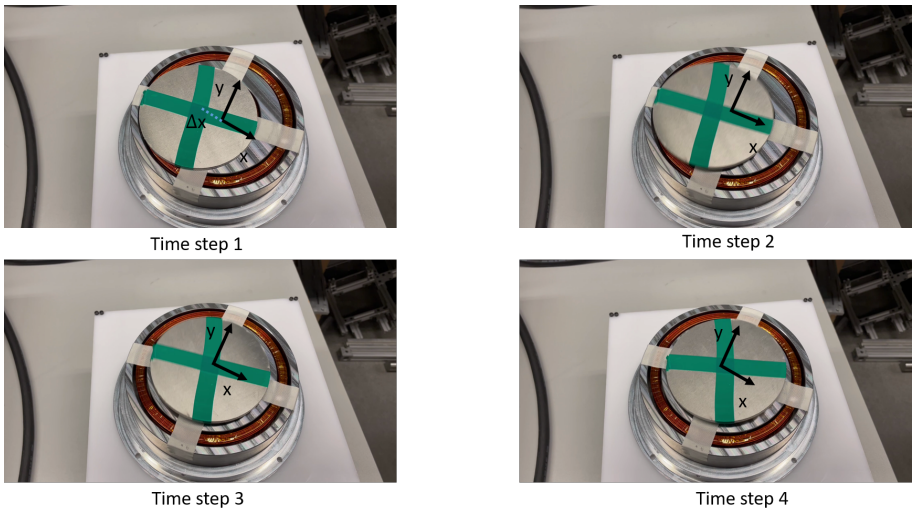

(e) Self-adjustment to center with an initial displacement of 30 mm

Figure 5.10: Impact of Powder Deposition

the disc as a function of time. As noted, the levitation height at a steady state was very similar despite the introduction of powder deposition force. Thus, the performance of the levitation system has been verified.

5.9 Performance of Levitation System in Different Environments

AM operations are conducted within a variety of different environments. For materials that are not stable within the air environment, it is critical to conduct the operations in an environment that ensures the stability of the materials. Thus, these are conducted within the vacuum environment or the AM machine is filled with argon to prevent the powders from reacting with air.

Thus, it was critical to study the performance of the levitation system within different environments. ANSYS Maxwell was utilized for the analysis. Different environments were considered: vacuum, air, and argon. An aluminum disc was placed 2 mm above the levitation system. 190 V at 150 Hz is supplied to the coils of the solid core system. From ANSYS Maxwell, it was found that the three environments produced an identical levitation force of 3.41 N. Thus, the performance of the levitation system was verified within different environments.

5.9.1 Stability within the Lateral Axes

Fig. 5.10e highlights the solid core systems stability within the lateral axes. As can be seen, in timestep 1, the disc has been provided a large displacement (about 30 mm) in the x-axis. However, timestep 2 - timestep 4 highlight the system's ability to bring the levitated disc back to the center with only the forces imposed on the disc from the levitation system. Thus, it has been highlighted that the system will retain its stability within the lateral axis.

5.10 Thermal Analysis

5.10.1 Laminated Core System

The key advantage of using laminated cores is the absence of induced eddy currents within the laminated sheets that form the core. Thus, there is no power loss within the core which would directly contribute to the overall temperature of the system. Since the coils also carry current below the ampacity of 20 AWG wire, which is the maximum temperature the wires can carry without exceeding the temperature rating of the wire, the temperature of the system is not anticipated to damage the system. The system operation is restricted to be below 5 A, while the ampacity of 20 AWG wires is highlighted to be 6 A [105] (17% lower than maximum current to ensure safe operation).

5.10.2 Solid Core System

Klein Tools MM300 Manual-Ranging 600V Digital Multimeter has been used to measure the temperature of the solid core system. An input of 200 V at 150 Hz was supplied to the coils. The measurement is conducted in the outer core for all measurements. A sample measurement of initial temperature is shown in Fig. 5.11a. The temperature was recorded after 1 min, 2 min... Up to 5 min of operation. The experimental data obtained was then documented in Fig. 5.11b and compared to the data obtained from the thermal simulation analysis.

Solidworks thermal module was used for the analysis. The analytical model previously developed and verified experimentally was used to determine the power dissipation of the coils. The calculated power dissipation was found using the equations highlighted in Section 3.6.4. The output power was calculated to be 128 W for both coils combined. The average eddy current losses were obtained from ANSYS Maxwell and found to be 114 W. These were subsequently fed into the skin depth of the core since the production of eddy current diminishes significantly beyond the skin depth. The skin depth at 150 Hz is calculated to be 6.6 mm. The model used for the thermal analysis is shown in Fig. 5.11c. The simulation data documented has been presented in Fig. 5.11d.

The error percentage has been plotted in Fig. 5.11e. The maximum error observed is 2.6%. This can be attributed to meshing errors. Thus, the simulation model developed is quite reliable for the solid core system. The simulation was subsequently run for 20 minutes to determine the viability of the system for 20 minutes of continuous operation for AM operations.

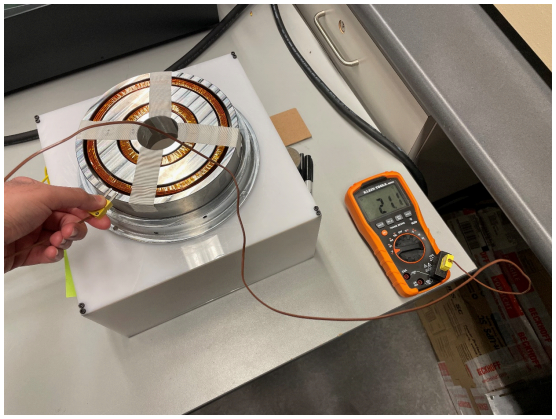

(a) Sample temperature measurement

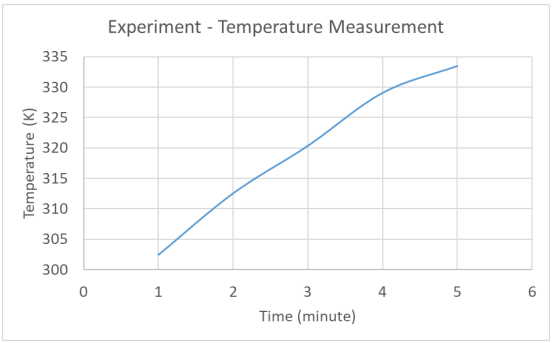

(b) Experimental measurement of temperature vs time for 5 min

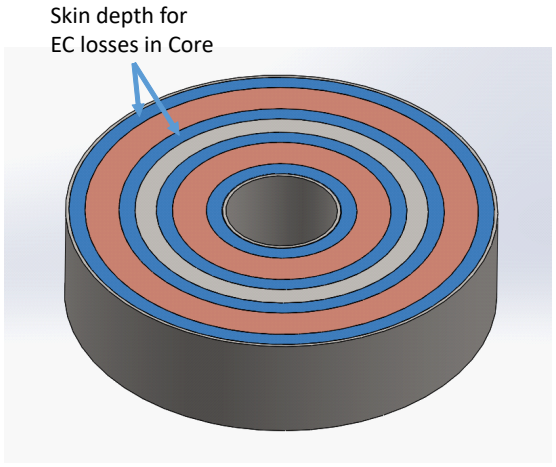

(c) Model for thermal analysis with skin depth highlighted

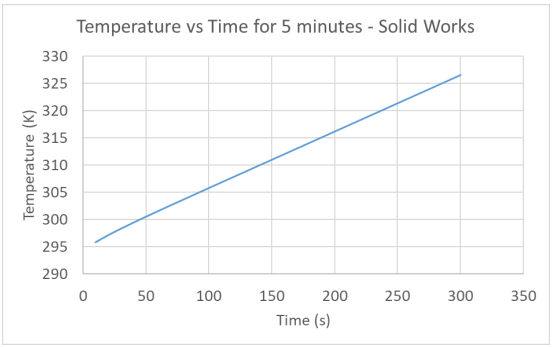

(d) Temperature vs time from thermal simulation analysis

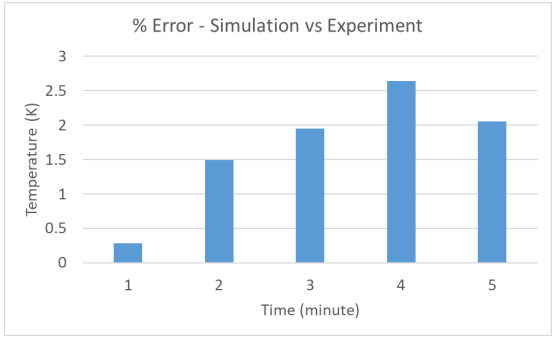

(e) Thermal analysis for 20 minutes of operation

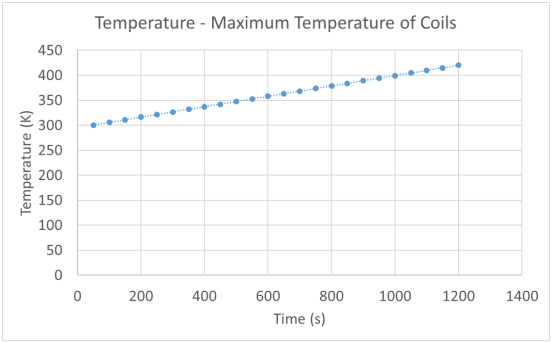

(f) Thermal analysis for 20 minutes of operation

Fig. 5.11f highlights the variation of temperature vs time for 20 minutes, as obtained from Solidworks thermal module. As can be seen, after 20 minutes of operation, the maximum temperature is 420 K (147 C). The epoxy of magnetic wire has a melting point of 200 C, which is the most vulnerable component of the levitation system. Thus, it has been shown that the system will be safe to use for 20 minutes.

5.11 Summary

The development of two distinct new levitation systems has been presented in this chapter. The two systems offer variations in dimension, wire AWG employed for coil development, and the core type.

The first system is developed within a laminated core system. The design decisions to select the optimum system have been presented. The comparison of simulation data is presented with experimental data, with a variation in current measurement restricted to 3.84%. The steady-state levitation position of the disc observed experimentally and through simulation is also in close agreement. The levitation experiment is deemed a success, with levitation height as high as 8 mm offered at 90 Hz. The compatibility of the levitation system with AM operations was also tested. The levitation system also offers the ability to levitate a disc with 66.74 g of added payload, therefore highlighting the system's ability to cope with added payload as a function of time. The impact force of powder deposition was also tested using simulation analyses. With the addition of the impact force in the negative axial axis, the steady state levitation height reduces by a mere 0.1 mm, therefore highlighting the system's ability to retain stability despite powder deposition activities.

The second system developed is embedded within a solid low-carbon steel system. The optimization and design decisions with the system development have been presented. As in the case with the laminated core system, the simulation and experimental data were compared and observed to be in close agreement, within 10% of one another. The levitation experiment was also successful at multiple frequencies, offering levitation heights as high as 8 mm at 150 Hz. Again, the compatibility of the system was tested with AM operations. First, the system's ability to cope with added payload as a function of time. The system displayed the ability to support 66.74 g of added mass with no loss in stability. Next, the stability within the lateral axis was also tested. A high initial displacement of 30 mm was provided to the disc. The system displayed the ability to bring the disc back to the equilibrium point with only the non-contact magnetic forces offered by the levitation system. The impact of powder deposition was also tested with the solid core levitation

system. The system retained stability and the steady state position was reduced by 0.14 mm with the incorporation of powder deposition forces.

Chapter 6

Design and Development of a Feedback Controller

6.1 Need for a Feedback Controller

Fig. 6.1a highlights the eddy currents produced with only the disc and Fig. 6.1b the disc with the added payload with the identical input (100 V RMS at 50 Hz). The added payload is an aluminum disc of 45 mm radius and 4 mm height with a total mass of 67 g. The initial disc is 60 mm in radius and 6 mm in height with a total mass of 121 g. The added payload is conductive, therefore there is an increase in volume within which eddy currents are produced. At 50 Hz, the skin depth, i.e., the characteristic length within which eddy currents are produced, is 11.6 mm. The sum of the height of the added payload and the initial disc is less than the skin depth. Therefore, significantly more eddy currents are produced with the added payload.

This would explain why the addition of 45% of the initial mass, results in a reduction of 13% reduction in levitation height (from 9.1 mm to 7.85 mm), as highlighted in Fig. 6.1d. Fig. 6.1c highlights the increase in levitation force with the addition of a conductive payload. This data was obtained using the transient mode of ANSYS Maxwell, the performance of which has been verified previously. It is a critical requirement of the magnetic levitation system for AM operations to maintain a constant position of the disc with no variation in position with powder deposition. The impact of powder deposition (as highlighted in Section 5.8.2) results in a slight deterioration of the levitation system performance by reducing the levitation height of the system. Thus, it was critical to develop a simple feedback controller to maintain the levitation height.

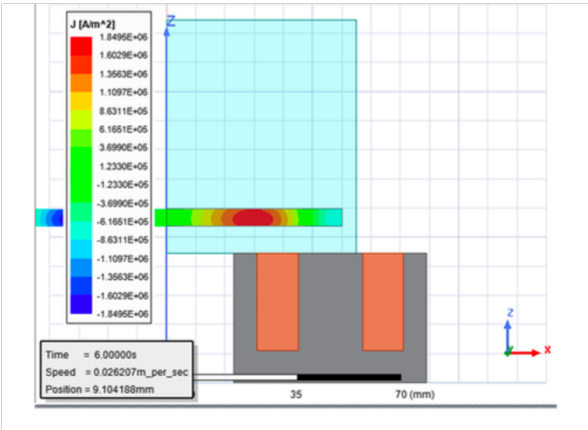

(a) Eddy Current Production from ANSYS Maxwell – With Only Disc

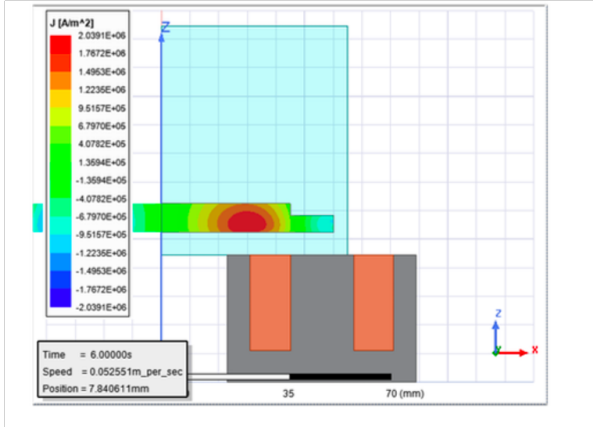

(b) Eddy Current Production from ANSYS Maxwell – Disc and Added Payload

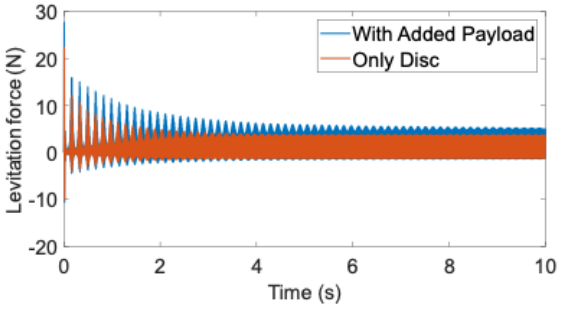

(c) Levitation Force vs Time from ANSYS Maxwell – With and Without Payload

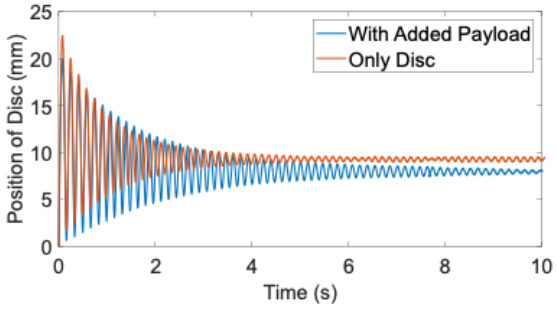

(d) Position of disc vs time from ANSYS Maxwell – With and without payload

Figure 6.1: Need for Feedback Controller

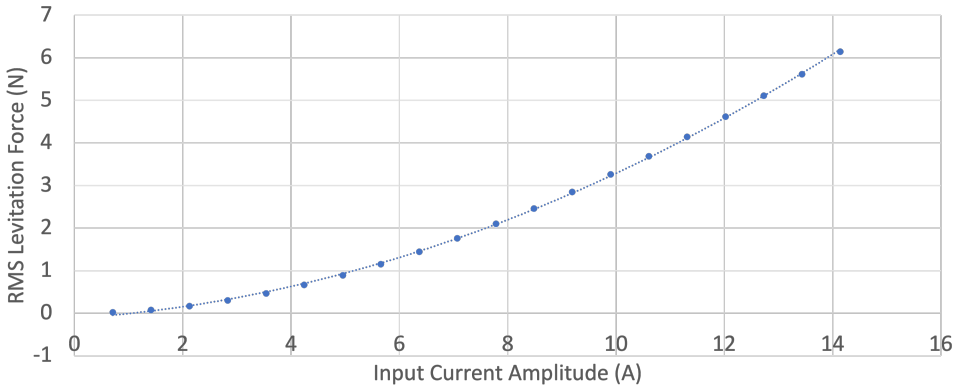

Figure 6.2: Levitation Force vs Amplitude of Input Current from ANSYS Maxwell

6.2 Controllability of the Magnetic Levitation System

The controllability of the system is defined as the ability to transfer the system from the initial state $x(0) = x_0$ to any desired final state $x(k_1) = x_f$ in a finite time. The first critical consideration for this is to study how effective the change of input (for this analysis, input current) is to the output (for this analysis, levitation force and position), keeping all other parameters constant. The initial study was conducted using ANSYS Maxwell. To determine the degree of controllability of the system, the input current was varied, and the levitation force was studied. The data was obtained from ANSYS Maxwell. For the analysis, the frequency and position of the disc were kept the same. The objective of the analysis is to develop a relationship between levitation force and input current to facilitate stable suspension 4 mm above the levitator at 150 Hz. As can be seen in Fig. 6.2, with a 0.5 A increase, there is an average 23% increase in levitation force when compared to the previous current step. This highlights a high degree of controllability of the system, according to ANSYS Maxwell.

6.3 Control System Performance Parameters

The three critical parameters used to study the performance of a control system and their associated measurement strategies are as follows:

- Rise Time: This parameter describes the time taken for the output (here, the position

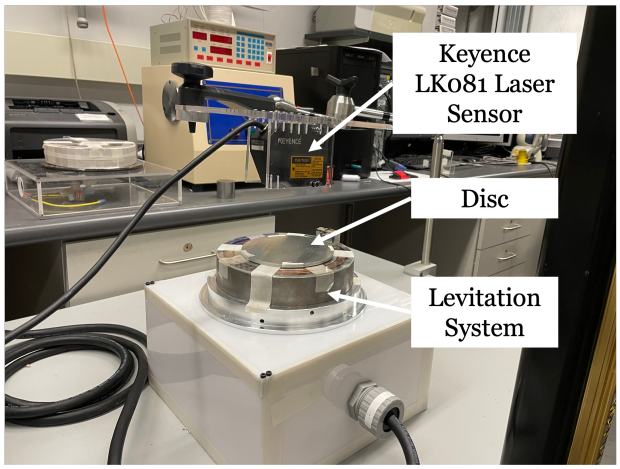

Figure 6.3: Experimental Apparatus for Feedback Controller

of the disc) to rise from one level to another level. The rise time is calculated for the output to rise from 10% to 90% for this system.

- Settling Time: The settling time is the amount of time needed after an input stimulation for an output to get to and stay in a specific error band. The settling time is calculated with the error threshold of 10%.
- Overshoot Error: Overshoot error is the deviation of the output signal above the desired setpoint. The overshoot error is calculated using the difference between the maximum output and the desired setpoint.

6.4 Experimental Apparatus

The system schematic of the experimental analysis of the control system is highlighted in Fig. 6.3. The hardware components used in the study of the positional feedback control system are as follows:

- Sensor: LK-081 laser sensor used. The sampling frequency is about 1000 Hz. The sensor has been used in an air environment. The use of the sensor in another environment would require recalibration to account for diffraction in different mediums.
- Controller: A simple Arduino Uno with digital Pulse Width Modulation (PWM) was used to supply output to the power supply.

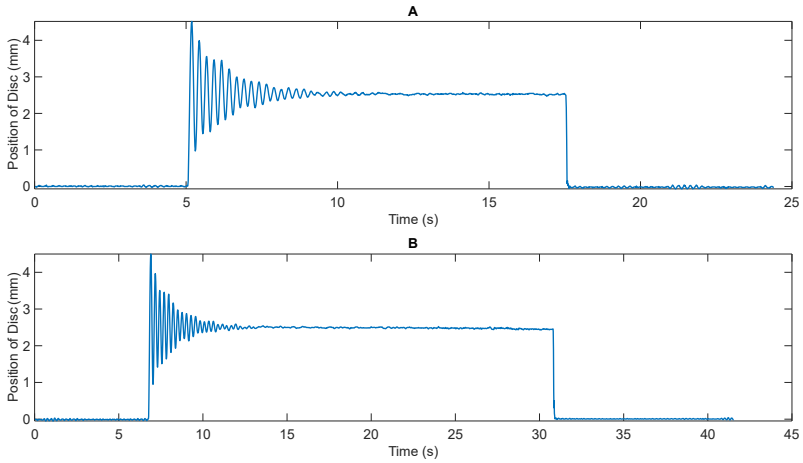

Figure 6.4: Position of the Disc Using LK081 sensor (a) No Averaging Filter (b) With an Averaging Filter

- Power Supply: The BK Precision 9832B power supply was used. The power supply can supply up to 300 V at frequencies between 50-1000 Hz.
- Interface: The digital I/O interface utilizing the DB25 connector was used to communicate between the Arduino Uno and the BK9832B. The Arduino supplied an analog output which was read by the power supply and resulted in the adjustment of the AC characteristics of the system.

6.5 Open Loop Performance of Levitation System

6.5.1 Sensor Output

Fig. 6.4a highlights the sensor output tracking the position of the disc vs time. A continuous sinusoidal wave of 150 V at 120 Hz is supplied to the coils.

It should be noted that even when the system is off, there are oscillations observed, as highlighted in Fig. 6.4a. When the system is off, the expected positional output should be constant, since no levitation occurs. This indicates a potential error in the read sensor data. The key culprit is suspected to be the analog-to-digital converter inbuilt within the Arduino Uno, with an absolute accuracy of 2 LSB [106].

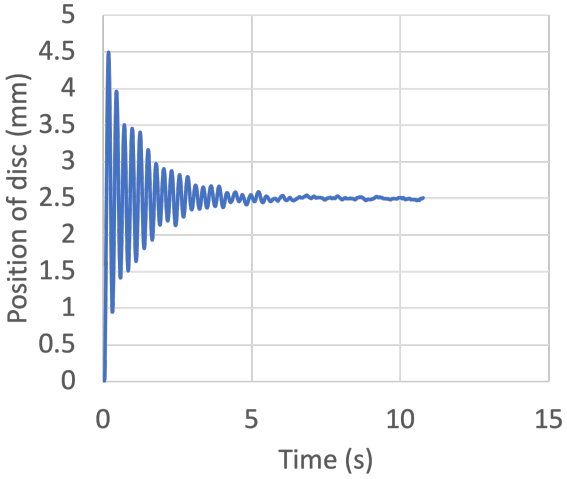

(a) Position of disc vs time with continuous harmonic input

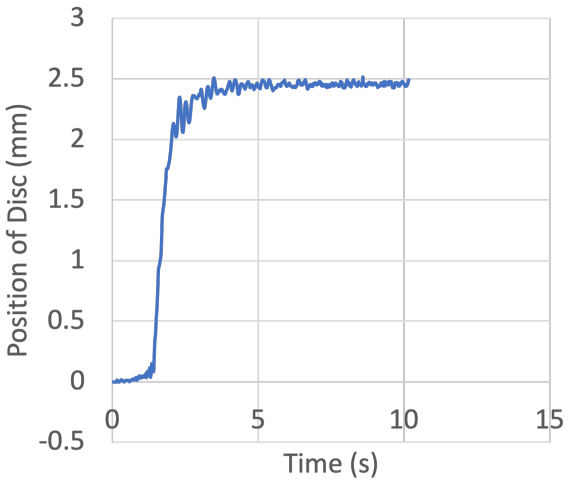

(b) Position of disc vs time with PWM input

Figure 6.5: Open Loop Performance of Levitation System

In order to overcome the error, a simple averaging filter was implemented. The averaging filter accepts several positional feedback data from the sensor and averages them to minimize the error. For this analysis, 50 sensor readings were averaged to obtain more reliable positional feedback data. The overall time for each cycle increased from 13 ms to 19 ms, however, the improvement in performance was worth the increase in time. The oscillations when the system is off are still not 0 probably due to some residual error from Arduino ADC error, as highlighted in Fig. 6.4b.

6.5.2 Types of Input to Levitation System

Fig. 6.5 highlights the comparison of the output position of the disc as a function of time with different modes of input. Fig. 6.5a highlights a continuous sinusoidal harmonic input. A significant overshoot of 1.992 mm and a settling time of 5.7 seconds are observed. However, the rise time is significantly lower, taking only 112 ms to achieve a levitation height within 10% of steady state levitation height.

Fig. 6.5b highlights the position of the disc as a function of time with the Arduino PWM input to the levitation coil. The rise time measured for this input is higher, taking 2.25 seconds to achieve 10% of the steady state levitation height. However, a significant

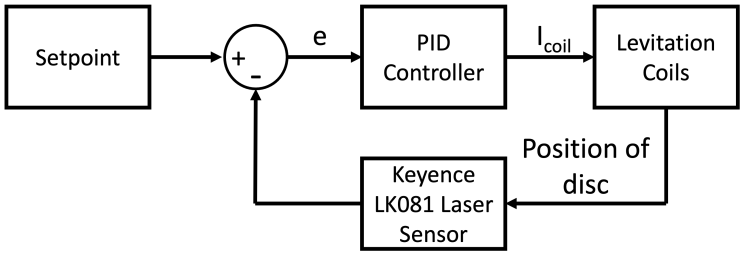

Figure 6.6: Schematic for Feedback PID Controller

improvement in settling time (2.51 s) and overshoot error (0 mm) is observed with the PWM input.

6.6 Closed Loop Performance of Levitation System - PID Controller

The feedback controller mechanism chosen is the proportional-integral-derivative (PID) controller. A PID controller is a feedback-based control loop that is frequently employed in industrial control systems and a wide range of other applications that call for continuously modulated control. When the desired setpoint (SP) and a measured process variable (PV) diverge, a PID controller constantly calculates an error value and makes a correction based on proportional, integral, and derivative terms (denoted P, I, and D respectively). This type of feedback controller is incorporated within the levitation system to improve the system's characteristics.

The PID control approach is chosen for this application owing to its simplicity in implementation, the widescale adoption of the control strategy in magnetic levitation applications [107, 108, 109] and the satisfactory performance produced by the controller, as highlighted in subsequent sections. The proposed controller is first analyzed in MATLAB/Simulink. The simulation of the feedback controller has been presented in Appendix A. The optimal gains for the controllers were obtained using the in-built Simulink PID tuner. Subsequently, the controller is implemented within the hardware infrastructure. Through experimental trial and error, the performance of the tuned parameters obtained from the Simulink tuner was verified. The block diagram for the developed PID controller is presented in Fig. 6.6. The controller implementation has been restricted to the laboratory setting.

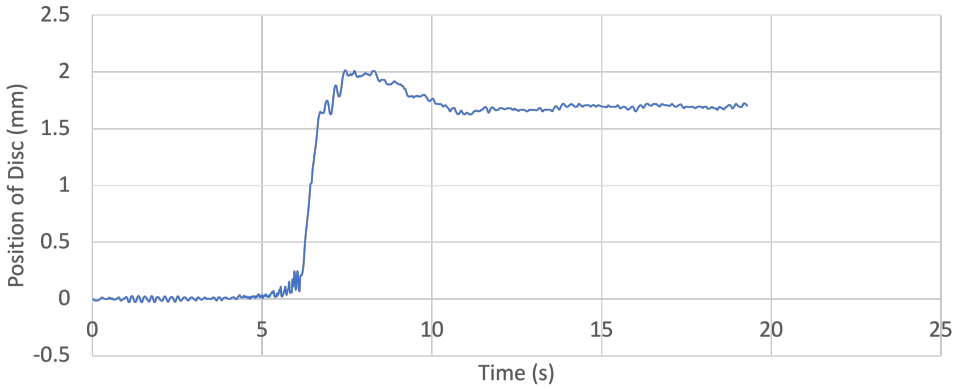

Figure 6.7: Position of Disc vs Time - With PID Controller

Table 6.1: Comparison of Open Loop PWM Input and PWM Input PID Control

Parameter	**Open Loop PWM Input**	**PID Controller with PWM Input**
Rise Time (s)	2.25	0.855
Settling Time (s)	2.51	9.234
Overshoot (mm)	0	0.3159

The averaging filter developed in Section 6.5.1 was incorporated into the controller. The tuned $K_p = 0, K_i = 0.25$, and $K_d = 0$ values obtained from the simulation analysis (Appendix A.1.2) were used in the experimental analysis. The input supplied is with PWM using the Arduino. The digital I/O interface of the power supply has been utilized to adjust the input. The resulting plot of the position of the disc vs time with the PID controller is highlighted in Fig. 6.7.

The comparison of the levitation system performance with PWM input and PID controller has been presented in Table 6.1. The PID controller has a significant improvement in rise time. However, there is an increase in overshoot error and settling time observed.

These errors can be attributed to the low K_i gain utilized for the controller. Due to the low K_i gain, the adjustment to input current is slower. This results in slower growth and slower adjustment to the controller. The critical consequence is an increase in settling time and an increase in overshoot error.

From Section 6.5.2 and Section 6.6, developing a control system with the overlapping features of the open loop system performance and closed loop PID controller will result in significant improvement in levitation system performance.

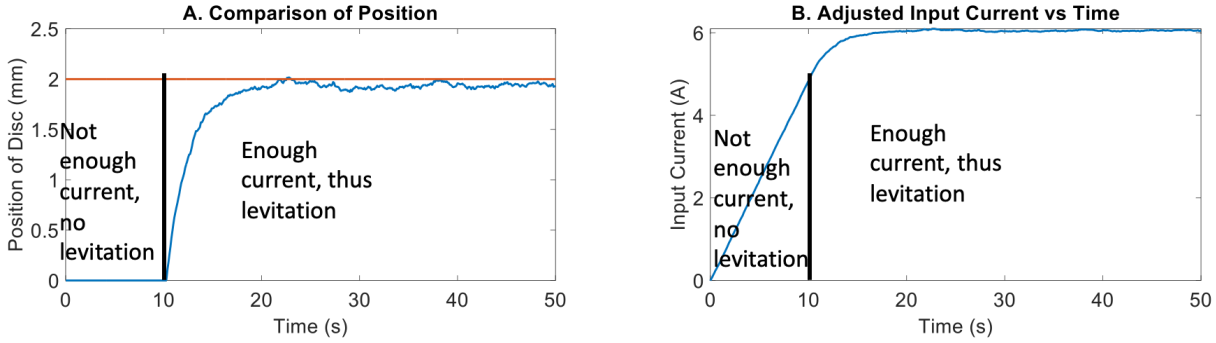

Figure 6.8: Performance of PID Controller - Simulation

6.7 Incorporation of Compensation Component

Fig. 6.8 highlights the impact of input current being initialized at 0. The adjustment of the input current is studied using the simulation, as presented in Appendix A.1. As can be seen, it takes a significant duration of time for the input current to reach the threshold of minimum current required for any levitation to be observed. Due to the small K_i value and K_p and K_d being 0, the controller takes a large duration of time to grow the input current to the required threshold. However, the incorporation of larger K_i, K_p, or K_d values results in the system overreacting to errors and increases system overshoot and steady-state error.

Through the incorporation of a compensator component that can initialize the current to a non-zero value depending on the desired setpoint, the overall performance of the levitation system can be improved.

6.7.1 Development of Compensator Component

The overall system schematic for the design of the PID controller with the compensator component is highlighted in Fig. 6.9a. The initial output is computed by modeling the relationship between the Arduino output and the position of the disc using the laser sensor. Through the developed relationship, the controller will initialize the input current as a non-zero value. The PID controller will then be tasked to adjust the input current to account for any deviations from the desired set point.

The Arduino Uno was connected to the power supply and given specific PWM values, following which the position of the disc was recorded using the LK081 sensor. For example,

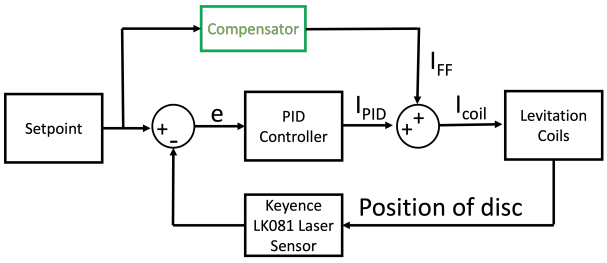

(a) Block diagram of Feedback Controller with Compensator

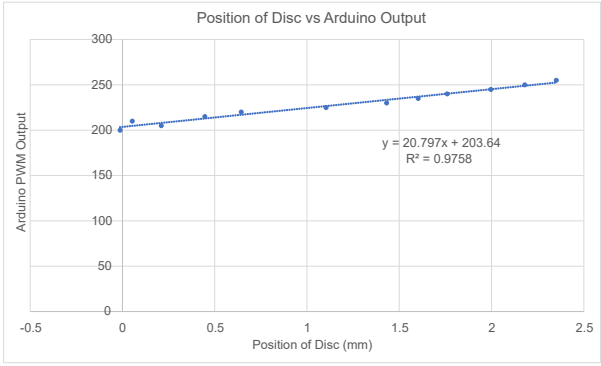

(b) Relationship between the position of the disc vs the output PWM of Arduino

Figure 6.9: Development of PID Controller With the Compensator Component

the output supplied using the Arduino PWM was set as 230, and the position read using the laser sensor was 1.43 mm. This process was repeated for several Arduino outputs. The resulting plot is shown in Fig. 6.9b. It should be noted that with a goodness of fit of 0.9758, the relationship developed will be quite reliable. However, the controller can tolerate some errors in this relationship since the feedback PID controller will adjust the input to account for any deviations from the set point.

6.7.2 Experimental Implementation of PID Controller with Compensator Component

The experimental result developed in Section 6.7.1 was used to initialize the input current, as highlighted in Equation 6.2. The remaining hardware components were identical to the conventional PID controller analysis presented in Section 6.6. The $K_p = 0, K_i = 0.25$, and $K_d = 0$ were also identical to the previous controller.

$$I_{compensator} = F(Position\ of\ Disc) \tag{6.1}$$

$$I_{input} = I_{compensator} + I_{PID} \tag{6.2}$$

Where $I_{compensator}$ is the initialized current using the compensator component, I_{PID} is the current input through the PID controller, and I_{input} is the input current to the levitation coils.

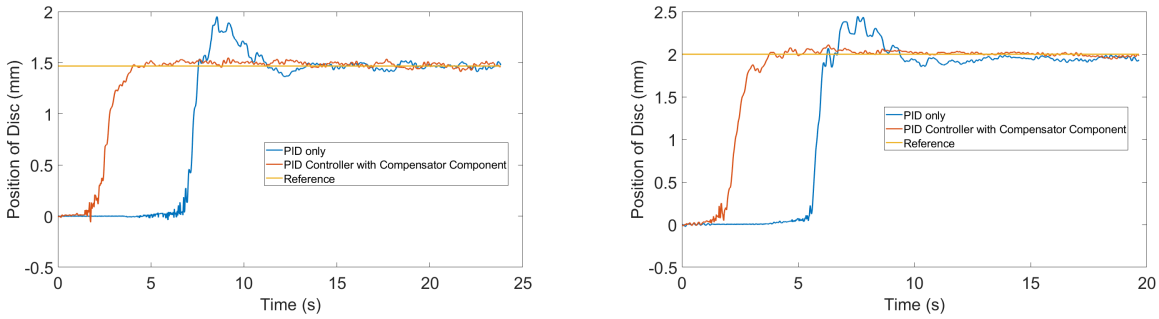

(a) Setpoint 1.468 mm

(b) Setpoint 2 mm

Figure 6.10: PID Controller with Compensator Component

Without any external disturbances, the performance of the PID controller with the compensator component is very similar to the open loop system performance with a PWM input. This is in line with expectations since the compensator component supplies a PWM input to initialize the current.

However, through the incorporation of the PID controller with the compensator component, the controller can adjust the input to overcome external disturbances. These disturbances are primarily caused by the addition of mass on the levitated disc, primarily through powder deposition within the AM environment.

The experiment with the compensator component was conducted for different desired setpoints. First, the desired setpoint was set as 1.468 mm, with the resulting comparison between PID controller and PID controller with compensator component highlighted in Fig. 6.10a. Next, the experiment was repeated with a setpoint of 2 mm, with the resulting comparison plot presented in Fig. 6.10b.

As can be seen, there is a significant improvement in the settling time and overshoot error with the incorporation of the compensator component with the PID controller for both setpoints. There is a decline in the rise time for both setpoints. However, due to the improvements in the settling time and overshoot error, the compensator component was selected as the optimum controller.

6.8 Multiple Level Control

Fig. 6.11 highlights the system's ability to levitate the disc at specific heights. Three distinct heights were selected here: First, the levitation occurs 1.6 mm above the levitator.

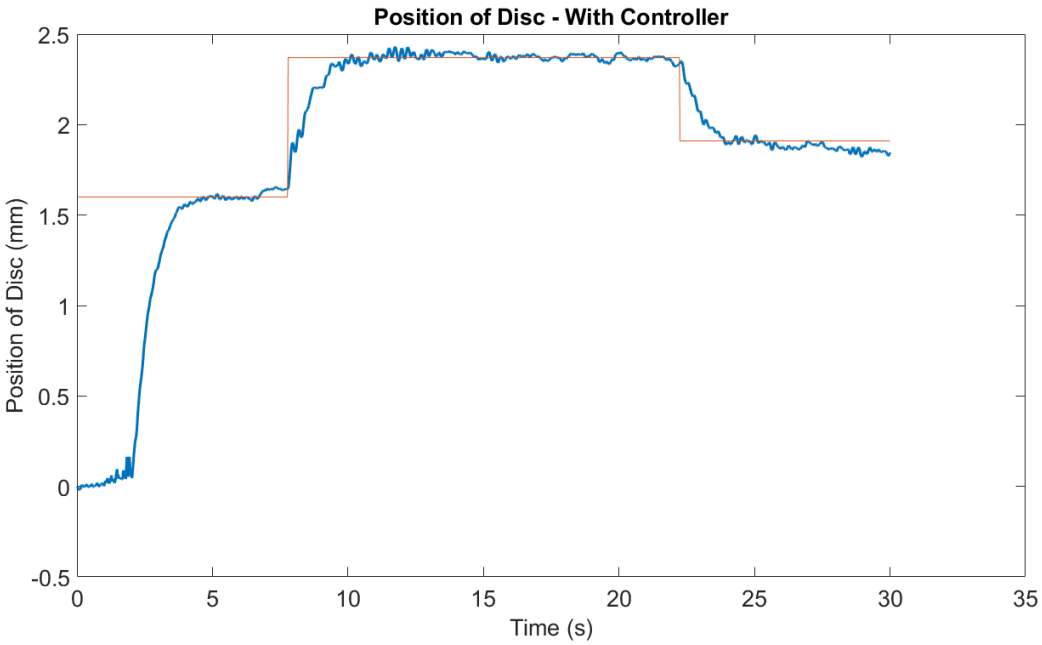

Figure 6.11: Levitation at Multiple Heights

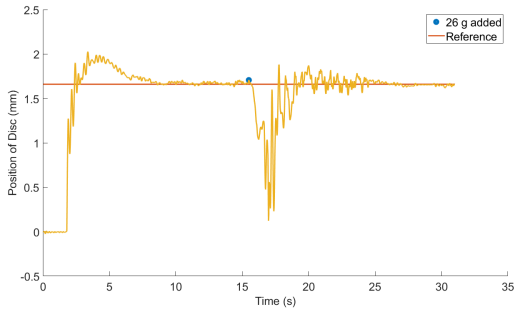

(a) Impact of the addition of 15.2 g weight

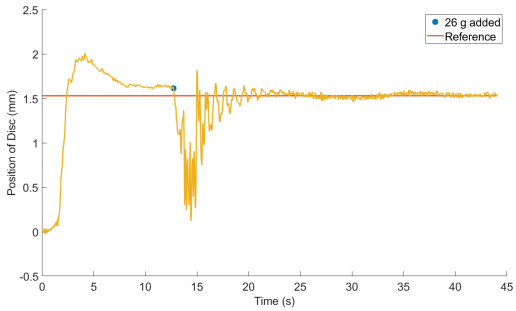

(b) Impact of the addition of 26 g weight

Figure 6.12: Performance of Levitation System with the Addition of Weight

Next, the levitation occurs at 2.37 mm above the levitation system. Finally, the levitation occurs at 1.91 mm above the levitation system.

6.9 Addition of Added Payload on Levitated Disc

A critical requirement of AM operations is the ability of the levitated disc to support added mass as a function of time. While within the AM environment, the added mass is anticipated to be more gradual, it was necessary to highlight the levitation system and its associated controller's ability to retain the desired levitation height despite the addition of an added payload. To conduct the analysis, a 16 g and 26 g weight was added to the levitated disc. The resulting plots are shown in Fig. 6.12a - 6.12b. The 15 g weight was added at 15.56 s, well after steady state levitation had been achieved, as highlighted in Fig. 6.12a. It took the system 5.72 s to settle between +/- 5% of steady state position (1.654 mm). For the addition of the 26 g aluminum disc, the weight was added at 12.72 s, well after steady state levitation had been achieved, as highlighted in Fig. 6.12b. It took the system 7.18 s to settle between +/- 5% of steady state position (1.52 mm). The higher settling time is in line with expectations since the addition of a heavier payload would result in higher disturbances.

6.10 Summary

To further improve the performance of the system to maintain stable steady state levitation to support AM applications, a one-dimensional controller was developed to adjust the input current. A conventional PID controller was developed that was able to significantly reduce the overshoot, however, the settling time and overshoot error of the PID controller was high. Through the incorporation of a compensator component to estimate the desired input to work in conjunction with the PID controller, the performance of the controller was improved. For the setpoint of 2 mm, a 58% reduction in settling time, and a 22% reduction in overshoot were observed. However, a decline of 83% is observed for the rise time. Due to the improvement in the performance of settling time and overshoot error, the PID controller with compensator component was pursued. The system's ability to support levitation height controllability and the ability to support added mass without losing any levitation height has also been highlighted. The PID controller and the compensator component with the PID controller have been implemented in the lab environment in this chapter.

Chapter 7

Levitation Ability of Materials

In [110], the physical characteristics of metals were studied to determine their viability for levitation. Two simple coil setups were used to do this. Through the use of eddy currents, the necessary levitation force was obtained to stably levitate the object. A ratio of **Levitation Force** to **Weight** of the object levitated was used for this analysis. The experiment was conducted with different metals to extract the levitation force for the two setups.

It was observed that the levitation ability of materials decreased with an increase in the atomic number of the element. This results in materials with small atomic numbers (like aluminum) being ideal for levitation. [110] also states that there is a detrimental impact of increasing the density of materials on their levitation ability.

7.1 Analytical Model

The working principle described in Section 3 is modeled analytically as shown in Eq. 7.1 (Faraday's Law), 7.2 (Ohm's Law) and 7.3 (Lorentz' Law):

$$E_{induced} = \frac{d\phi}{dt} \tag{7.1}$$

$$J = E_{induced}\,\frac{\sigma A_{conductor}}{l} \tag{7.2}$$

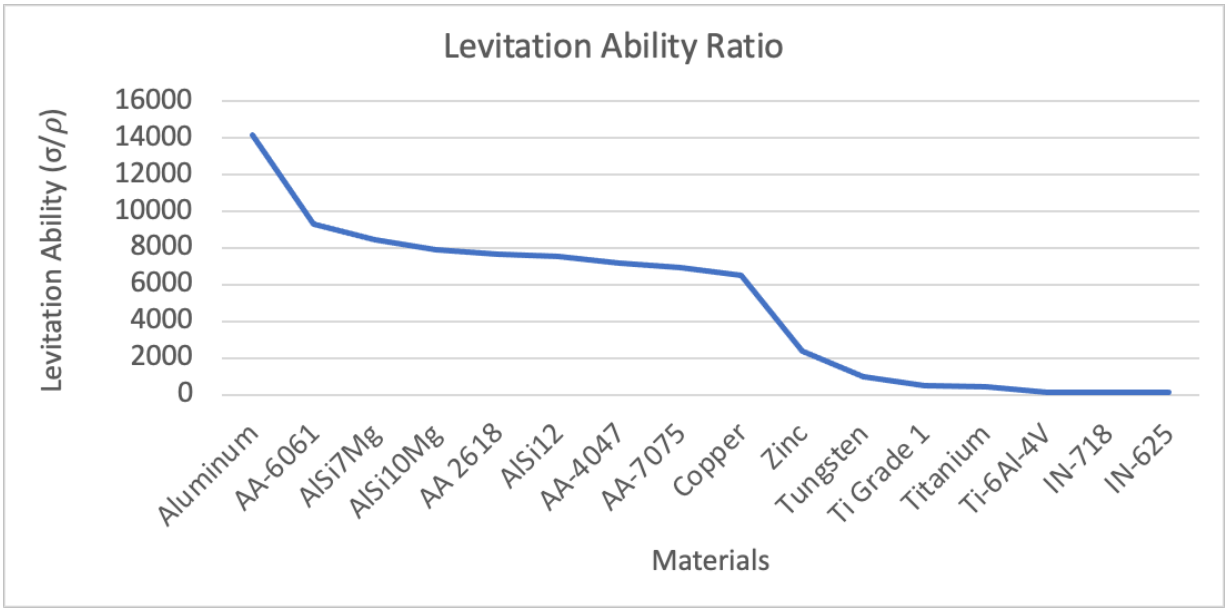

Figure 7.1: Levitation Ability: Ratio of $\frac{\sigma}{\rho}$ for Different Materials.

$$F_{lev} = \int J \times B dV \tag{7.3}$$

where J is the induced eddy currents, ϕ is the magnetic flux, B is the magnetic field, F_{Lev} is the levitation force, $E_{induced}$ is the induced emf, l is the length of the conductor, $A_{conductor}$ is the area of the conductor, σ is the conductivity of the material and dV is the differential volume of the conductor. The gravitational force of the levitated object is modeled as in Eq. 7.4.

$$F_{gravity} = mg = \rho V g \tag{7.4}$$

Where m is the mass of the object, ρ is the density of the material of the conductor, V is the volume of the levitated object and g is the gravitational constant. According to [110], the levitation ability of a material is defined as the ratio of the maximum levitation force experienced by the levitated object to the gravitational force experienced by the levitated object. This is described analytically in Eq. 7.4.

According to [110], the levitation ability of a material is defined as the ratio of the maximum levitation force experienced by the levitated object to the gravitational force experienced by the levitated object. This is described analytically in Eq. 7.5.

Table 7.1: Material Properties

Materials	Density ($\frac{kg}{m^3}$)	Conductivity $\frac{S}{m}$	Materials	Density ($\frac{kg}{m^3}$)	Conductivity $\frac{S}{m}$
Aluminum	38000000	2689	Copper	58000000	8933
AA 6061	25063000	2700	Zinc	16700000	7140
AlSi7Mg	22700000	2680	Tungsten	18200000	19300
AlSi10Mg	20400000	2590	Ti Grade 1	2222200	4510
AA 2618	21277000	2770	Titanium	1820000	4500
AlSi12	20000000	2650	Ti6Al4V	561800	4430
AA 4047	19140000	2660	IN 718	800000	8190
AA 7075	19417000	2810	IN 625	775190	8440

$$Lev\ Ability = \frac{F_{lev}}{F_{gravity}} = \frac{\int J \times BdV}{\rho V g} \tag{7.5}$$

As it can be seen from Eq. 7.1 - 7.3, the only material property that affects the levitation force of the conductor is the conductivity of the material. As evident from Eq. 7.4, the only material property of the material that affects the gravitational force on the object is the density of the material. Thus, the levitation ability of materials can be represented as the ratio of conductivity to the density of the material, as shown in Eq. 7.6.

$$Lev\ Ability = \frac{F_{lev}}{F_{gravity}} = \frac{\int J \times BdV}{\rho V g}\ \alpha\ \frac{\sigma}{\rho} \tag{7.6}$$

The pertinent material properties have been highlighted in Table 7.1. The material properties have been obtained from [111, 112]. Several different materials were considered for the analysis with applications within AM techniques, as highlighted in Table 7.2. A strong emphasis is placed on materials used for additive manufacturing applications since the technique is critical to determining the compatibility of different materials employed for AM operations with the levitation system and its associated application. The levitation ability of different materials using the levitation ability parameter developed has been highlighted in Fig. 7.1.

Table 7.2: Applications of Materials in AM

Materials	**Application**
AA 6061	Manufacturing of bars, sheets, foils using Laser Powder Bed Fusion AM [113]
AlSi7Mg	Used in applications of Wire Arc AM and Laser Powder Bed Fusion AM [114] - [114]
AlSi10Mg	Used in Selective Laser Melting (SLM) AM applications [115] - [116]
AA 2618	Used in the autmotive, defence, aircraft industry using SLM AM technique [117]
AlSi12	Used in SLM AM applications [115]
AA 4047	Used in LDED-PF AM techniques [118]
AA 7075	Applications in the aerospace industry using various AM techniques [119]
Copper	Applications in SLM, Selective Electron Beam Melting (SEBM) and binder jetting (BJ) AM applications [120]
Zinc	Applications in the biomedical industry using Laser Powder Bed Fusion AM [121]
Tungsten	Used in SLM AM technique [122]
Titanium	Biomedical applications using SLM AM applications [123]
Ti6Al4V	Applications in the aerospace and medical implants using laser powder bed fusion (LPBF) technique [124]
IN 718	Applications using SLM AM technique [125]
IN 625	Applications in the aerospace and gas turbine using electron beam powder bed fusion (EPBF), LPBF AM, and binder jetting technology [126]

Table 7.3: Specifications for Simulation Analyses

Specifications	Prototype 0	Prototype 1	Prototype 2	Prototype 3
Diameter of Disc	50 mm	50 mm	120 mm	120 mm
Height of disc	5 mm	5 mm	5 mm	5 mm
Height of Suspension	2 mm above lev	2 mm above lev	2 mm above lev	2 mm above lev
Input: Coil 1	5 A	4.6582 A	300 V	200 V
Input: Coil 2		2.7844 A		
Frequency of Input	50 Hz	50 Hz	85 Hz	150 Hz

7.2 Simulation Analysis

ANSYS Maxwell has been used for the simulation analyses. The levitation force is extracted from ANSYS Maxwell. Through the use of ANSYS Maxwell, the performance of the levitation ability parameter has been verified for Prototype 0, Prototype 1, Prototype 2, and Prototype 3. The specifications and pertinent parameters for the simulation analysis of each prototype are highlighted in Table 7.3. The levitation force in the axial (z-axis) is extracted from ANSYS Maxwell and the weight is calculated analytically. The resulting ratio of Levitation Force to the weight of the disc is compared to the analytically developed levitation ability parameter.

Fig. 7.2 highlights the overall performance of the levitation ability parameter through simulation analysis. The general trend of the levitation ability parameters through all prototype simulations has been highlighted in Fig. 7.2a. As it can be seen, the performance of different materials relative to aluminum has been highlighted. The general trend of output levitation ability follows the same trajectory as the simulation-based data, thereby verifying the overall performance of the parameter.

The direct numerical comparison in the form of a bar graph has been highlighted in Fig. 7.2b. The maximum deviation from the analytical model recorded for materials is 8%. This error can be attributed to meshing errors of simulations.

7.3 Summary

The novel methodology of using the ratio of conductivity of the levitated geometry's material (σ) to the density of the material (ρ) to determine the compatibility of different materials within the AM sphere with magnetic levitation applications were also discussed.

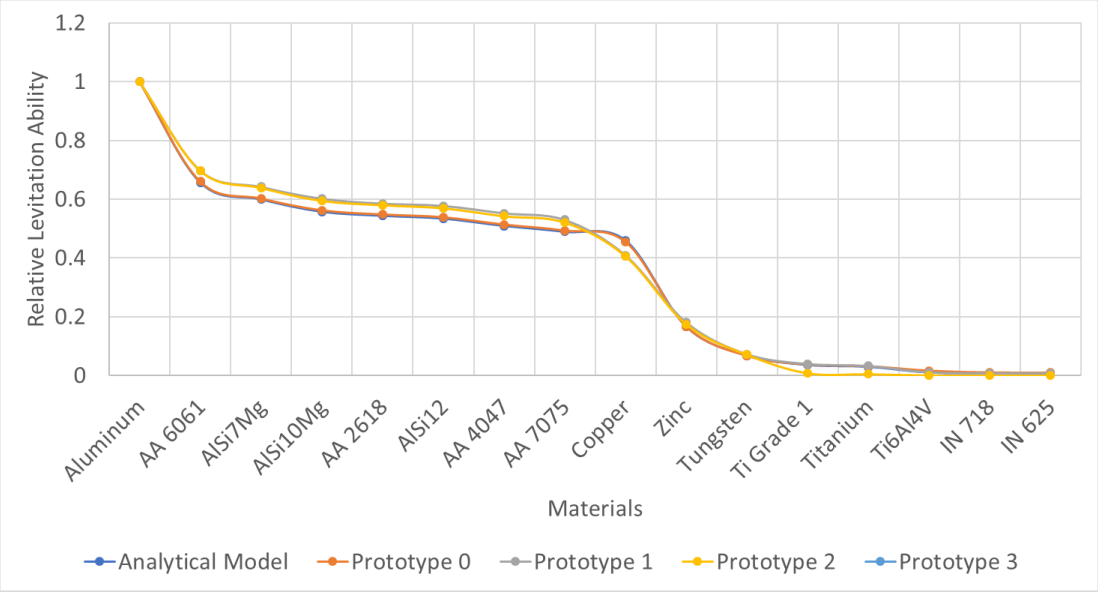

(a) General trend of relative levitation ability

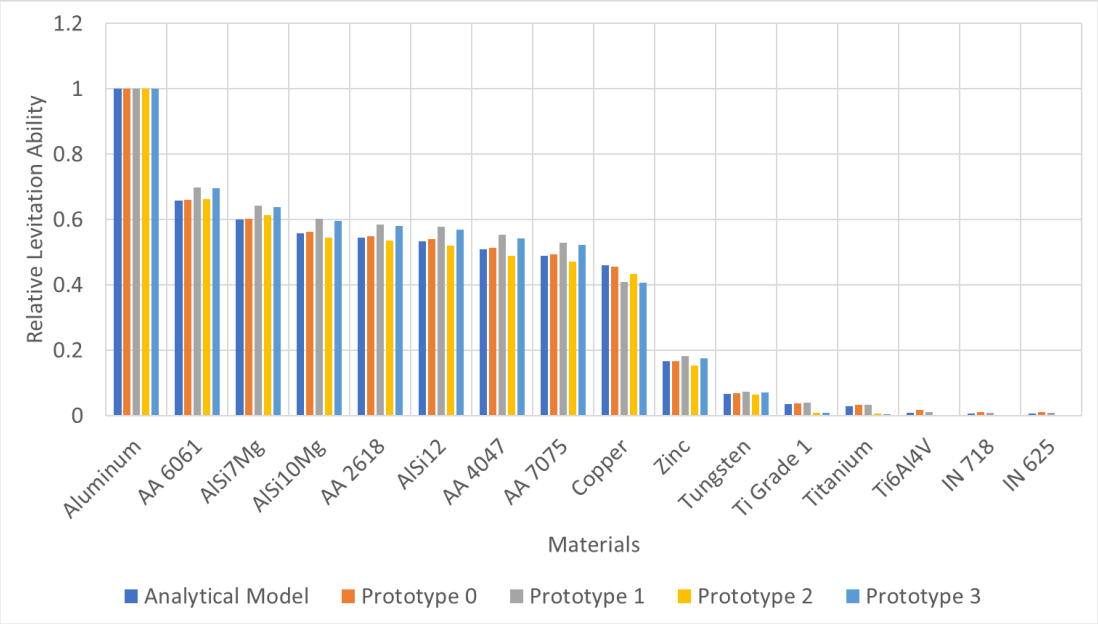

(b) Bar graphical comparison of levitation ability of different materials with different prototypes

Figure 7.2: Simulation-Based Verification of the Levitation Ability Parameter

The newly developed method relies solely on material properties for the determination of the levitation ability of materials, as opposed to experimental analyses.

The technique offers a simple analytical model to determine the compatibility of different materials with magnetic levitation techniques. The parameter was verified across the four levitation system prototypes developed throughout this research. The resulting data verifies the performance of the parameter across a wide variety of paramagnetic materials.

Chapter 8

Magnetic Levitation Experiments within Laser Directed Energy Deposition via Powder Feeding Applications

8.1 System Description

The levitation system developed in Chapter 5 was subsequently used for the experimental implementation within the LDED-PF setup. The DMDIC106 machine was utilized for the study. The system has a working envelope of $35 \times 35 \times 35\ cm^3$ and relies on the use of a robotic arm to facilitate the build. The coaxial nozzle comprises a high-power laser in the center with two powder feeders. The experimental apparatus for the levitation experiment has been highlighted in Fig. 8.1.

There were several critical considerations that needed to be addressed to facilitate the safe operation of this experimental setup (highlighted in Fig. 8.1a). First, the levitation system's electrical safety was addressed by enclosing all wiring inside the enclosure. The enclosure and the levitation system were subsequently covered and sealed to prevent powder instrusion. Next, the overall volume of the levitation system was only 38.4% of the available working space within the DMDIC106 machine, as shown in Fig. 8.1b. Therefore, a sufficient clearance was provided to facilitate all AM operations safely. Finally, the levitated geometry, i.e., the disc was sand blasted to minimize laser back reflection that might damage the laser.

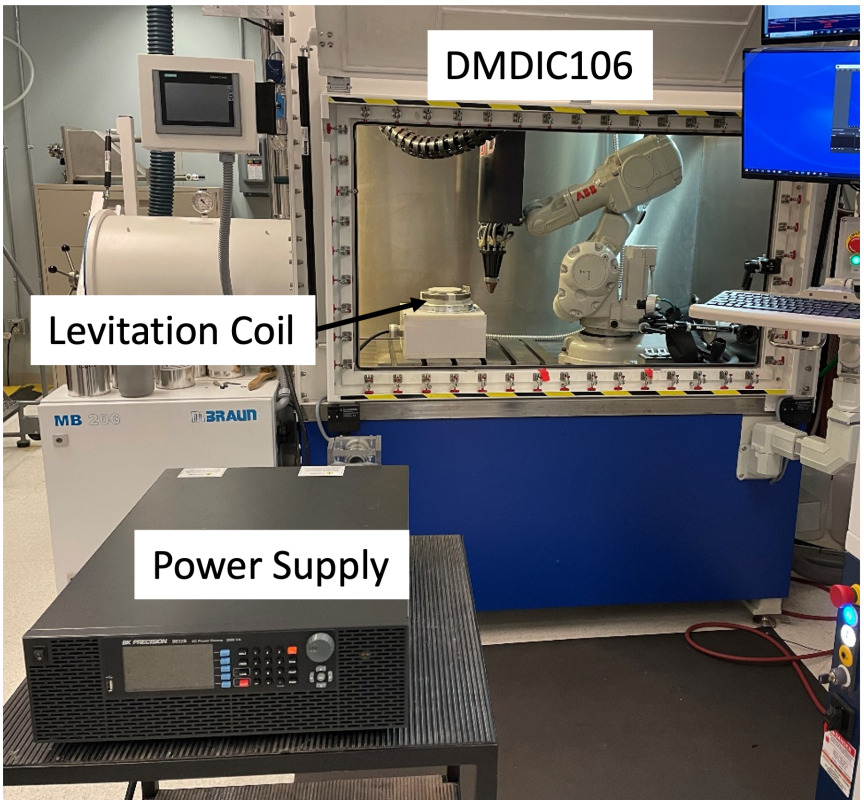

(a)

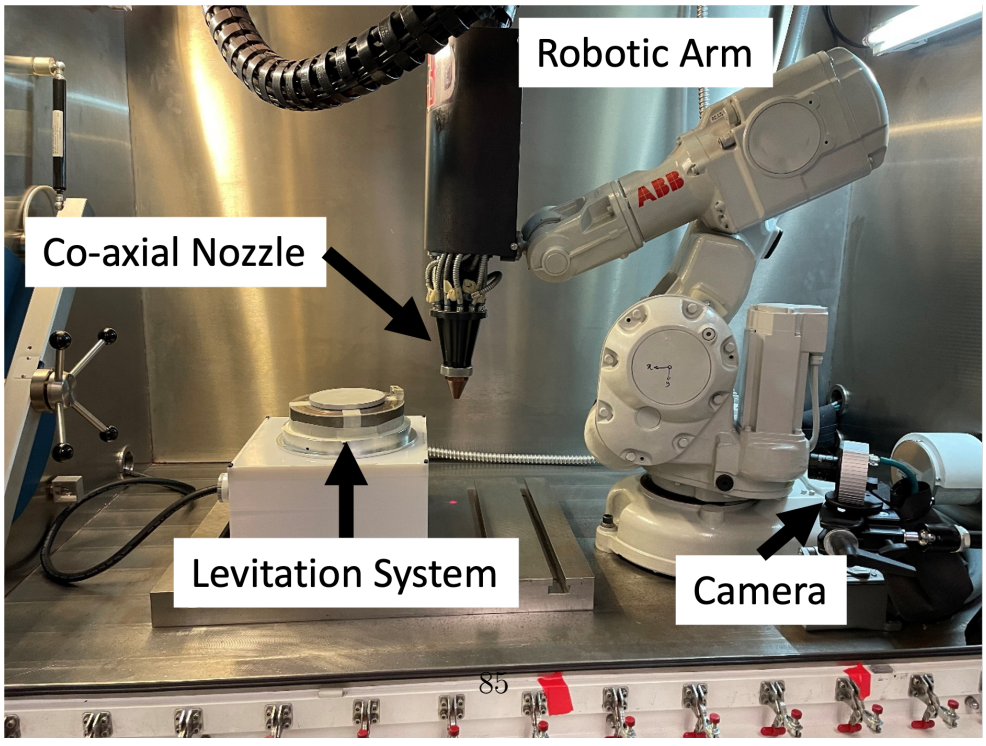

(b)

Figure 8.1: Experimental Apparatus for Magnetic Levitation Experiment in AM Machine

Table 8.1: Process Parameters for AM Operation

Parameter	Value
Powder feed rate	12 g/min
Laser power	1500 W
Laser scanning speed	5 mm/s
Powder material	Copper
Disc material	A7075, A6061
Velocity of powder	2.546 m/s

Table 8.1 highlights the selected process parameter to conduct the powder deposition operations. [127] presents the process parameters for the deposition of copper on a stainless steel disc. It uses a laser power of 600-1800 W, a scan speed of 5-11.6 mm/s, and a powder feed rate of 4-8 g/min. A powder feed rate of 12 g/min was used in this study to verify the stability of the levitated disc with high powder feed rates. The velocity of powders was calculated using the radius of the outlet of the material nozzle and the volumetric flow rate through the nozzle [99].

8.1.1 Experimental Verification of Compatibility of the Magnetic Levitation System

Section 5.8.2 highlighted the simulated performance of the magnetic levitation system while incorporating the effect of powder deposition through a worst-case scenario analysis. The study presented in this section aims to verify the validity of the simulation-based analysis. It is also critical to determine whether the levitation system could withstand the impact of powder deposition on the ends of the disc as well as in the center.

The disc was suspended above the levitation system. The powder deposition process was facilitated without the laser. For the analysis, a 60 mm radius and 7.5 mm height disc of A7075 were used. The levitation system was operated with an input of 190 V at 150 Hz (resulting in a 7 A input current).

The material nozzle was initially placed on one end of the levitated disc. Following this, the material nozzle was moved to the center of the disc. Finally, the material nozzle was moved to the other end of the disc. The levitated disc maintained its stability throughout the study. This verifies the conclusion drawn in Section 5.8.2: The levitated disc will maintain its stability with the impact of powder particles.

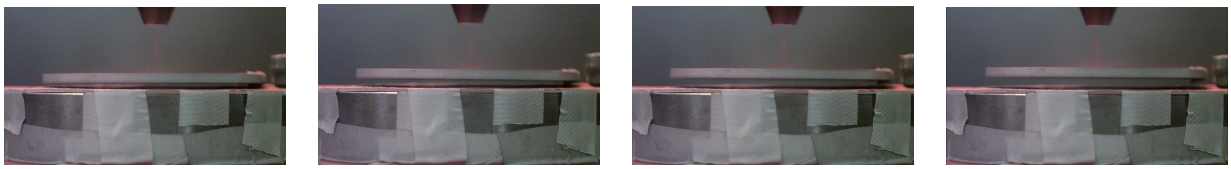

(a) Height 1 = 4.9 mm (b) Height 2 = 6.5 mm (c) Height 3 = 7.2 mm (d) Height 4 = 8.1 mm

Figure 8.2: Powder Deposition with Disc Levitated at Different Heights

The experiment was repeated with the laminated core system as well. For the analysis, the levitation system was given an input of 300 V at 90 Hz (resulting in about 5 A input). The levitation disc maintains its stability despite the impact of powder particles.

8.2 Powder Deposition with Laser

Having established the stability of the levitation input at the maximum allowable input, the next critical consideration was the stability of the levitation system at lower inputs. It should be noted that both the levitation force in the axial and lateral axes and the restoration forces in the lateral axes are contingent on the input supplied to the levitation system. Thus, providing a lower input to the levitation coils would also result in lower forces in the axial axis. 4 different levitation heights were considered for this analysis: 4.9 mm (Fig. 8.2a), 6.5 mm (Fig. 8.2b), 7.2 mm (Fig. 8.2c) and 8.1 mm (Fig. 8.2d). The input to the levitation system varied between 150 V and 200 V (resulting in 5.5 - 7.3 A current) at 150 Hz. As highlighted in Fig. 8.2, the system maintained its stability at the various heights discussed. The resulting data clearly highlights the system's ability to produce sufficient forces in the lateral and axial axes at inputs lower than the maximum allowable input.

The A7075 disc of 120 mm diameter and 7.5 mm height was utilized for the first analysis. Fig. 8.3 highlights the deposition of copper powder from a layer-by-layer perspective. A 190 V at 150 Hz input (7 A) was supplied to the coils. As highlighted in Fig. 8.3a - 8.3g, it is evident that there is an increase in the levitation height of the disc for the same input. 7 layers were deposited successfully.

The variation of measured levitation height with the addition of each layer is highlighted in Fig. 8.4a. The increase in the levitation height can be explained by the additional eddy currents induced within the deposited copper. Copper is a highly conductive material. With the deposition of additional layers, there is an increase in the volume within which

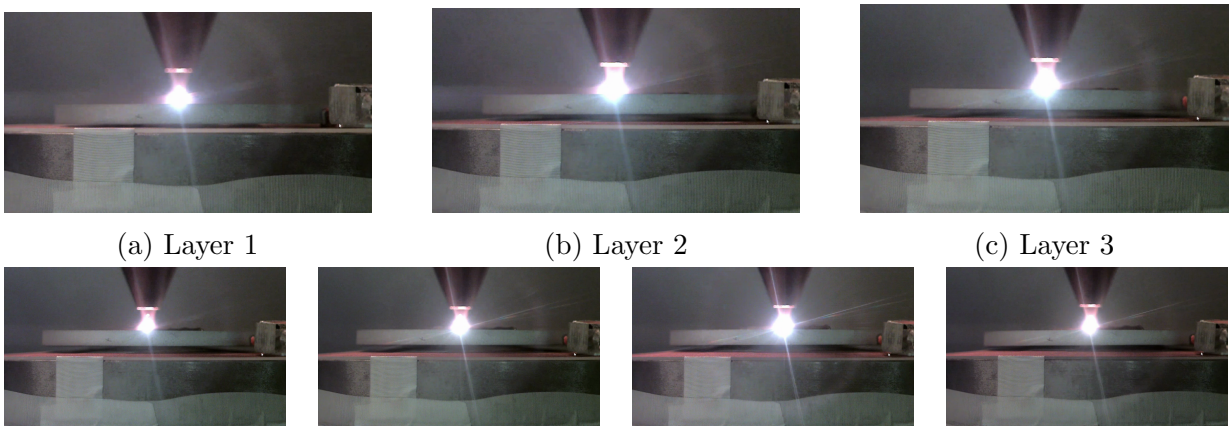

(a) Layer 1 (b) Layer 2 (c) Layer 3

(d) Layer 4 (e) Layer 5 (f) Layer 6 (g) Layer 7

Figure 8.3: Powder Deposition with Laser on AA7075 Aluminum Alloy Disc

eddy currents can be induced. This increased volume for eddy current induction results in more eddy current generation, since these deposited layers are still within the skin depth at 150 Hz (skin depth of aluminum $\delta = 6.7\ mm$, the skin depth of copper $\delta = 5.323\ mm$ according to Equation. 3.10). Thus, there are more eddy currents interacting with the source magnetic field to produce the lifting force responsible for the stable suspension of the aluminum disc.

This was tested using ANSYS Maxwell. The layer length, width, and deposited mass per layer were known. The height of each deposited layer was calculated from these parameters. These layers were then fed into ANSYS Maxwell and the levitation force was extracted with the addition of each layer. It should be noted that for this analysis, the disc was held 5 mm above the levitation system.

The resulting data of levitation force extracted from ANSYS Maxwell has been highlighted in Fig. 8.4b. As it can be seen, there is a clear increase in the levitation force with the addition of each copper layer, confirming the effect of adding a conductor and the subsequent increase in volume available for eddy current induction. The levitation force tends to increase with the addition of layers and subsequently stagnate. This would result in the weight, eventually, becoming higher than the levitation force to result in the deterioration of the levitation performance, which is in line with expectations.

The effective levitation force, which is the difference between the levitation force and weight of the levitated geometry, was also documented in Fig. 8.4c. As evident, the effective force reaches a peak and then decreases, which is in agreement with the observed

trend of an initial rise and the subsequent fall of the levitated geometry with the addition of layers. The effective force of the levitated disc becomes negative after reaching a threshold beyond which the weight of the disc and deposited layer is greater than the levitation force the geometry is able to produce. This is also in line with expectations.

Further testing was conducted using ANSYS Maxwell, where the disc was held at the measured levitation height and the layers were added on top of the A7075 disc, as shown in Fig. 8.4a. Fig. 8.4d highlights the comparison of levitation force extracted from ANSYS Maxwell and the weight (i.e., the gravitational force the levitation system must overcome to facilitate stable suspension). As it can be seen, the levitation force extracted from ANSYS Maxwell is in relatively close agreement, with a maximum error of 13% observed. This error can be attributed to the meshing errors of the simulation analysis and slight inaccuracies associated with the measurement of levitation height.

The powder deposition experiment was repeated with the laminated core system as well. Here, an A6061 aluminum disc of 60 mm diameter and 5 mm height was utilized. The levitation coils were given an input of 300 V at 90 Hz, which resulted in a 4.35 A of current. The deposition process on a layer-by-layer basis has been highlighted in Fig. 8.5a - Fig. 8.5d.

ANSYS Maxwell was utilized to study the levitation force at the measured levitation heights. The measured levitation heights are highlighted in Fig. 8.5e. As highlighted in Fig. 8.5f, the levitation force at the measured levitation height is in close agreement with the anticipated force, i.e., the weight of the levitated geometry.

8.3 Deposition on Both Sides of the Disc

Following the success of powder deposition with laser on one side of the levitated disc, there was a need to expand the overall build surface available for AM applications. This entailed conducting deposition activities on one side and facilitating deposition on the other side of the levitated disc. Thus, an analysis was conducted where the powder deposition activities were conducted on both sides of the levitated disc. Here, side 1 refers to an arbitrarily selected side used for the first set of deposition activities and side 2 refers to the other side of the levitated geometry used for the second set of deposition activities. An A6061 disc of 60 mm radius and 5 mm height was used for the analysis.

The results of these deposition activities have been highlighted in Fig. 8.6 and Fig. 8.7. Four layers of copper were deposited on side 1 and 5 layers were deposited on the other side. For side 1, the input to the coils was 200 V at 150 Hz. For side 2, the input was 300

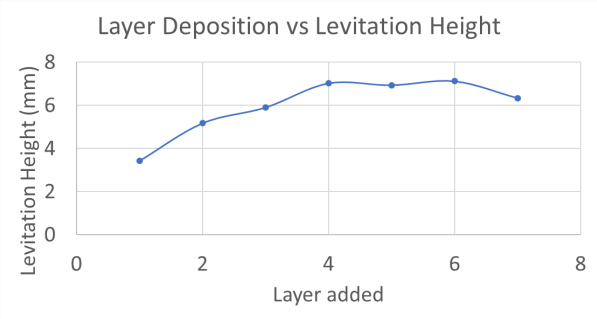

(a) Measured levitation height with incremental layer deposited

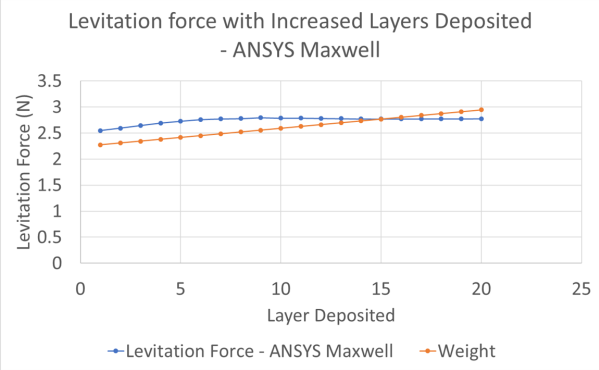

(b) Variation of levitation force vs layer deposited with the disc at 2 mm above the levitation system

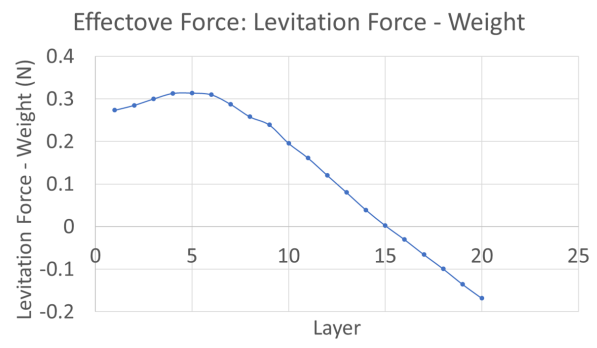

(c) Progression of effective force vs layers deposited

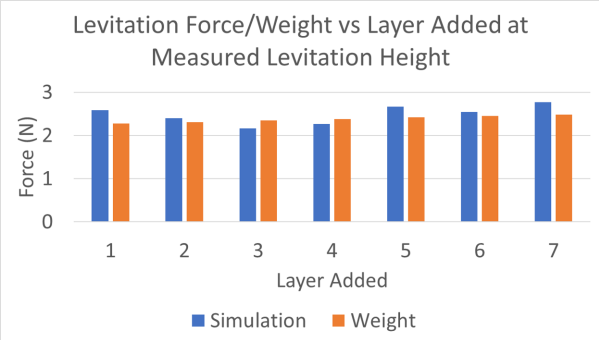

(d) Levitation forces extracted from ANSYS Maxwell at measured levitation height

Figure 8.4: Analysis for A7075 Powder Deposition with Laser Process

(a) Layer 1

(b) Layer 2

(c) Layer 3

(d) Layer 4

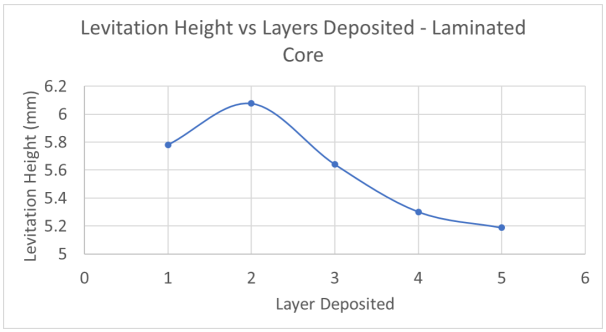

(e) Measured levitation height

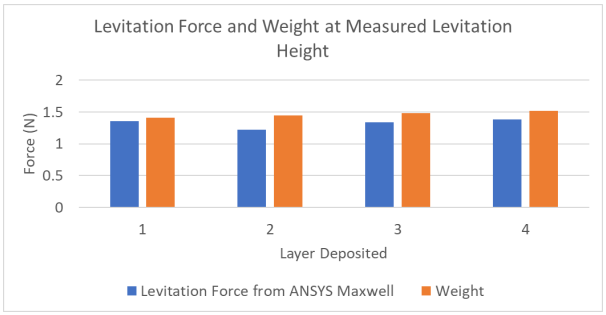

(f) Levitation force at measured levitation height with added layer from ANSYS Maxwell

Figure 8.5: Powder Deposition with Laser - Laminated Core System

V at 250 Hz, to increase the overall levitation force and facilitate stable suspension despite the added mass.

The levitation height was measured for both deposition activities, as highlighted in Fig. 8.6e for side 1 and Fig. 8.7f for side 2. As done previously, the levitation force was extracted from ANSYS Maxwell at these levitation heights and was in close agreement with the anticipated force, i.e., the weight of the disc and layers deposited.

Throughout the process, the system maintained its stability and performed in line with expectations. Thus, the overall build surface to build the part was increased by flipping the levitated substrate.

8.4 Results and Discussions

8.4.1 Successful Levitation and Layer Deposition

The deposition of copper powder on a levitated aluminum disc has been successfully presented in this chapter. The quality of the layers deposited in the first experiment (highlighted in Section 8.2) has been highlighted in Fig. 8.8a. The deposition activities were

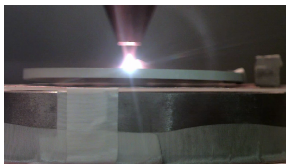

(a) Layer 1

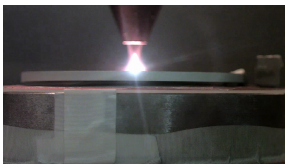

(b) Layer 2

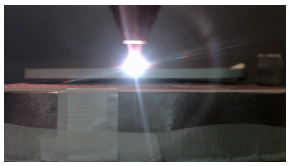

(c) Layer 3

(d) Layer 4

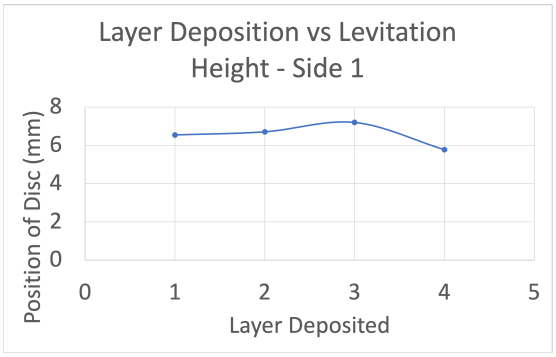

(e) Measured levitation height with each layer

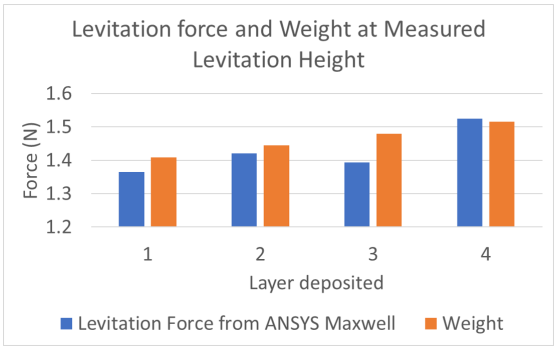

(f) Levitation force at measured levitation height with added layer from ANSYS Maxwell

Figure 8.6: Power Deposition with Laser on AA6065 Aluminum Disc - Side 1

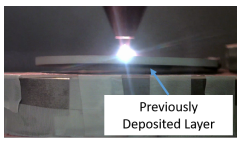

(a) Layer 1

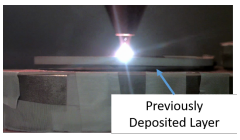

(b) Layer 2

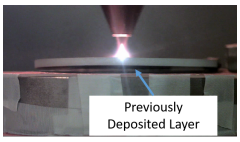

(c) Layer 3

(d) Layer 4

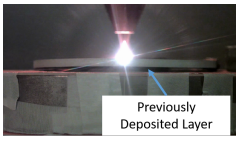

(e) Layer 5

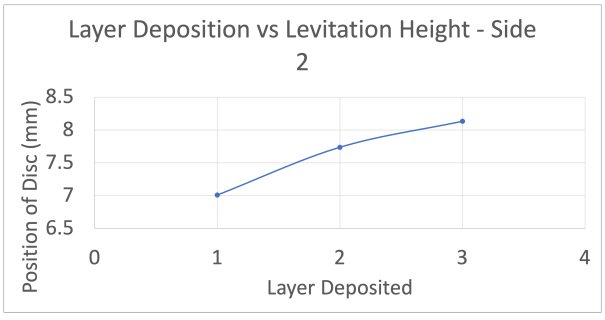

(f) Measured levitation height

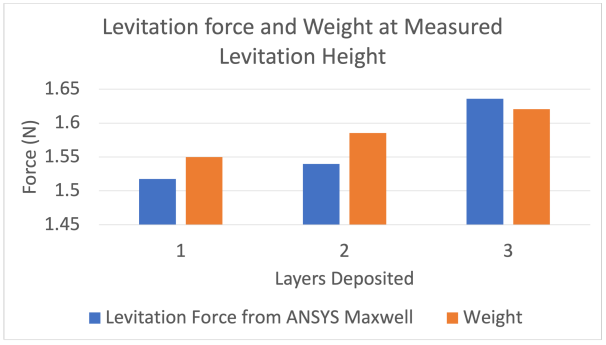

(g) Levitation force at measured levitation height with added layer from ANSYS Maxwell

Figure 8.7: Power Deposition with Laser on AA6065 Aluminum Disc - Side 2

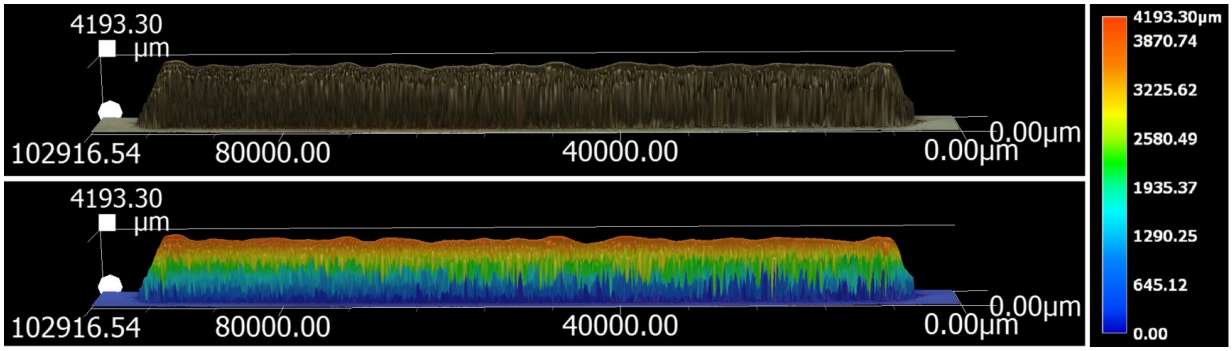

(a) Quality of layers deposited in Section 8.2

(b) Deposition of 'MAGLEV' on side 1 of disc

(c) Deposition of 'MSAM' on side 1 of disc

Figure 8.8: Results of Deposition with Magnetic Levitation System

also conducted on either side of the disc, with 'MAGLEV' being deposited on one side and 'MSAM' being deposited on the other. It resulted in an increase in the weight of the disc by 40 g. Parts built using this magnetic levitation system have been highlighted in Fig. 8.8b - 8.8c. The figure also highlights 3D printing activity results on both sides of the disc.

8.4.2 Effect of Powder Feed Rate

According to [127], conventional copper deposition on stainless steel disc operations requires the use of a powder feed rate of 4 g/min to 8 g/min. Thus, the use of 12 g/min is considered a relatively high powder feed rate for AM operations. In addition, the simulation analyses highlighted in Section 5.8.2 show that the levitation disc retains its stability with significantly higher powder dispersion force. Thus, the stability of the levitation system has been clearly highlighted.

8.4.3 Effect of Laser Power

According to [127], the laser power utilized for the deposition of copper on stainless steel disc was between 600 W to 1800 W. Thus, the levitation system maintains its stability with a high laser power of 1500 W without losing stability. This highlights the compatibility of the levitation system with other AM operations utilizing lower laser power.

8.4.4 Effect of Increase in Temperature of Levitated Disc

Following the deposition of over 5 layers, there is a steep increase in temperature observed within the levitated geometry, from room temperature ($24°C$ to $105°C$), measured using a Digi-Sense Infrared Thermometer Model 20250-06 before and after the deposition activities. According to [128], there is a 16% decrease in the conductivity of aluminum with the increase in temperature highlighted.

As highlighted in Chapter 7, the levitation force on the levitated disc is directly proportional to the conductivity of the material. Thus, there is a reduction in levitation force expected.

According to the analysis conducted in ANSYS Maxwell, the decrease in conductivity results in a 10% reduction in the overall levitation force experienced by the levitated aluminum alloy disc. However, the system can maintain its stability despite the 10% reduction in the levitation force.

8.4.5 Effect of Input Voltage and Frequency on Levitation System

The input voltage and frequency of the input to the coils within the levitation system play a critical role in the performance of the system. The input voltage and frequency are crucial to determine the levitation height of the levitated disc and the stabilizing restoration forces in the lateral axes to maintain stable levitation over time. Thus, it was critical to determine if the levitation system would maintain stability for input lower than the maximum allowable input. As highlighted in Section 8.2, the levitated disc can maintain stability with powder dispersion at different levitation heights.

8.5 Summary

This chapter highlights the first successful implementation of a magnetic levitation system capable of supporting additive manufacturing applications using nonmagnetic materials. The primary emphasis is placed on LDED-PF techniques. Two distinct systems have been developed for this analysis, as highlighted in Chapter 5.

The levitation system is able to facilitate stable suspension of the levitated disc with the incorporation of the effect of powder particle impact has been verified through both simulations (as highlighted in Section 5.8.2) and experimentally (as highlighted in Section 8.1.1).

Next, the levitated disc was also subjected to powder deposition activities with the laser on. Two different aluminum alloy discs of different dimensions were used for the study. Both systems developed in Chapter 5 highlighted the ability to support the deposition of at least 5 layers while maintaining stability.

With the addition of a highly conductive material (copper), an increase in the volume of eddy current induction was observed. This subsequently resulted in an increase in levitation force which produced an increase in the measured levitation height of the disc. The experimental observation was verified through simulation analyses.

The most significant contribution of this research is that the levitated geometry is replacing the conventional substrate utilized within the additive manufacturing environment. Since the levitated geometry is anticipated to be a portion of the final built part, there is an anticipated reduction in the number of post-manufacturing operations. The technique also allows for both sides of the levitated geometry to be used for deposition activities. This results in a 100% increase in the build surface available for deposition activities.

Finally, the levitation system was subjected to high process parameters for the powder deposition of copper on an aluminum disc. With a 12 g/min powder feed rate and 1500 W laser power, the levitated disc maintained stability. This observation offers confidence that the levitated disc will maintain stability for lower powder feed rates and lower laser powers.

Chapter 9

Conclusions and Future Work

9.1 Conclusions

This thesis aims and succeeds in developing a magnetic levitation system with applications and compatibility within the AM environment using the principle of eddy current repulsive levitation. The levitated geometry serves as a build surface to facilitate AM operations. This is a novel technique of overlapping magnetic levitation technique with LDED-PF operations with no previous precedence within the literature. The following conclusions can be drawn from this research:

- The initial viability of a magnetic levitation system was established through simulation analyses. Three specific test cases were considered: a levitated disc, a disc with one layer of material, and a disc with two layers of material. The minimum inputs to overcome the effect of gravitational force were also calculated. The system highlighted successful performance with several different inputs, therefore confirming the initial viability of a magnetic levitation system for AM applications.

Table 9.1: Comparison of System Prototypes

Parameter	Value from [96] Prototype	Laminated Core	Solid Core
hline Surface area of Levitated disc	1963 mmˆ2	11309.73 mmˆ2	11309.73 mmˆ2
Supported added mass	15.2 g	66.74 g	66.74 g
Mass deposition time for AM (assuming m =1g/min)	15.2 min	1.11 hour	1.11 hour
Levitation height	4.5 mm at 85 Hz	8 mm at 90 Hz	8 mm at 150 Hz

- Two distinct prototypes were designed and optimized to maximize the levitation force with a controllable input voltage to facilitate the stable suspension of paramagnetic materials. The developed prototypes highlighted improved performances the prototype developed in [96], as highlighted in Table 9.1.

- The two prototypes were subjected to compatibility testing with AM operations using simulation. This entailed testing the system's ability to support a time-varying payload and the stability in the axial and lateral axes while incorporating the effects of the impact of powder deposition with FEA tools. Both prototypes highlighted successful performance, despite being subjected to worst-case scenario analysis.

- A simple PID controller was built and tuned using Simulink. The tuned PID controller was then tested within the experimental environment. The system possessed a low rise time but a high settling time and overshoot error. To facilitate improved performance, a compensator component was added to work in conjunction with the feedback controller. For a 2 mm setpoint, the incorporation of the compensator component results in a 58% reduction in the settling time and a 22% reduction in overshoot error, therefore improving the overall performance of the feedback control system. This feedback controller has been implemented in the lab environment through this research.

- Following the successful development of the improved levitation system prototypes, the following integral step was the incorporation of the levitation system within the LDED-PF machine. The levitation system was successful in supporting powder deposition activities associated with LDED-PF operations. With a high powder feed rate of 12 g/min and high laser powder of 1500 W, the levitated disc maintained stable suspension.

- There is an increase in the measured levitation height of the disc during the deposition of copper. This is caused by the deposition of highly conductive copper on the levitated disc, resulting in an increase in the volume available for eddy current induction. Thus, there is an increase in levitation force caused by the deposition activities.

- A crucial improvement offered by the incorporation of the levitation system within the AM machine is the ability to utilize both sides of the levitated geometry for deposition activities. By flipping the levitated disc, there is a 100% increase in the build surface available for deposition activities. Conducting deposition activities on both sides of the levitated disc can have significant applications in fields like repair and reconditioning existing components.

- The levitation system developed serves as a modular add-on for existing AM machines. This entails no adjustments to the AM machine infrastructure to facilitate experimentation with the levitation system. This allows the levitation system to be compatible with all AM machines with the minimum working envelope to fit the levitation system.
- The research presented in this report also develops a viable alternative to testing the compatibility of different paramagnetic materials with magnetic levitation applications. As highlighted in [110], there is a strong dependence on conducting levitation experiments with different materials to determine its 'levitation ability. Through the analytical model developed in Chapter 7, the relative performance of a paramagnetic material with magnetic levitation applications can be determined based solely on the ratio of the conductivity to the density of the material. This parameter was verified across all prototypes developed and produced consistent results within the simulation environment.

9.2 Future Scope of Work

- Incorporation of a feedback controller during the deposition activity:
  - The most critical challenge encountered during the implementation of the levitation system in the AM machine was the change in the levitation height of the levitated geometry. As discussed in Section 6.1, the incorporation of added payloads will result in a change in the levitated height. During the experiment, the addition of layers on the levitated disc resulted in variation in the levitation height of the disc. This is in line with the anticipated outcome of the implementation of the levitation system with no feedback controller.
  - The feedback control controller developed in Chapter 6 utilizes a laser sensor above the levitation system. This feedback controller was only implemented within the lab environment.
  - The compatibility of the laser sensor with LDED-PF applications is not ideal for two reasons. First, the laser sensor would be subjected to significant noise due to the nomadic powder particles encountered within the AM machine. This would render the readings unreliable within the AM machine. Second, the laser sensor is placed above the levitation system, as highlighted in Fig. 9.1a. Thus, the laser sensor would serve as a barrier between the AM infrastructure and the levitated build surface, as highlighted in Fig. 9.1b.

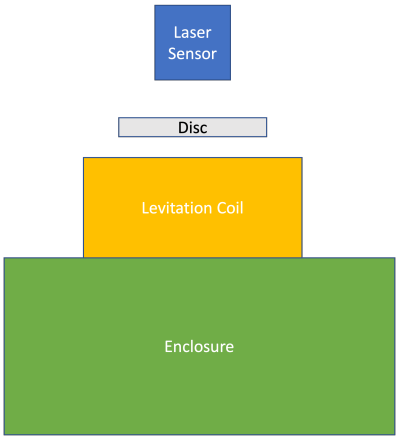

(a) Implementation of laser sensor for feedback controller

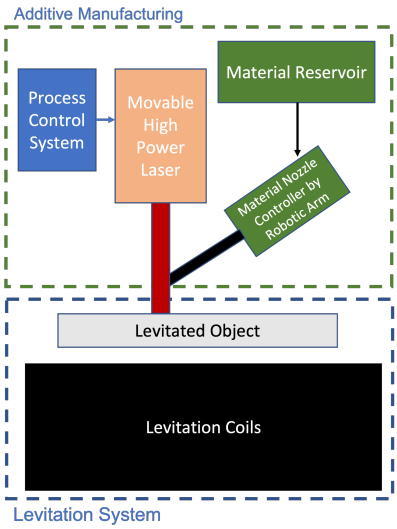

(b) Implementation of levitation system in AM machine

Figure 9.1: Issues with use of Laser Sensor within AM environment

  - Thus, the critical next step would be incorporating a feedback controller with a sensor compatible with the AM machine.
  - Through the incorporation of a reliable feedback controller within the AM machine, the levitation height of the system could be kept constant with added powder layers. This would facilitate a more reliable comparison of the powder deposition activities within a conventional substrate and a magnetically levitated substrate.

- Selection of sensor for use within the AM machine:
  - The selection of a sensor with higher feasibility within the AM machine and the subsequent implementation within the AM machine are the pertinent next steps.
  - The use of cameras coupled can serve as a viable alternative sensor input, as highlighted by [129, 130].
  - According to Section 2.5.1 , the most common sensors incorporated within the AM machine are high-frame cameras.

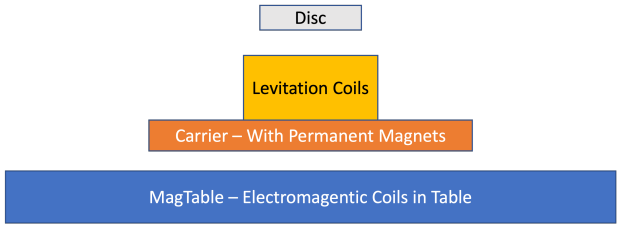

Figure 9.2: Potential incorporation of MagTable

- The performance of the feedback controller can be subjected to further improvement. Using other feedback control techniques with precedence with magnetic levitation systems can result in further improvement in performance. This includes techniques such as Linear–Quadratic Regulator (LQR) [131] and Pole Placement Controller (PPC), [132] amongst others.

- Elimination of Robotic Arm for LDED-PF Operations:

  - [36, 133, 134] highlight the development of a 'MagTable'. A 'MagTable' includes an array of electromagnetic coils embedded within a table. Permanent magnets can subsequently be levitated on the table containing the electromagnets. Through the variation of input currents to specific coils within the table, the magnetic field over the table can be adjusted to facilitate the movement of the permanent magnet over the coils.

  - The idea of a 'MagTable' can also work in conjunction with the levitation system developed through this research. As highlighted in Fig. 9.2, the levitation system developed can be placed on top of a carrier place consisting of a permanent magnet array to facilitate motion of the levitation system and levitated disc over the 'MagTable'. Through the incorporation of this idea, the need for a robotic arm can be bypassed.

References

[1] W. A. Harkness and J. H. Goldschmid, "Free-form spatial 3-d printing using part levitation," Mar. 6 2018. US Patent 9,908,288.

[2] "Small metal 3d printer specialized for medical products." https://www.eos.info/en/additive-manufacturing/3d-printing-metal/eos-metal-systems/eos-m-100, Accessed: December 2022.

[3] "Msam - infrastucture." https://msam.uwaterloo.ca/infrastructure/, Accessed: December 2022.

[4] E. Okress, D. Wroughton, G. Comenetz, P. Brace, and J. Kelly, "Electromagnetic levitation of solid and molten metals," *Journal of applied physics*, vol. 23, no. 5, pp. 545–552, 1952.

[5] F. Ghayoor and A. Swanson, "Modelling and analysis of electrodynamic suspension of an aluminium disc as a complex engineering problem," *The International Journal of Electrical Engineering & Education*, vol. 55, no. 2, pp. 91–108, 2018.

[6] H. Karl, J. Fetzer, S. Kurz, G. Lehner, and W. M. Rucker, "Description of team workshop problem 28: An electrodynamic levitation device," in *Proc. of the TEAM Workshop, Graz, Austria*, pp. 48–51, 1997.

[7] P. H. Smith, J. W. Murray, A. Jackson-Crisp, J. Segal, and A. T. Clare, "Magnetic manipulation in directed energy deposition using a programmable solenoid," *Journal of Materials Processing Technology*, vol. 299, p. 117342, 2022.

[8] M. Alimardani, C. Paul, E. Toyserkani, and A. Khajepour, "Multiphysics modelling of laser solid freeform fabrication techniques," in *Advances in Laser Materials Processing*, pp. 765–791, Elsevier, 2010.

[9] Y. Huang, M. B. Khamesee, and E. Toyserkani, "Electrodynamic concentration of non-ferrous metallic particles in the moving gas-powder stream: Mathematical modeling and analysis," *International Journal of Magnetics and Electromagnetism*, vol. 5, no. 1, 2019.

[10] H. E Farag, E. Toyserkani, and M. B. Khamesee, "Non-destructive testing using eddy current sensors for defect detection in additively manufactured titanium and stainless-steel parts," *Sensors*, vol. 22, no. 14, p. 5440, 2022.

[11] Y. Sanagawa, H. Ueda, M. Tsuda, A. Ishiyama, S. Kohayashi, and S. Haseyama, "Characteristics of lift and restoring force in hts bulk-application to two-dimensional maglev transporter," *IEEE transactions on applied superconductivity*, vol. 11, no. 1, pp. 1797–1800, 2001.

[12] R. Moser, F. Barrot, J. Sandtner, and H. Bleuler, "Optimization of two-dimensional permanent magnet arrays for diamagnetic levitation," in *17th International Conference on Magnetically Levitated Systems and Linear Drives (Maglev)*, 2002.

[13] P. Kazemzadeh Heris and M. B. Khamesee, "Design and fabrication of a magnetic actuator for torque and force control estimated by the ann/sa algorithm," *Micromachines*, vol. 13, no. 2, p. 327, 2022.

[14] E. S. Motta, D. H. N. Dias, G. G. Sotelo, H. O. C. Ramos, J. H. Norman, and R. M. Stephan, "Optimization of a linear superconducting levitation system," *IEEE Transactions on Applied Superconductivity*, vol. 21, no. 5, pp. 3548–3554, 2011.

[15] "Transformer: Why is the core laminated?." https://www.cyberphysics.co.uk/topics/magnetsm/electro/Transfromer/laminated.htm.

[16] "Transformer construction of the core and transformer design." https://www.electronics-tutorials.ws/transformer/transformer-construction.html.

[17] "Impact on efficiency of core materials." https://www.electricmotorengineering.com/impact-on-efficiency-of-core-materials/., journal=Electric Motor Engineering, Accessed: July 20, 2022.

[18] M. Kacki, M. S. Ryłko, J. G. Hayes, and C. R. Sullivan, "A study of flux distribution and impedance in solid and laminar ferrite cores," in *2019 IEEE Applied Power Electronics Conference and Exposition (APEC)*, pp. 2681–2687, IEEE, 2019.

[19] C. Boniface and P. Barendse, "Impedance behavioural study of silicon steel laminated core inductor," in *2020 International SAUPEC/RobMech/PRASA Conference*, pp. 1–6, IEEE, 2020.

[20] "Magnetics." https://www.mag-inc.com/.

[21] "The difference between ferrite core and iron powder core." http://www.gsmagnetics.com/news/the-difference-between-ferrite-core-and-iron-p-23212644.html.

[22] "Difference between ferrite core and iron core base inverters." https://microcontrollerslab.com/ferrite-core-and-iron-core-inverter/.

[23] I. Ahmad and M. A. Javaid, "Nonlinear model & controller design for magnetic levitation system," *Recent advances in signal processing, robotics and automation*, pp. 324–328, 2010.

[24] S. K. Pandey, V. Laxmi, *et al.*, "Pid control of magnetic levitation system based on derivative filter," in *2014 Annual International Conference on Emerging Research Areas: Magnetics, Machines and Drives (AICERA/iCMMD)*, pp. 1–5, IEEE, 2014.

[25] W. G. Hurley, M. Hynes, and W. H. Wolfle, "Pwm control of a magnetic suspension system," *IEEE Transactions on education*, vol. 47, no. 2, pp. 165–173, 2004.

[26] X. Zhang, M. Mehrtash, and M. B. Khamesee, "Dual-axial motion control of a magnetic levitation system using hall-effect sensors," *IEEE/ASME Transactions on Mechatronics*, vol. 21, no. 2, pp. 1129–1139, 2015.

[27] T. Kumar, S. Shimi, D. Karanjkar, and S. Rana, "Modeling, simulation and control of single actuator magnetic levitation system," in *2014 Recent Advances in Engineering and Computational Sciences (RAECS)*, pp. 1–6, IEEE, 2014.

[28] N. Shawki, S. Alam, and A. K. S. Gupta, "Design and implementation of a magnetic levitation system using phase lead compensation technique," in *2014 9th International Forum on Strategic Technology (IFOST)*, pp. 294–299, IEEE, 2014.

[29] E. W. Reutzel and A. R. Nassar, "A survey of sensing and control systems for machine and process monitoring of directed-energy, metal-based additive manufacturing," *Rapid Prototyping Journal*, 2015.

[30] A. R. Nassar, E. W. Reutzel, S. W. Brown, J. P. Morgan Jr, J. P. Morgan, D. J. Natale, R. L. Tutwiler, D. P. Feck, and J. C. Banks, "Sensing for directed energy deposition and powder bed fusion additive manufacturing at penn state university," in *Laser 3D Manufacturing III*, vol. 9738, pp. 77–90, SPIE, 2016.

[31] M. Khanzadeh, W. Tian, A. Yadollahi, H. R. Doude, M. A. Tschopp, and L. Bian, "Dual process monitoring of metal-based additive manufacturing using tensor decomposition of thermal image streams," *Additive Manufacturing*, vol. 23, pp. 443–456, 2018.

[32] G. B. Arfken, D. F. Griffing, D. C. Kelly, and J. Priest, "chapter 32 - magnetism and the magnetic field," in *International Edition University Physics* (G. B. Arfken, D. F. Griffing, D. C. Kelly, and J. Priest, eds.), pp. 602–627, Academic Press, 1984.

[33] T. Zhu, B. Cazzolato, W. S. Robertson, and A. Zander, "Vibration isolation using six degree-of-freedom quasi-zero stiffness magnetic levitation," *Journal of Sound and Vibration*, vol. 358, pp. 48–73, 2015.

[34] H.-W. Lee, K.-C. Kim, and J. Lee, "Review of maglev train technologies," *IEEE transactions on magnetics*, vol. 42, no. 7, pp. 1917–1925, 2006.

[35] G. E. Fúnez, A. M. Carrasco, and J. L. Ordoñez-Ávila, "Study case: Electromechanical design of a magnetic damper for robotic systems," *International Journal of Mechanical Engineering and Robotics Research*, vol. 11, no. 2, 2022.

[36] X. Zhang, C. Trakarnchaiyo, H. Zhang, and M. B. Khamesee, "Magtable: A tabletop system for 6-dof large range and completely contactless operation using magnetic levitation," *Mechatronics*, vol. 77, p. 102600, 2021.

[37] R. Zhou, M. Yan, F. Sun, J. Jin, Q. Li, F. Xu, M. Zhang, X. Zhang, and K. Nakano, "Experimental validations of a magnetic energy-harvesting suspension and its potential application for self-powered sensing," *Energy*, vol. 239, p. 122205, 2022.

[38] G. Aldawood and H. Bardaweel, "Self-powered self-contained wireless vibration synchronous sensor for fault detection," *Sensors*, vol. 22, no. 6, 2022.

[39] P. J. Widodo, E. P. Budiana, U. Ubaidillah, F. Imaduddin, and S.-B. Choi, "Effect of time and frequency of magnetic field application on mrf pressure performance," *Micromachines*, vol. 13, no. 2, 2022.

[40] D. M. Rote, "Magnetic levitation," in *Encyclopedia of Energy* (C. J. Cleveland, ed.), pp. 691–703, New York: Elsevier, 2004.

[41] V. Vostokov and S. Lebedeva, "Stability of electromagnetic suspension of a rotor," *Journal of Computer and Systems Sciences International*, vol. 50, no. 2, pp. 181–185, 2011.

[42] S.-M. Yang and Y.-H. Tsai, "Design of a thrust actuator for magnetic bearings with low radial attraction force," *IEEE Transactions on Magnetics*, vol. 48, no. 11, pp. 3587–3590, 2012.

[43] J.-M. Jo, Y.-J. Han, and C.-Y. Lee, "The design of the feedback control system of electromagnetic suspension using kalman filter," *International Journal of Railway*, vol. 4, no. 4, pp. 93–96, 2011.

[44] K. S. Jung and Y. S. Baek, "Precision stage using a non-contact planar actuator based on magnetic suspension technology," *Mechatronics*, vol. 13, no. 8-9, pp. 981–999, 2003.

[45] L. Hao, Z. Huang, F. Dong, D. Qiu, B. Shen, and Z. Jin, "Study on electrodynamic suspension system with high-temperature superconducting magnets for a high-speed maglev train," *IEEE Transactions on Applied Superconductivity*, vol. 29, no. 2, pp. 1–5, 2019.

[46] H.-W. Lee, K.-C. Kim, and J. Lee, "Review of maglev train technologies," *IEEE transactions on magnetics*, vol. 42, no. 7, pp. 1917–1925, 2006.

[47] M.-Y. Chen, M.-J. Wang, and L.-C. Fu, "Modeling and controller design of a maglev guiding system for application in precision positioning," *IEEE Transactions on Industrial Electronics*, vol. 50, no. 3, pp. 493–506, 2003.

[48] E. E. Covert, M. Finston, M. Vlajinac, and T. Stephens, "Magnetic balance and suspension systems for use with wind tunnels," *Progress in Aerospace Sciences*, vol. 14, pp. 27–107, 1973.

[49] K. Nagaya and M. Ishikawa, "A noncontact permanent magnet levitation table with electromagnetic control and its vibration isolation method using direct disturbance cancellation combining optimal regulators," *IEEE Transactions on Magnetics*, vol. 31, no. 1, pp. 885–896, 1995.

[50] W. Hurley and J. Kassakian, "Induction heating of circular ferromagnetic plates," *IEEE Transactions on Magnetics*, vol. 15, no. 4, pp. 1174–1181, 1979.

[51] M. Simon and A. Geim, "Diamagnetic levitation: Flying frogs and floating magnets," *Journal of applied physics*, vol. 87, no. 9, pp. 6200–6204, 2000.

[52] E. Beaugnon, D. Fabregue, D. Billy, J. Nappa, and R. Tournier, "Dynamics of magnetically levitated droplets," *Physica B: Condensed Matter*, vol. 294, pp. 715–720, 2001.

[53] A. K. Geim and H. Ter Tisha, "Detection of earth rotation with a diamagnetically levitating gyroscope," *Physica B: Condensed Matter*, vol. 294, pp. 736–739, 2001.

[54] M. Boukallel, E. Piat, and J. Abadie, "Passive diamagnetic levitation: theoretical foundations and application to the design of a micro-nano force sensor," in *Proceedings 2003 IEEE/RSJ International Conference on Intelligent Robots and Systems (IROS 2003)(Cat. No. 03CH37453)*, vol. 2, pp. 1062–1067, IEEE, 2003.

[55] R. Moser, "Passive diamagnetic levitation for flywheels," in *8th International Symposium on Magnetic Bearing, August 26-28, 2002, Mito, Japan*, 2002.

[56] U. Hasirci, A. Balikci, Z. Zabar, and L. Birenbaum, "Experimental performance investigation of a novel magnetic levitation system," *IEEE Transactions on Plasma Science*, vol. 41, no. 5, pp. 1174–1181, 2013.

[57] D. K. Bwambok, M. M. Thuo, M. B. Atkinson, K. A. Mirica, N. D. Shapiro, and G. M. Whitesides, "Paramagnetic ionic liquids for measurements of density using magnetic levitation," *Analytical chemistry*, vol. 85, no. 17, pp. 8442–8447, 2013.

[58] P. Samanta and H. Hirani, "Magnetic bearing configurations: Theoretical and experimental studies," *IEEE Transactions on Magnetics*, vol. 44, no. 2, pp. 292–300, 2008.

[59] H. Shakir and W.-J. Kim, "Nanoscale path planning and motion control with maglev positioners," *IEEE/ASME Transactions on Mechatronics*, vol. 11, no. 5, pp. 625–633, 2006.

[60] M. P. Kummer, J. J. Abbott, B. E. Kratochvil, R. Borer, A. Sengul, and B. J. Nelson, "Octomag: An electromagnetic system for 5-dof wireless micromanipulation," *IEEE Transactions on Robotics*, vol. 26, no. 6, pp. 1006–1017, 2010.

[61] M. Ono, S. Koga, and H. Ohtsuki, "Japan's superconducting maglev train," *IEEE Instrumentation & Measurement Magazine*, vol. 5, no. 1, pp. 9–15, 2002.

[62] Q. Lin, W. Wang, Z. Deng, D. Jiang, D. Shin, Z. Xie, X. Gu, N. Lin, M. Shao, Z. Yang, *et al.*, "Measurement and calculation method of the radial stiffness of radial high-temperature superconducting bearings," *Journal of Superconductivity and Novel Magnetism*, vol. 28, no. 6, pp. 1681–1685, 2015.

[63] J. L. Perez-Diaz, I. Valiente-Blanco, E. Diez-Jimenez, and J. Sanchez-Garcia-Casarrubios, "Superconducting noncontact device for precision positioning in cryogenic environments," *IEEE/ASME Transactions on Mechatronics*, vol. 19, no. 2, pp. 598–605, 2013.

[64] S. A. Tofail, E. P. Koumoulos, A. Bandyopadhyay, S. Bose, L. O'Donoghue, and C. Charitidis, "Additive manufacturing: scientific and technological challenges, market uptake and opportunities," *Materials today*, vol. 21, no. 1, pp. 22–37, 2018.

[65] I. Golubev, "Possibilities of 3d scanning of parts during repair of agricultural machinery," in *BIO Web of Conferences*, vol. 37, p. 00003, EDP Sciences, 2021.

[66] V. Mohanavel, K. A. Ali, K. Ranganathan, J. A. Jeffrey, M. Ravikumar, and S. Rajkumar, "The roles and applications of additive manufacturing in the aerospace and automobile sector," *Materials Today: Proceedings*, vol. 47, pp. 405–409, 2021.

[67] C. Basgul, H. Spece, N. Sharma, F. M. Thieringer, and S. M. Kurtz, "Structure, properties, and bioactivity of 3d printed paeks for implant applications: A systematic review," *Journal of Biomedical Materials Research Part B: Applied Biomaterials*, vol. 109, no. 11, pp. 1924–1941, 2021.

[68] L. F. Velásquez-García and Y. Kornbluth, "Biomedical applications of metal 3d printing," *Annual review of biomedical engineering*, vol. 23, pp. 307–338, 2021.

[69] Y. Tian, C. Chen, X. Xu, J. Wang, X. Hou, K. Li, X. Lu, H. Shi, E.-S. Lee, and H. B. Jiang, "A review of 3d printing in dentistry: Technologies, affecting factors, and applications," *Scanning*, vol. 2021, 2021.

[70] J. Li and M. Pumera, "3d printing of functional microrobots," *Chemical Society Reviews*, vol. 50, no. 4, pp. 2794–2838, 2021.

[71] I. Gibson, D. Rosen, and B. Stucker, "Vat photopolymerization processes," in *Additive Manufacturing Technologies*, pp. 63–106, Springer, 2015.

[72] W. L. Ng, J. M. Lee, M. Zhou, Y.-W. Chen, K.-X. A. Lee, W. Y. Yeong, and Y.-F. Shen, "Vat polymerization-based bioprinting—process, materials, applications and regulatory challenges," *Biofabrication*, vol. 12, no. 2, p. 022001, 2020.

[73] C. Yan, Y. Shi, J. Yang, and J. Liu, "Multiphase polymeric materials for rapid prototyping and tooling technologies and their applications," *Composite Interfaces*, vol. 17, no. 2-3, pp. 257–271, 2010.

[74] J. Dilag, T. Chen, S. Li, and S. A. Bateman, "Design and direct additive manufacturing of three-dimensional surface micro-structures using material jetting technologies," *Additive Manufacturing*, vol. 27, pp. 167–174, 2019.

[75] A. Kalkal, S. Kumar, P. Kumar, R. Pradhan, M. Willander, G. Packirisamy, S. Kumar, and B. D. Malhotra, "Recent advances in 3d printing technologies for wearable (bio) sensors," *Additive Manufacturing*, vol. 46, p. 102088, 2021.

[76] F. Acquaticci, M. M. Yommi, S. N. Gwirc, S. E. Lew, *et al.*, "Rapid prototyping of pyramidal structured absorbers for ultrasound," *Open Journal of Acoustics*, vol. 7, no. 03, p. 83, 2017.

[77] M. Ziaee and N. B. Crane, "Binder jetting: A review of process, materials, and methods," *Additive Manufacturing*, vol. 28, pp. 781–801, 2019.

[78] F. Zhang, M. Wei, V. V. Viswanathan, B. Swart, Y. Shao, G. Wu, and C. Zhou, "3d printing technologies for electrochemical energy storage," *Nano Energy*, vol. 40, pp. 418–431, 2017.

[79] R. Trombetta, J. A. Inzana, E. M. Schwarz, S. L. Kates, and H. A. Awad, "3d printing of calcium phosphate ceramics for bone tissue engineering and drug delivery," *Annals of biomedical engineering*, vol. 45, no. 1, pp. 23–44, 2017.

[80] J. K. Placone and A. J. Engler, "Recent advances in extrusion-based 3d printing for biomedical applications," *Advanced healthcare materials*, vol. 7, no. 8, p. 1701161, 2018.

[81] T. DebRoy, H. Wei, J. Zuback, T. Mukherjee, J. Elmer, J. Milewski, A. Beese, A. Wilson-Heid, A. De, and W. Zhang, "Additive manufacturing of metallic components – process, structure and properties," *Progress in Materials Science*, vol. 92, pp. 112–224, 2018.

[82] "Powder bed fusion: Additive manufacturing research group: Loughborough university." https://www.lboro.ac.uk/research/amrg/about/the7categoriesofadditivemanufacturing/powderbedfusion/, Accessed: July 20, 2022.

[83] D. W. Gibbons, J.-P. L. Serfontein, and A. F. Van der Merwe, "Mapping the path to certification of metal laser powder bed fusion for aerospace applications," *Rapid Prototyping Journal*, 2021.

[84] I. Yadroitsava, A. Du Plessis, and I. Yadroitsev, "Bone regeneration on implants of titanium alloys produced by laser powder bed fusion: A review," *Titanium for Consumer Applications*, pp. 197–233, 2019.

[85] N. Asnafi, "Application of laser-based powder bed fusion for direct metal tooling," *Metals*, vol. 11, no. 3, p. 458, 2021.

[86] W. E. Frazier, "Metal additive manufacturing: a review," *Journal of Materials Engineering and performance*, vol. 23, no. 6, pp. 1917–1928, 2014.

[87] M. Juhasz, R. Tiedemann, G. Dumstorff, J. Walker, A. Du Plessis, B. Conner, W. Lang, and E. MacDonald, "Hybrid directed energy deposition for fabricating metal structures with embedded sensors," *Additive Manufacturing*, vol. 35, p. 101397, 2020.

[88] P. Azhagarsamy, K. Sekar, and K. Murali, "An overview of metallic materials fabrication by direct energy deposition," *Key Engineering Materials*, vol. 882, pp. 11–20, 2021.

[89] W. J. Oh, W. J. Lee, M. S. Kim, J. B. Jeon, and D. S. Shim, "Repairing additive-manufactured 316l stainless steel using direct energy deposition," *Optics & Laser Technology*, vol. 117, pp. 6–17, 2019.

[90] I.-H. Kim, Y.-I. Jung, H.-G. Kim, and J.-I. Jang, "Oxidation-resistant coating of fecral on zr-alloy tubes using 3d printing direct energy deposition," *Surface and Coatings Technology*, vol. 411, p. 126915, 2021.

[91] T. Niendorf, F. Brenne, P. Hoyer, D. Schwarze, M. Schaper, R. Grothe, M. Wiesener, G. Grundmeier, and H. J. Maier, "Processing of new materials by additive manufacturing: iron-based alloys containing silver for biomedical applications," *Metallurgical and Materials Transactions A*, vol. 46, no. 7, pp. 2829–2833, 2015.

[92] I. Rishmawi, M. Salarian, and M. Vlasea, "Tailoring green and sintered density of pure iron parts using binder jetting additive manufacturing," *Additive Manufacturing*, vol. 24, pp. 508–520, 2018.

[93] E. M. Palmero and A. Bollero, "3d and 4d printing of functional and smart composite materials," in *Encyclopedia of Materials: Composites* (D. Brabazon, ed.), pp. 402–419, Oxford: Elsevier, 2021.

[94] Huang, Yuze, *Comprehensive Analytical Modeling of Laser Powder-Bed/Fed Additive Manufacturing Processes and an Associated Magnetic Focusing Module*. PhD thesis, 2019.

[95] M. T. Thompson, "Electrodynamic magnetic suspension-models, scaling laws, and experimental results," *IEEE Transactions on Education*, vol. 43, no. 3, pp. 336–342, 2000.

[96] P. Kumar, S. Malik, E. Toyserkani, and M. B. Khamesee, "Development of an electromagnetic micromanipulator levitation system for metal additive manufacturing applications," *Micromachines*, vol. 13, no. 4, 2022.

[97] J. O. Bird and P. J. Chivers, "10 - electromagnetism and magnetic circuits," in *Newnes Engineering and Physical Science Pocket Book* (J. O. Bird and P. J. Chivers, eds.), pp. 77–87, Newnes, 1993.

[98] S. Carty, I. Owen, W. Steen, B. Bastow, and J. Spencer, "Catchment efficiency for novel nozzle designs used in laser cladding and alloying," in *Laser processing: surface treatment and film deposition*, pp. 395–410, Springer, 1996.

[99] M. Ansari, A. Martinez-Marchese, Y. Huang, and E. Toyserkani, "A mathematical model of laser directed energy deposition for process mapping and geometry prediction of ti-5553 single-tracks," *Materialia*, vol. 12, p. 100710, 2020.

[100] Malik, Saksham, "Hardware design and implementation of an electromagnetic levitation system in an additive manufacturing environment," Master's thesis, 2022.

[101] P. Kumar and M. B. Khamesee, "Development and analysis of a novel magnetic levitation system with a feedback controller for additive manufacturing applications," in *Actuators*, vol. 11, p. 364, Multidisciplinary Digital Publishing Institute, 2022.

[102] P. R. Upadhyay and K. Rajagopal, "Fe analysis and cad of radial-flux surface mounted permanent magnet brushless dc motors," *IEEE Transactions on Magnetics*, vol. 41, no. 10, pp. 3952–3954, 2005.

[103] Y. Huang, M. B. Khamesee, and E. Toyserkani, "A comprehensive analytical model for laser powder-fed additive manufacturing," *Additive Manufacturing*, vol. 12, pp. 90–99, 2016.

[104] S. Carty, I. Owen, W. Steen, B. Bastow, and J. Spencer, "Catchment efficiency for novel nozzle designs used in laser cladding and alloying," in *Laser processing: surface treatment and film deposition*, pp. 395–410, Springer, 1996.

[105] "Awg - american wire gauge current ratings." https://www.engineeringtoolbox.com/wire-gauges-d_419.html, Accessed: July 20, 2022.

[106] "Arduino adc: Everything you must know about the built-in adc." https://www.best-microcontroller-projects.com/arduino-adc.html.

[107] A. Ghosh, T. R. Krishnan, P. Tejaswy, A. Mandal, J. K. Pradhan, and S. Ranasingh, "Design and implementation of a 2-dof pid compensation for magnetic levitation systems," *ISA transactions*, vol. 53, no. 4, pp. 1216–1222, 2014.

[108] S. Yadav, S. Verma, and S. Nagar, "Optimized pid controller for magnetic levitation system," *Ifac-PapersOnLine*, vol. 49, no. 1, pp. 778–782, 2016.

[109] S. K. Swain, D. Sain, S. K. Mishra, and S. Ghosh, "Real time implementation of fractional order pid controllers for a magnetic levitation plant," *AEU-International Journal of Electronics and Communications*, vol. 78, pp. 141–156, 2017.

[110] W. Nan, X. Wen-jun, and W. Bing-bo, "Physical characteristics of electromagnetic levitation processing," *Chinese Physics B*, vol. 8, no. 7, pp. 503–513, 1999.

[111] "Matweb: Online materials information resource." https://www.matweb.com. Accessed: 2022-07-01.

[112] "Asm aerospace specifications metals inc.." https://asm.matweb.com. Accessed: 2022-07-01.

[113] C. S. Kannan, S. S. S. Chandra, G. P. Krishnan, and S. P. Raj, "A review on additive manufacturing of aa2024 and aa6061 alloys using powder bed fusion," in *IOP Conference Series: Materials Science and Engineering*, vol. 988, p. 012002, IOP Publishing, 2020.

[114] J. A. Muñiz-Lerma, A. Nommeots-Nomm, K. E. Waters, and M. Brochu, "A comprehensive approach to powder feedstock characterization for powder bed fusion additive manufacturing: a case study on alsi7mg," *Materials*, vol. 11, no. 12, p. 2386, 2018.

[115] A. H. Maamoun, M. A. Elbestawi, and S. C. Veldhuis, "Influence of shot peening on alsi10mg parts fabricated by additive manufacturing," *Journal of Manufacturing and Materials Processing*, vol. 2, no. 3, p. 40, 2018.

[116] P. Ansari and M. U. Salamci, "On the selective laser melting based additive manufacturing of alsi10mg: The process parameter investigation through multiphysics simulation and experimental validation," *Journal of Alloys and Compounds*, vol. 890, p. 161873, 2022.

[117] A. Hadadzadeh, B. S. Amirkhiz, S. Shakerin, J. Kelly, J. Li, and M. Mohammadi, "Microstructural investigation and mechanical behavior of a two-material component fabricated through selective laser melting of alsi10mg on an al-cu-ni-fe-mg cast alloy substrate," *Additive Manufacturing*, vol. 31, p. 100937, 2020.

[118] G. Dinda, A. Dasgupta, S. Bhattacharya, H. Natu, B. Dutta, and J. Mazumder, "Microstructural characterization of laser-deposited al 4047 alloy," *Metallurgical and Materials Transactions A*, vol. 44, no. 5, pp. 2233–2242, 2013.

[119] A. Ramanathan, P. K. Krishnan, and R. Muraliraja, "A review on the production of metal matrix composites through stir casting–furnace design, properties, challenges, and research opportunities," *Journal of Manufacturing processes*, vol. 42, pp. 213–245, 2019.

[120] Q. Jiang, P. Zhang, Z. Yu, H. Shi, D. Wu, H. Yan, X. Ye, Q. Lu, and Y. Tian, "A review on additive manufacturing of pure copper," *Coatings*, vol. 11, no. 6, p. 740, 2021.

[121] Y. Zhou, J. Wang, Y. Yang, M. Yang, H. Zheng, D. Xie, D. Wang, and L. Shen, "Laser additive manufacturing of zinc targeting for biomedical application," *International Journal of Bioprinting*, vol. 8, no. 1, 2022.

[122] A. v. Müller, G. Schlick, R. Neu, C. Anstätt, T. Klimkait, J. Lee, B. Pascher, M. Schmitt, and C. Seidel, "Additive manufacturing of pure tungsten by means of selective laser beam melting with substrate preheating temperatures up to 1000 c," *Nuclear Materials and Energy*, vol. 19, pp. 184–188, 2019.

[123] Y. Dong, J. Tang, D. Wang, N. Wang, Z. He, J. Li, D. Zhao, and M. Yan, "Additive manufacturing of pure ti with superior mechanical performance, low cost, and biocompatibility for potential replacement of ti-6al-4v," *Materials & Design*, vol. 196, p. 109142, 2020.

[124] K. Dietrich, J. Diller, S. Dubiez-Le Goff, D. Bauer, P. Forêt, and G. Witt, "The influence of oxygen on the chemical composition and mechanical properties of ti-6al-4v during laser powder bed fusion (l-pbf)," *Additive Manufacturing*, vol. 32, p. 100980, 2020.

[125] Q. Jia and D. Gu, "Selective laser melting additive manufacturing of inconel 718 superalloy parts: Densification, microstructure and properties," *Journal of Alloys and Compounds*, vol. 585, pp. 713–721, 2014.

[126] J. Gonzalez, J. Mireles, S. Stafford, M. Perez, C. Terrazas, and R. Wicker, "Characterization of inconel 625 fabricated using powder-bed-based additive manufacturing technologies," *Journal of Materials Processing Technology*, vol. 264, pp. 200–210, 2019.

[127] S. Yadav, C. Paul, A. Jinoop, A. Rai, and K. Bindra, "Laser directed energy deposition based additive manufacturing of copper: process development and material characterizations," *Journal of Manufacturing Processes*, vol. 58, pp. 984–997, 2020.

[128] J. Hrbek, "Induction heating of thin nonmagnetic sheets in transverse time-variable magnetic field," *Acta Tech*, vol. 60, no. 1, pp. 15–29, 2015.

[129] E. W. Reutzel and A. R. Nassar, "A survey of sensing and control systems for machine and process monitoring of directed-energy, metal-based additive manufacturing," *Rapid Prototyping Journal*, 2015.

[130] A. R. Nassar, E. W. Reutzel, S. W. Brown, J. P. Morgan Jr, J. P. Morgan, D. J. Natale, R. L. Tutwiler, D. P. Feck, and J. C. Banks, "Sensing for directed energy deposition and powder bed fusion additive manufacturing at penn state university," in *Laser 3D Manufacturing III*, vol. 9738, pp. 77–90, SPIE, 2016.

[131] K. Anurag and S. Kamlu, "Design of lqr-pid controller for linearized magnetic levitation system," in *2018 2nd International Conference on Inventive Systems and Control (ICISC)*, pp. 444–447, IEEE, 2018.

[132] M. Hypiusová and D. Rosinová, "Discrete-time robust lmi pole placement for magnetic levitation," in *2018 Cybernetics & Informatics (K&I)*, pp. 1–6, IEEE, 2018.

[133] T. Murai and H. Hasegawa, "Electromagnetic analysis of inductrack magnetic levitation," *Electrical Engineering in Japan*, vol. 142, no. 1, pp. 67–74, 2003.

[134] K. Nagaya and M. Ishikawa, "A noncontact permanent magnet levitation table with electromagnetic control and its vibration isolation method using direct disturbance cancellation combining optimal regulators," *IEEE Transactions on Magnetics*, vol. 31, no. 1, pp. 885–896, 1995.

APPENDICES

Appendix A

Simulation of Controller

Simulink, a block diagram-based simulation software, has been utilized to study the effectiveness of the PID control strategy with the magnetic levitation system.

A.1 Simulation of the PID Controller

The critical first step to simulate the controller is to develop the plant model. The plant block is the combination of the process of actuators modeled in the system. For the levitation system in consideration, the plant model will highlight the variation of the position of the disc as a function of the input current supplied to the coils. The constant weight was taken to be the weight of the disc + 10% (1.5N) to ensure the capability of the system to develop the control system. The controller is developed at a 120 Hz frequency of input current.

A.1.1 Development of Plant Block

The levitation forces as a function of input current were obtained from ANSYS Maxwell. The force vs current was obtained for positions 1 mm, 2 mm... up to 10 mm above the levitator. Using the equation of curve fitting, the current required to develop the force of 1.5 N was extracted. A sample plot for the development of the lift current is shown in Fig. A.1a.

In Fig. A.1a, the position of the disc is set as 1 mm above the levitation system. The variation of force is plotted as a function of current. The quadratic curve fit equation, with

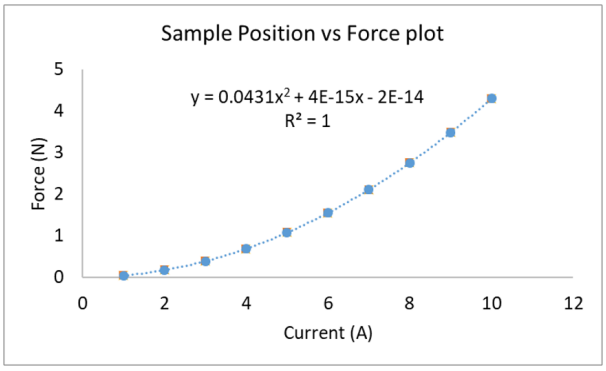

(a) Position of Disc 1 mm above the levitator

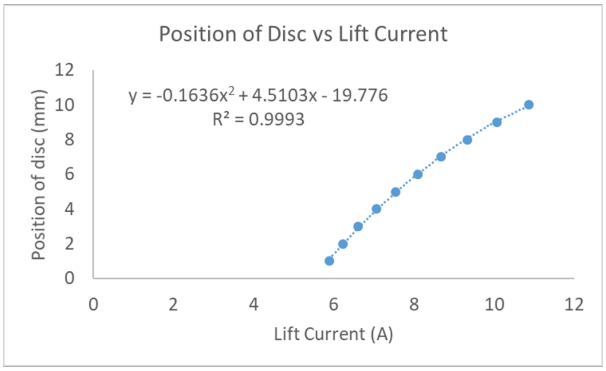

(b) Plant model - Position of Disc vs Input Current producing a constant force

a goodness of fit of 0.9999, was then equated to 1.5 N to obtain the current required to produce the force. The current output was found to be 4.9 A for this case. The process was repeated up to 10 mm and the resulting position of the disc vs input current model was developed, as shown in Fig. A.1b. The quadratic equation obtained through curve-fitting was set as the plant model and the goodness of fit of 1 highlights the high degree of reliability of the model.

A.1.2 Simulation of PID Controller

A simple 1D PID controller was developed using Simulink, as shown in Fig. A.2. Gaussian noise with a mean of 0 and variance of 5% was added to mimic noise encountered with sensor feedback, with a maximum error to the positional feedback as +/- 0.5 mm. The tuned value of the PID controller, as obtained from the in-built Simulink PID tuner, was found to be $K_p = 0, K_i = 0.25, K_d = 0$.

The critical results have been highlighted in Fig.A.3. Fig. A.3a highlights the position of the disc, A.3b highlights the variation of input current, Fig. A.3 highlights the added Gaussian noise and Fig. A.3d highlights the error, i.e., the difference between the setpoint and the position of the disc.

As it can be seen, the input current (Fig. A.3b) is shown to grow from 0 A to 6 A slowly as a function of time. Thus, initially, no levitation is observed. However, as the input current grows as a function of time and crosses the threshold of about 5.5 A (minimum current required to observe levitation), the disc rises. This has been highlighted in Fig. A.4.

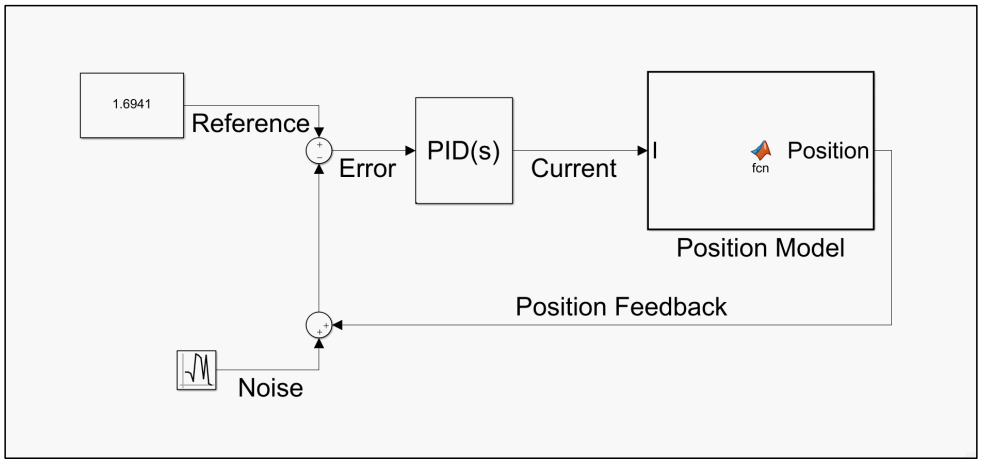

Figure A.2: Simulink model of the closed-loop controller with position feedback

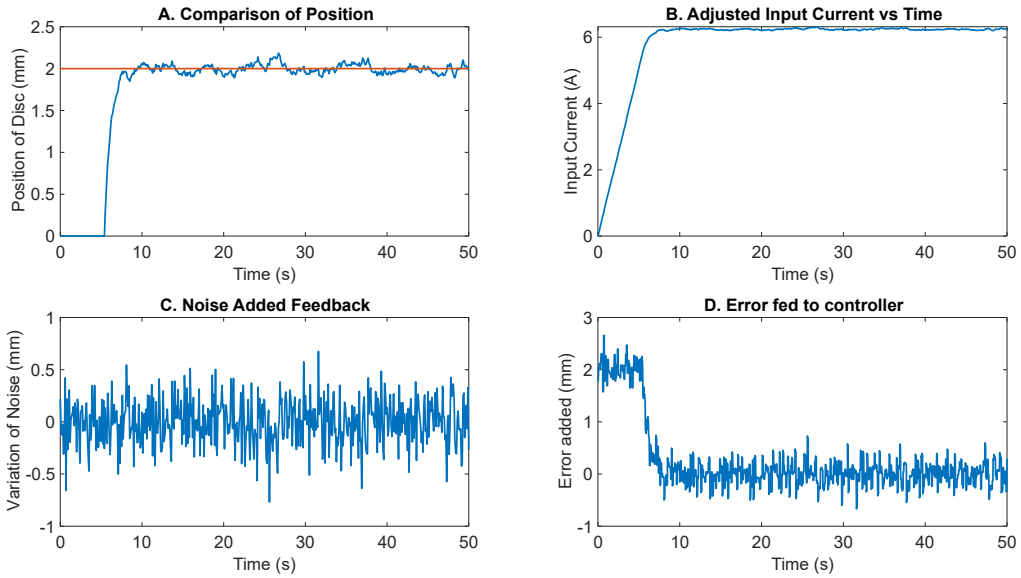

Figure A.3: Resulting Plots from Simulink Simulation (a) Position of Disc vs Time (b) Input Current RMS vs Time (c) Noise Added to the Sensor Feedback (d) Error Fed to Controller

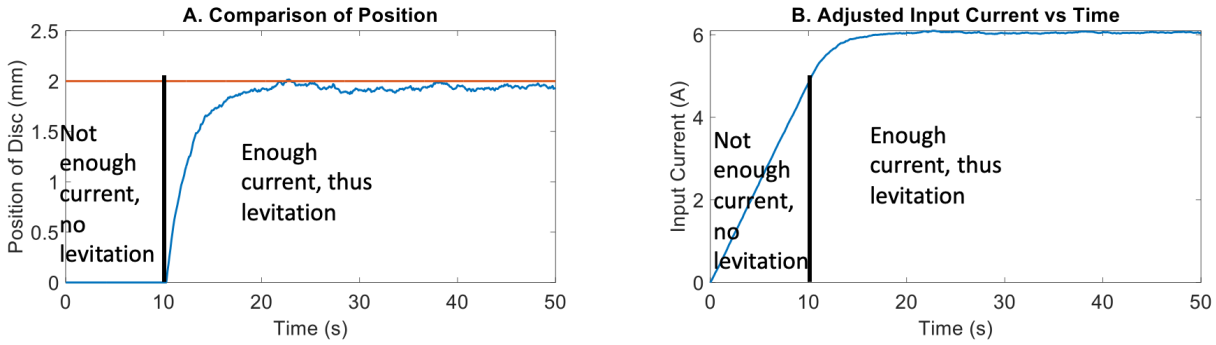

Figure A.4: Growth of Input Current and Associated Impact on Levitation Height

Through the incorporation of a compensating component, the input current can be initialized to a non-zero value at time t=0 to facilitate an improvement in settling time. This is discussed subsequently.

A.2 Simulation of Feedback PID Controller with Compensator Component

The Simulink block diagram to conduct the simulation-based analysis of the PID controller with a compensator component is highlighted in Fig. A.5. The inclusion of a compensator component in the simulation diagram is the critical difference. The compensator component accepts the output of the PID controller and initializes the input current based on the desired setpoint. This is given by Equation A.1-A.2.

$$P = F(I) \tag{A.1}$$

$$Input\ Current = (P(I))^{-1} + PID(I) \tag{A.2}$$

Equation A.1 highlights the plant model with P being the position of the disc and I being the input current to the coils. The compensator component uses the inverse of the plant model to predict the initial current based on the desired setpoint. The PID output provides the feedback controller to correct any potential errors encountered.

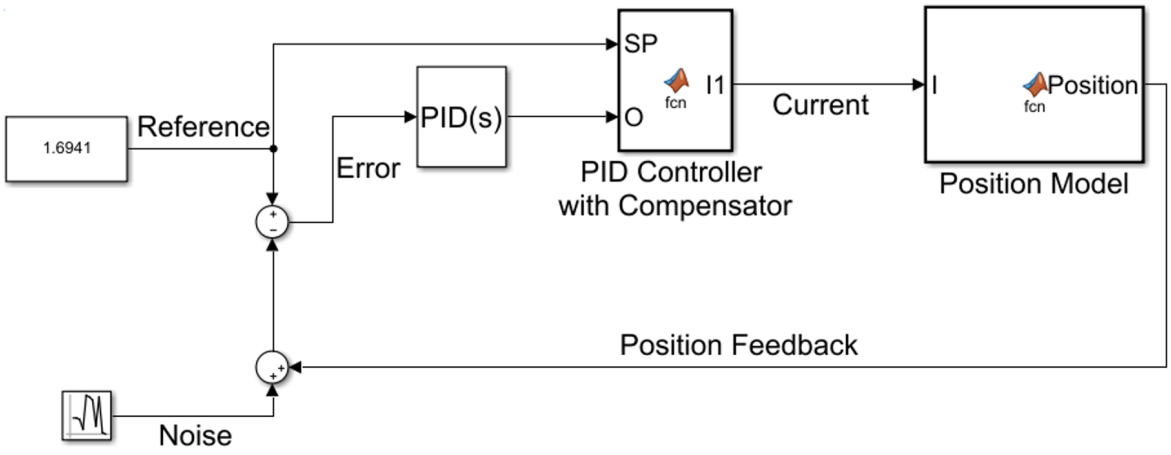

Figure A.5: Simulink Model of the Closed-Loop Controller with Position Feedback and PID Controller with a Compensator Component

The results of the simulations are shown in Fig. A.6. A similar Gaussian noise of mean 0.5 and 5% variance was added to the positional feedback. As it can be seen in Fig. A.6a, the overall settling time reduces quite significantly due to the initialization of the input current using the compensator component.

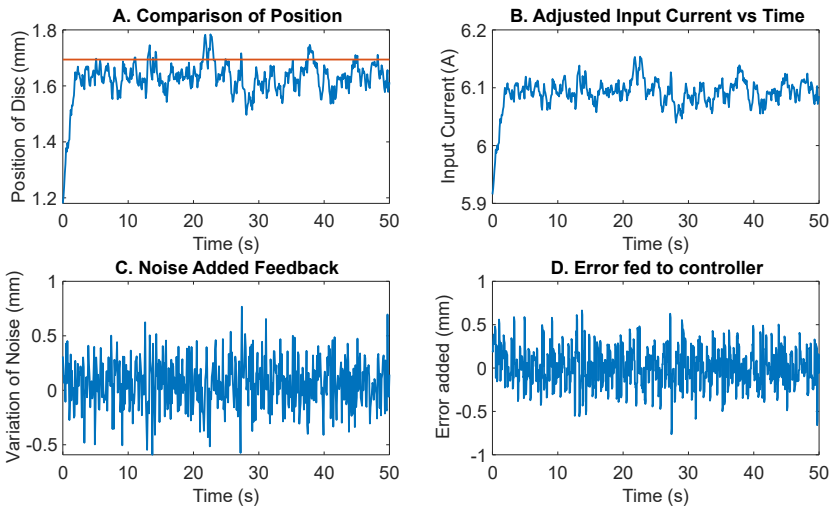

Figure A.6: Simulation Results Using the PID Controller with Compensator Component